

國立臺灣海洋大學

河海工程學系

碩士學位論文

指導教授：陳正宗 博士

零場積分方程求解含圓形邊界拉普拉斯與赫  
姆茲方程之格林函數

Derivation of the Green's function for Laplace  
and Helmholtz problems with circular  
boundaries by using the null-field integral  
equation approach

研究生：柯佳男 撰

中華民國 96 年 7 月



零場積分方程求解含圓形邊界拉普拉斯與赫姆茲  
方程之格林函數

Derivation of the Green's function for Laplace and  
Helmholtz problems with circular boundaries by using the  
null-field integral equation approach

研究生：柯佳男

Student : Jia-Nan Ke

指導教授：陳正宗

Advisor : Jeng-Tzong Chen

國立臺灣海洋大學  
河海工程學系  
碩士論文

A Thesis  
Submitted to Department of Harbor and River Engineering  
College of Engineering  
National Taiwan Ocean University  
In Partial Fulfillment of the Requirements  
for the Degree of  
Master of Science  
in  
Harbor and River Engineering  
July 2007  
Keelung, Taiwan, Republic of China

中華民國 96 年 7 月

國立台灣海洋大學  
河海工程學系

2007  
年

碩士學位論文

零場積分方程求解含圓形邊界拉普拉斯與赫姆茲方程之格林函數

柯佳男  
撰

## 謝誌

兩年碩士生活隨著論文結束而終止，還記得當初剛進入海大的我心情是多麼忐忑不安，承蒙 陳正宗 終身特聘教授的鼓勵下加入了力學聲響振動實驗室。回首過往，對於學問從懵懵懂懂、玩世不恭到了解做學問應有的深思熟慮、嚴謹態度，「學海無涯勤為岸，青雲有路志為梯」，可說是做研究最佳的捷徑。感謝老師於生活上對學生的關心，撰寫論文期間，不厭其煩地審閱修改，得於完成這本論文。

論文口試期間，承蒙國立高雄海洋科技大學造船工程系 陳義麟 博士、中華技術學院機械系 李為民 博士、航空機械系 呂學育 博士、稻江管理學院資訊管理學系 陳桂鴻 博士，悉心指教並提供寶貴的意見使文章內容更臻完善，由衷感謝。

一路走來除了憑靠著自己的堅毅與努力，很幸運地也得到許多人的幫助，修業其間所有曾提供協助關懷的學長、同學、實驗室學弟、至親及益友，願與各位共享榮譽與喜悅。更要感謝國科會計畫 NSC 95-2221-E-019-065 提拱之碩士生研究助學金，讓我在做研究時無經濟之壓力，能更加專心於學業上。

夕陽無限好，只是近黃昏，雖然這段旅程即將結束，但是學習的路途是如此的無邊無盡，此階段的結束象徵著人生另一個歷練的到來，期許自己在未來更加努力。

輕輕的我走了，正如我悄悄的來~

基隆 仲夏 2007

# Derivation of the Green's function for Laplace and Helmholtz problems with circular boundaries by using the null-field integral equation approach

## Contents

Contents	I
Table captions	III
Figure captions	IV
Notations	VII
Abstract	IX
中文摘要	X
<b>Chapter 1 Introduction</b>	
1.1 Overview of BEM and Motivation	1
1.2 Organization of the thesis	6
<b>Chapter 2 Construction of Green's function using null-field integral approach for Laplace problems with circular boundaries</b>	
Abstract	8
2.1 Introduction	8
2.2 Formulation of null-field integral equation	9
2.2.1 Dual boundary integral equations and dual null-field integral equations	9
2.2.2 Expansion of kernel function and boundary density	10
2.2.3 Adaptive observer system	11
2.2.4 Vector decomposition technique for the potential gradient in the hypersingular equation	12
2.2.5 Linear algebraic equation	12
2.2.6 Matching of interface conditions for problems of apertures and inclusions	15

2.3 Illustrative examples and discussions	15
2.4 Concluding remarks	16
<b>Chapter 3 Derivation of anti-plane dynamic Green's function for several circular inclusions with imperfect interfaces</b>	
Abstract	18
3.1 Introduction	18
3.2 Derivation of anti-plane dynamic Green's function for Helmholtz problems with imperfect circular boundaries	19
3.2.1 Problem statement and null-field integral formulation	19
3.2.2 Expansions of kernel function and boundary density	21
3.3 Series representation for the Green's function of an inclusion case	22
3.4 Illustrative examples and discussions	24
3.5 Conclusions	26
<b>Chapter 4 Conclusions and further research</b>	27
4.1 Conclusions	27
4.2 Further research	29
<b>References</b>	30
<b>Appendix</b>	
Appendix 1 Special cases	38
Appendix 2 Derivation of the static solution by using the limiting process ( $k \rightarrow 0$ )	43
Appendix 3 Special cases of $\beta \rightarrow \infty$ and $\beta = 0$	48

## Table captions

Table 1-1	Bibliographic database search based on the Web of Science	51
Table 2-1	Comparisons of the BIE between the conventional BIEM and the present method	52
Table 2-2	Comparison of the numerical results	53
Table 3-1	Series-form & closed-form solutions for the static case (ideally bonded interface)	54
Table 3-2	Stress contours of $\sigma_{zx}$ and $\sigma_{zy}$ for the static and dynamic solutions (a concentrated force in the matrix)	55
Table 3-3	Stress contours of $\sigma_{zx}$ and $\sigma_{zy}$ for the static and dynamic solutions (a concentrated force in the inclusion)	56

## Figure captions

Figure 1-1	A brief history of the BEM	57
Figure 1-2 (a)	Bump contour	58
Figure 1-2 (b)	Limiting process	58
Figure 1-3	The boundary value problems with arbitrary boundaries	59
Figure 1-4	Mesh generation	60
Figure 1-5	Convergence test	61
Figure 1-6	Boundary-layer effect analysis	62
Figure 1-7	The frame of the thesis	63
Figure 2-1	Problem statement	64
Figure 2-2 (a)	Sketch of the null-field integral equation in conjunction with the adaptive observer system	65
Figure 2-2 (b)	Sketch of the boundary integral equation for the domain point in conjunction with the adaptive observer system	65
Figure 2-3	Vector decomposition for the potential gradient in the hypersingular equation (collocation point $x$ integration on $B_j$ )	66
Figure 2-4	Decomposition of the inclusion problem using the subdomain approach by taking free body	67
Figure 2-5 (a)	Green's function for the eccentric ring	68
Figure 2-5 (b)	Potential contour using the Melnikov's method	69
Figure 2-5 (c)	Potential contour using the present method (M=50)	69
Figure 2-6 (a)	Green's function for the half-plane with an aperture	70
Figure 2-6 (b)	Potential contour using the Melnikov's method	71
Figure 2-6 (c)	Potential contour using the present method (M=50)	71
Figure 2-7 (a)	Green's function for the half-plane problem with the Robin boundary condition	72
Figure 2-7 (b)	Potential contour by using the Melnikov's approach	73
Figure 2-7 (c)	Potential contour by using the null-field integral equation approach (M=50)	73
Figure 2-8 (a)	Problem sketch of half-plane problem with a circular hole and a semi-circular inclusion	74

Figure 2-8 (b)	Potential contour by using the Melnikov's method approach	75
Figure 2-8 (c)	Potential contour by using the null-field integral equation approach (M=50)	75
Figure 3-1 (a)	An infinite matrix containing a circular inclusion with a concentrated force at $\xi$ in the matrix	76
Figure 3-1 (b)	An infinite matrix containing a circular inclusion with a concentrated force at $\xi$ in the inclusion	76
Figure 3-1 (c)	An infinite matrix containing a circular inclusion with a concentrated force at $\xi$ in the matrix (take free body)	77
Figure 3-2 (a)	Distribution of $\sigma_{zr}^*$ for the dynamic ( $k_M a = 0.01$ ) solution along the circular boundary (Wang and Sudak's solution)	78
Figure 3-2 (b)	Distribution of $\sigma_{zr}^*$ for the dynamic ( $k_M a = 0.01$ ) solution along the circular boundary by using the present solution	78
Figure 3-3 (a)	Parameter study of $\lambda = a\beta / \mu_M$ for the stress response (Wang and Sudak's solution)	79
Figure 3-3 (b)	Parameter study of $\lambda = a\beta / \mu_M$ for the stress response by using the present solution	79
Figure 3-4 (a)	Test of convergence for the Fourier series with a concentrated force in the matrix (real part)	80
Figure 3-4 (b)	Test of convergence for the Fourier series with a concentrated force in the matrix (imaginary part)	80
Figure 3-5 (a)	The distribution of displacement $u_I^*$ along the circular boundary (Wang and Sudak's solution)	81
Figure 3-5 (b)	The distribution of displacement $u_I^*$ along the circular boundary by using the present solution	81
Figure 3-6	Distribution of $\sigma_{zr}^*$ for the dynamic ( $k_M a = 0.01$ ) solution along the circular boundary ( $e = 0.9a$ )	82
Figure 3-7	Parameter study of $\lambda = a\beta / \mu_M$ for the stress response ( $e = 0.9a$ )	82
Figure 3-8	The distribution of displacement $u_I^*$ along the circular boundary for the case of $\lambda = 1$ ( $k_M a = 1, 2, 3, 4, 5$ ) ( $e = 0.9a$ )	83
Figure 3-9	An infinite matrix containing two circular inclusions with a concentrated force at $\xi$ in the matrix	84

Figure 3-10	Distribution of $\sigma_{zr}^*$ of the matrix at the position of $(a_1, \pi)$ various $d$	85
Figure 3-11	The contour of the displacement for an infinite matrix containing two inclusions with a concentrated force at $\xi$ in the matrix	85
Figure 3-12	The absolute amplitude of displacement for an ideally bonded case	86
Figure 3-13	The absolute amplitude of displacement for $\beta = 10^{32}$	86
Figure 3-14	A matrix with a debonded inclusion	87
Figure 3-15	The absolute amplitude of displacement for the cavity	88
Figure 3-16	The absolute amplitude of displacement for $\beta = 10^{-32}$	88

## Notations

$a$	radius of a circular aperture
$a_n, b_n$	Fourier coefficients of boundary density $G(s, \xi)$
$B$	boundary
$C.P.V.$	Cauchy principal value
$D$	domain of interest
$D^c$	complementary domain
$d$	distance between the circles
$G(x, \xi)$	Green's function
$H_0^{(1)}(\cdot)$	Zerth order Hankel function of the first kind
$J_n(\cdot)$	the $n$ th order Bessel function of the first kind
$J'_n(\cdot)$	the derivative of $J_n(\cdot)$
$k$	wave number
$L(s, x)$	kernel function in the hypersingular formulation
$L^i(s, x)$	degenerate kernel function of $L(s, x)$ for $R > \rho$
$L^e(s, x)$	degenerate kernel function of $L(s, x)$ for $\rho > R$
$M$	truncated terms of Fourier series
$M(s, x)$	kernel function in the hypersingular formulation
$M^i(s, x)$	degenerate kernel function of $M(s, x)$ for $R \geq \rho$
$M^e(s, x)$	degenerate kernel function of $M(s, x)$ for $\rho > R$
$N$	number of the circles
$n$	normal vector
$n_s$	normal vector at the source point $s$
$n_x$	normal vector at the field point $x$
$R$	radius of the outer boundary
$R.P.V.$	Riemann principal value
$s$	source point
$T(s, x)$	kernel function in the singular formulation
$T^i(s, x)$	degenerate kernel function of $T(s, x)$ for $R > \rho$
$T^e(s, x)$	degenerate kernel function of $T(s, x)$ for $\rho > R$
$t(s)$	normal derivative of $u(s)$ at $s$
$t(x)$	normal derivative of $u(x)$ at $x$
$t^I$	normal derivative of $u^I$
$t^M$	normal derivative of $u^M$
$U(s, x)$	kernel function in the singular formulation

$U^i(s, x)$	degenerate kernel function of $U(s, x)$ for $R \geq \rho$
$U^e(s, x)$	degenerate kernel function of $U(s, x)$ for $\rho > R$
$u(s)$	potential function on the source point $s$
$u(x)$	potential function on the field point $x$
$u^I$	Fourier coefficients of boundary densities for the inclusion
$u^M$	Fourier coefficients of boundary densities for the matrix
$x$	field point
$Y_n(\cdot)$	the $n$ th order Bessel function of the second kind
$Y'_n(\cdot)$	the derivative of $Y_n(\cdot)$
$\beta$	the imperfect interface parameter
$\omega$	the circular frequency
$\mu$	shear modulus
$\lambda$	material conductivity
$p_n, q_n$	Fourier coefficients for the boundary density of $\partial G(s, \xi) / \partial n_s$
$r$	distance between the source point $s$ and the field point $x$ , $r \equiv  x - s $
$[\mathbf{U}]$	influence matrix of the kernel function $U(s, x)$
$\{\mathbf{u}\}$	vector of Fourier coefficients $\{a_0 \ a_1 \ b_1 \ \cdots \ a_M \ b_M\}^T$
$[\mathbf{T}]$	influence matrix of the kernel function $T(s, x)$
$\{\mathbf{t}\}$	vector of Fourier coefficients $\{p_0 \ p_1 \ q_1 \ \cdots \ p_M \ q_M\}^T$
$(x_k, y_k)$	boundary point for the $k$ th circle
$\delta(x - s)$	Dirac-delta function
$[\boldsymbol{\mu}]$	diagonal matrix of shear modulus
$\xi, \xi'$	location of a concentrated source and image source of Green's function
$\theta$	polar angle measured with respect to $x_1$ direction
$(R, \theta)$	polar coordinate of $s$
$(\rho, \phi)$	polar coordinate of $x$
$\nabla^2$	Laplacian operator
“ $I$ ”	index of inclusion
“ $M$ ”	index of matrix

## Abstract

In this thesis, we derive the Green's function for Laplace and Helmholtz problems with circular apertures and/or inclusions subjected to the Dirichlet, Neumann, mixed and imperfect-interface boundary conditions by using the null-field integral equation approach in conjunction with degenerate kernels, Fourier series and the adaptive observer system. After exactly collocating points on each real circular boundary to satisfy the boundary conditions, a linear algebraic system is obtained. Then unknown coefficients can be easily determined. Five advantages: (1) mesh-free generation (2) well-posed model, (3) principal value free (4) elimination of boundary-layer effect (5) exponential convergence, are achieved. Finally, several examples, including the eccentric case, half-plane Laplace problems with circular apertures and inclusions, and anti-plane dynamic Green's function for several circular inclusions problems, were demonstrated to see the validity of the present formulation and match well with available solutions in the literature. Besides, parameter study of wave number and interface constant is done. Special cases of cavity and ideal bonding are also examined. A general-purpose program for deriving the Green's function of Laplace or Helmholtz problems with arbitrary number of circular apertures and/or inclusions of arbitrary radii and various positions involving the Dirichlet or the Neumann or mixed boundary condition was developed.

**Keyword:** degenerate kernel, Fourier series, null-field approach, inclusion, anti-plane, Green's function, imperfect, Laplace or Helmholtz problems, imperfect-interface

## 中文摘要

本文係使用零場積分方程搭配分離核函數、傅立葉級數與自適性座標系統推導含圓孔洞和/或置入物 Dirichlet、Neumann、混合型或非理想界面邊界條件之格林函數。然後經由佈點於每個真實圓邊界上，在滿足邊界條件後可由所得的線性代數系統輕易地解出未知係數。此方法有五大優勢 (1) 無需網格；(2) 良態模式；(3) 無需主值計算；(4) 無邊界層效應；(5) 指數收斂。最後，偏心圓、半平面含多個置入物之靜、動力格林函數被用來驗證此方法的正確性。靜力格林函數與單置入物之動力格林函數分別和 Melnikov 與 Wang 及 Sudak 結果比較，獲得滿意的結果。除此之外，界面常數與波數的參數也進行探討。其中圓孔洞和理想界面亦可視為本文的特例。我們並發展一套程式可求解含任意數目、不同大小與位置的圓孔洞和/或置入物 Dirichlet、Neumann、混合型邊界條件之拉普拉斯或赫姆茲方程的格林函數。

**關鍵字：**分離核函數、傅立葉級數、零場積分方程、置入物、反平面、格林函數、拉普拉斯或赫姆茲問題、非理想界面。

# Chapter 1 Introduction

## 1.1 Overview of BEM and motivation

For many problems involving complicated geometry shape, initial condition or boundary condition, numerical solutions are generally required in engineering applications. Researchers and scholars mainly proposed several numerical methods as shown in the Table 1-1, e.g., boundary element method (BEM), finite element method (FEM), finite difference method (FDM). FDM approximates the derivatives in the differential equations which govern each problem using some types of truncated Taylor expansion and thus express them in terms of the values at a number of discrete mesh points. FDM has main difficulties of the technique in the consideration of curved geometries and the application of boundary condition. For the case of general boundaries, the regular finite difference grid is unable to accurately reproduce the geometry of the problem. In the past decade, FEM has been widely applied to carry out many engineering problems. FEM utilizes a weighted residual method of the minimum potential energy theorem. The disadvantages of FEM are inconvenient in modeling infinite regions, moving boundary problems, concentrated load and dealing with quantities of data, especially for three-dimensional problems. BEM was developed as a response to the above difficulties. The method requires only discretization of the boundary thus reducing the quantity of data in numerical implementation. BEM is suitable for the general boundaries regardless of the dimensionality of the problem. Because of the problem formulation in terms of fundamental solutions, discontinuities and singularities can be modeled without special difficulties. There are also no difficulty for free and moving boundaries. Another important advantage of the method is that it can deal with problems extending to infinity without having to truncate the domain at a finite distance. The integral equation was introduced by Fredholm in 1903. The origin of the boundary element method can be traced to the work carried out by some groups of researchers in the 1960's on the applications of boundary integral equations to potential flow and stress analysis problems. In the 1960 period, the BEM was utilized to solve 2-D elasticity by Rizzo [Rizzo (1967)] and 2-D elastodynamics problem by Cruse and

Rizzo [Cruse and Rizzo (1968)], respectively. In 1978, the first book on boundary elements in its title was published [Brebbia (1978)], and the first international conference on the topic was organized. From 1978 to 1986, the mathematical foundation of BEM is the singular integral equation with Cauchy kernel. In order to solve the boundary value problem with degenerate boundaries, Hong and Chen [Hong and Chen (1988)] introduced the dual BEM with hypersingularity. Another breakthrough of BEM is the introduction of degenerate kernels which makes fast multipole BEM possible. A brief history of BEM is shown in Figure 1-1. Although the study of BEM has been popular for solving engineering problems, five critical issues are of concern.

### **(1) Treatment of weak, strong and hypersingular singularity**

Singularity of BEM appears when the source and response points coincide. One way is to face the singularity. First, Guiggiani [Guiggiani (1995)] has derived the free terms for Laplace and Navier equations using differential geometry and bump contour approach in Figure 1-2(a). Second, Gray and Manne [Gray and Manne (1993)] have employed a limiting process to ensure a finite value from an interior point to boundary by using a symbolic software in Figure 1-2(b). On the other hand, many scholars proposed several skills to regularize singularity. Achenbach *et al.* [Achenbach, Kechter and Xu (1988)] proposed the off-boundary approach in order to overcome the fictitious frequencies free of singularity and Waterman used null-field approach to deal with the singularity. Although, fictitious BEM or null-field approach can avoid the singularity, but they result in an ill-posed matrix which will be elaborated on later.

### **(2) Ill-posed model**

In order to avoid directly calculating the singular and hypersingular integrals, two approaches, null-field approach or fictitious BEM [Achenbach, Kechter and Xu (1988)], have been used. However, they result in an ill-conditioned matrix. The influence matrix is not diagonally dominated and needs preconditioning. To approach the fictitious boundary to the real boundary or to move the null-field point to the real boundary can make the system well-posed. However, singularity occurs. In the thesis, we may wonder whether it is possible to push the null-field

point on the real boundary but free of calculating singularity and hypersingularity. The answer is yes. Instead of determining the singular (hypersingular) integrals using the definition of CPV (HPV), the kernel function is described in an analytical form for interior and exterior potentials by employing the separable technique since the double-layer potential is discontinuous behavior when across the boundary. Therefore, degenerate kernels, namely separable kernels, are employed to represent the potential of the perforated domain which satisfies the governing equation.

### **(3) Boundary-layer effect**

Boundary-layer effect in BEM occurs when the collocation point approaches near the boundary. Kisu and Kawahara [Kisu and Kawahara (1988)] proposed a concept of relative quantity to eliminate the boundary-layer effect. Chen and Hong in Taiwan [Chen and Hong (1994)] as well as Chen et al. in China [Chen, Lu and Schnack (2001)] independently extended the idea of relative quantity to two regularization techniques which the boundary densities are subtracted by constant and linear terms. For the stress calculation, Sladek et al. [Sladek and Sladek (1991)] used a regularized version of the stress boundary integral equation ( $\sigma$  BEM) to compute the correct values of stresses close to the boundary. Others proposed a regularization of the integrand by using variable transformations. For example, Telles [Telles (1987)] used a cubic transformation such that its Jacobian is minimum at the point on the boundary close to the collocation point and can smooth the integrand. Similarly, Huang and Cruse [Huang and Cruse (1993)] proposed rational transformations which regularized the nearly singular integrals. We concern how to develop a BIEM formulation free of boundaries-layer effect.

### **(4) Convergence rate**

How to speed up the convergence rate is an important issue for numerical methods. The different boundary shape has different interpolation function for boundary densities. Fourier series for circular boundary, spherical harmonic function for surface of sphere, Methieu function for the boundary densities of elliptic boundaries and Legendre polynomials for the boundary densities on the regular and degenerate straight boundaries were incorporated into BEM,

respectively. Regarding to constant, linear and quadratic elements, the discretization scheme does not take the special geometry into consideration. It results in the slow convergence rate about these geometry. Figure 1-3 shows randomly distributed apertures and/or inclusions with square, elliptic and circular shapes, etc. Bird and Steele [Bird (1992); Bird and Steele (1991); Bird and Steele (1992)] presented a Fourier series procedure to solve circular plate problems containing multiple circular apertures in a similar way of Trefftz method by adopting the interior and exterior T-complete sets. The T-complete function can be found in the degenerate kernels of fundamental solution [Chen, Wu, Lee and Chen (2007)]. Barone and Caulk [Barone and Caulk (1981, 1982, 1985, 2000); Caulk (1983, 1983, 1983, 1984)] have solved the boundary potential and its normal derivative of Laplace problem by using Fourier series on each aperture in two-dimensional region with circular apertures by using the special boundary integral equations. Crouch and Mogilevskaya [Crouch and Mogilevskaya (2003)] utilized Somigliana's formula and Fourier series for elasticity problems with circular boundaries. Mogilevskaya and Crouch [Mogilevskaya and Crouch (2001)] have solved the problem of an infinite plane containing arbitrary number of circular inclusions based on the complex singular integral equation. In their analysis procedure, the unknown tractions are approximated by using complex Fourier series. However, for calculating an integral over a circular boundary, they didn't express the fundamental solution using the local polar coordinate. However, they didn't employ the null-field integral equation and degenerate kernels to fully capture the circular boundary, although they all employed Fourier series expansion. Kress has proved that the exponential convergence instead of the algebraic convergence in the BEM can be achieved by using the degenerate kernels and Fourier expansion [Kress (1989)]. This thesis will take advantage of this higher rate of exponential convergence to derive the Green's function for problems with circular boundaries by using Fourier series in conjunction with degenerate kernels.

##### **(5) Mesh generation**

Although BEM is free of domain discretization, boundary mesh generation is also

required since collocation point is on the boundary. We introduce the generalized Fourier coefficients for problems with circular boundaries. In Figure 1-4, domain type methods, FEM and FDM, have been widely used to solve the engineering problem. Boundary type methods, BEM, MFS and Trefftz method have received more attention in the recent years. In analogy of clinical medicine, FEM behaves like operation, BEM is similar to diagnosis by feeling the pulse and boundary collocation method behaves like acupuncture and moxibustion [Chen and Lee (2007)].

In this thesis, we focus on the Green's function for problems with circular apertures and/or inclusions since the fundamental solutions can be expanded into separable forms in the polar coordinate. Chen and Weng [Chen and Weng (2001)] have introduced the conformal mapping with a Laurent series expansion to analyze the Saint-Venant torsion of a circular compound bar with an imperfect interface. Lebedev et al. [Lebedev, Skalskaya and Uflyand (1979)] solved the problem by using the bipolar coordinate. Recently, Honein et al. [Honein, Honein and Herrmann (1992)] have investigated the harmonic problem with two circular inclusions by using the Mobius transformation. To fully capture the geometry of circular boundary, the fundamental solution and boundary densities are expanded into the degenerate form and Fourier series in the polar coordinate, respectively. Five advantages are obtained, (1) singularity free, (2) boundary-layer effect free, (3) exponential convergence, (4) well-posed model, (5) mesh-free generation. In the recent three years, Chen [Chen (2005)] and his coworkers applied the null-field integral formulation, Fourier series and degenerate kernels to solve Laplace [Chen, Shen and Wu (2005); Chen, Shen and Chen (2006); Chen and Wu (2006); Chen and Wu (2007); Shen, Chen and Chen (2005)], Helmholtz [Chen (2005); Chen, Chen and Chen (2005); Chen, Chen and Chen (2005)], biHelmholtz and biharmonic [Chen, Hsiao and Leu (2006)] problems with circular apertures. Exponential convergence by using their methods was achieved as demonstrated by Hsiao [Hsiao (2005)] in Figure 1-5. Then, Chen and Wu have developed this approach to solve inclusion problems in their theses. The boundary-layer effect is eliminated by using the null-field integral equation. A demonstration to eliminate the boundary-layer effect is shown in Figure 1-6 which

was done by Wu [Wu (2006)]. In mathematics, Green's function is important to solve the ordinary and partial differential equations [Kellogg (1953); Bergman and Schiffer (1953); Morse and Fechbach (1953); Courant and Hilbert (1962); Melnikov (1977); Roach (1982)]. Analytical Green's function have been presented for only a few simple configurations, Boley [Boley (1956)] analytically constructed the Green's function by using the successive approximation. Adewale [Adewale (2006)] proposed an analytical solution for an annular plate subjected to a concentrated load. Numerical Green's function has received attention by many researchers [Telles, Castor and Guimaraes (1995); Guimaraes and Telles (2000); Ang and Telles (2004)]. Melnikov [Melnikov (1982, 1995); Melnikov and Melnikov (2001)] utilized the method of modified potentials (MMP) to solve boundary value problems from various areas of computational mechanics. Later, Melnikov [Melnikov and Melnikov (2006)] studied in computing Green's functions and matrices of Green's type for mixed boundary value problems stated on 2-D regions of irregular configuration. For the different field problems, dynamic Green's functions for time-harmonic problems [Kitahara (1985); Denda, Wang and Yong (2003); Denda, Araki and Yong (2004)], piezoelectricity problems [Wang and Zhong (2003); Chen and Wu (2006)], and scattering problems in elastodynamics [Willis (1980a, b); Talbot and Willis (1983)] have been solved by using BEM. Following the experiences of previous investigators and the success of Chen's group using null field integral formulation, the null-field approach will be extended to derive Green's function for Laplace and Helmholtz equations with multiple circular apertures and/or inclusions subjected to the Dirichlet, Neumann, mixed and imperfect interface boundary conditions, respectively. We will revisit the dynamic Green's function for the imperfect interface by Wang and Sudak [Wang and Sudak (2007)].

## **1.2 Organization of the thesis**

The frame of the thesis is shown in Figure 1-7. In this thesis, the null-field integral equations in conjunction with degenerate kernels and Fourier series, namely the null-field integral equation approach, are utilized to derive the Green's function with circular apertures and/or inclusions. The organization of each chapter is summarized

below:

In the chapter 2, we introduce the formulation of null-field integral equation and construct the Green's function of Laplace problems. To fully utilize the geometry of circular boundary, Fourier series for boundary densities, degenerate kernels for fundamental solutions and the adaptive observer system will be incorporated into the null-field integral equation. A linear algebraic system is obtained after collocating points on each circular boundary and satisfying the boundary conditions. The unknown coefficients in the algebraic system can be determined easily. It is straightforward to obtain the field solution by substituting the unknown coefficients to integral equation for domain point. For solving the potential gradient by using the hypersingular equation, vector decomposition should be considered. Furthermore, the derivation of Green's function for 2-D Laplace problem containing circular apertures or inclusions is the main concern. Green's functions for eccentric or half-plane problems with a circular hole as well as an aperture and a semi-circular inclusion are found. The results of eccentric case and half-plane problems with a circular aperture or an aperture and a semi-circular inclusion are compared with those by Melnikov.

In the chapter 3, we focus on the applications in deriving the anti-plane dynamic Green's function of the Helmholtz equation for several circular inclusions with imperfect interfaces. Not only special cases of cavity and ideal bonding but also parameter study of wave number and interface constant are considered. Numerical examples were given to test our programs and some results were compared with those of Wang and Sudak to verify the validity of our formulation.

In the chapter 4, we draw out some conclusions item by item and reveal some further topics.

## **Chapter 2 Construction of Green's function using the null-field integral approach for Laplace problems with circular boundaries**

### **Summary**

A null-field integral approach is employed to derive the Green's function for boundary value problems stated for the Laplace equation with circular boundaries. The kernel function and boundary density are expanded by using the degenerate kernel and Fourier series, respectively. Not only an eccentric ring but also a half-plane problems with a circular aperture subject to Dirichlet or Robin boundary condition are demonstrated to verify the validity of the present approach. Besides, a half-plane problem with a circular aperture as well as a semi-circular inclusion is solved. Good agreement is made after comparing with the Melnikov's results.

### **2.1 Introduction**

Mathematicians as well as engineers have studied Green's function in many fields [Jaswon and Symm (1977); Melnikov (1977)]. But, only a few of simple regions allow a closed-form Green's function for Laplace equation. For example, one aperture or circular sector in half-plane, infinite strip, semi-strip or infinite wedge are mapped by elementary analytic functions, making their Green's function expressed in a closed form. A closed-form Green's function of Laplace equation by using the mapping function becomes impossible for complicated domain except for the annular case. Numerical Green's function has received attention from BEM researchers by Telles et al. [Telles, Castor and Guimaraes (1995); Guimaraes and Telles (2000); Ang and Telles (2004)]. Melnikov [Melnikov (1982), (1995); Melnikov and Melnikov (2001)] utilized the method of modified potentials (MMP) to solve boundary value problems from various areas of computational mechanics. Later, Melnikov [Melnikov and Melnikov (2006)] studied in computing Green's functions and matrices of Green's type for mixed boundary value problems stated on 2-D regions of irregular configuration. For the image method, Thomson [Thomson (1848)] proposed the concept of reciprocal radii to find the image source to satisfy the homogeneous

Dirichlet boundary condition. Chen and Wu [Chen and Wu (2006)] proposed an alternative way to find the location of image through the degenerate kernel. In this chapter, we will construct the Green's function of multiply connected domain by using the null-field integral equation. Green's function for eccentric case and half-plane problems with a circular hole or an aperture as well as a semi-circular inclusion are solved semi-analytically and match well with Melnikov's results.

## 2.2 Formulation of null-field integral equation

The null-field integral equation combining degenerate kernels of the fundamental solution and Fourier series of boundary densities is utilized to solve problems with circular apertures and/or inclusions. An adaptive observer system is addressed to fully employ the property of degenerate kernels for circular boundaries. After exactly collocating points on each real circular boundary to satisfy the boundary conditions, a linear algebraic system is obtained. How to use the hypersingular equation and match of interface conditions is also introduced for multiply-connected problems in this formulation.

### 2.2.1 Dual boundary integral equations and dual null-field integral equations

Considering the problem with  $N$  randomly distributed circular cavities and/or inclusions bounded in the domain  $D$  and enclosed with the boundaries,  $B_k$  ( $k = 0, 1, 2, \dots, N$ ) as shown in Figure 2-1. We define

$$B = \bigcup_{k=0}^N B_k \quad (2-1)$$

In mathematical physics, many engineering problems subjected to the concentrated source satisfy

$$\nabla^2 G(x, \xi) = \delta(x - \xi), \quad x \in D \quad (2-2)$$

where  $G(x, \xi)$  is the Green's function and can be seen as the potential,  $\nabla^2$  indicates the Laplacian operator,  $\delta(x - \xi)$  denotes the Dirac-delta function of source at  $\xi$  and  $D$  is the domain of interest. Based on the dual boundary integral formulation for the domain point, we have

$$2\pi G(x, \xi) = \int_B T(s, x) G(s, \xi) dB(s) - \int_B U(s, x) \frac{\partial G(s, \xi)}{\partial n_s} dB(s) + U(\xi, x) \quad (2-3)$$

,  $x \in D$

$$2\pi \frac{G(x, \xi)}{\partial n_x} = \int_B M(s, x) G(s, \xi) dB(s) - \int_B L(s, x) \frac{\partial G(s, \xi)}{\partial n_s} dB(s) + L(\xi, x) \quad (2-4)$$

,  $x \in D$

where  $s$  and  $x$  are the source and field points, respectively,  $B$  is the boundary,  $n_x$  and  $n_s$  denote the outward normal vector at field point  $x$  and source point  $s$  and the kernel function  $U(s, x) = \ln r$  is the fundamental solution which satisfies

$$\nabla^2 U(s, x) = 2\pi \delta(x - s), \quad (2-5)$$

The other kernel functions,  $T(s, x)$ ,  $L(s, x)$  and  $M(s, x)$ , are defined by

$$T(s, x) \equiv \frac{\partial U(s, x)}{\partial n_s}, \quad L(s, x) \equiv \frac{\partial U(s, x)}{\partial n_x}, \quad M(s, x) \equiv \frac{\partial^2 U(s, x)}{\partial n_s \partial n_x} \quad (2-6)$$

By collocating the field point  $x$  outside the domain (including boundary), the null-field integral equations yield

$$0 = \int_B T(s, x) G(s, \xi) dB(s) - \int_B U(s, x) \frac{\partial G(s, \xi)}{\partial n_s} dB(s) + U(\xi, x), \quad x \in D^c \quad (2-7)$$

$$0 = \int_B M(s, x) G(s, \xi) dB(s) - \int_B L(s, x) \frac{\partial G(s, \xi)}{\partial n_s} dB(s) + L(\xi, x), \quad x \in D^c \quad (2-8)$$

where  $D^c$  is the complementary domain. By using the degenerate kernels, the BIE for the “boundary point” can be easily derived through the null-field integral equation by exactly collocating  $x$  on  $B$  in Eq. (2-7) [Chen, Shen and Chen (2006)]. All the singular integrals disappear in the present formulation since that the potential across the boundary can be explicitly determined in both sides by using degenerate kernels as shown in the Table 2-1. Mathematically speaking, our domain is a closed set  $(D \cup B)$ , instead of the open set ( $D$  only) of the conventional method.

### 2.2.2 Expansion of kernel function and boundary density

Based on the separable property, the kernel function  $U(s, x)$  can be expanded into series form by separating the field point  $x(\rho, \phi)$  and source point  $s(R, \theta)$  in the polar coordinate:

$$U(s, x) = \begin{cases} U^i(R, \theta; \rho, \phi) = \ln R - \sum_{m=1}^{\infty} \frac{1}{m} \left(\frac{\rho}{R}\right)^m \cos m(\theta - \phi), & R \geq \rho \\ U^e(R, \theta; \rho, \phi) = \ln \rho - \sum_{m=1}^{\infty} \frac{1}{m} \left(\frac{R}{\rho}\right)^m \cos m(\theta - \phi), & \rho > R \end{cases} \quad (2-9)$$

It is noted that the leading term and the numerator in the above expansion involve the larger argument to ensure the log singularity and the series convergence, respectively.

According to the definition of  $T(s, x)$  in Eq. (2-6), we have

$$T(s, x) = \begin{cases} T^i(R, \theta; \rho, \phi) = \frac{1}{R} + \sum_{m=1}^{\infty} \left( \frac{\rho^m}{R^{m+1}} \right) \cos m(\theta - \phi), & R > \rho \\ T^e(R, \theta; \rho, \phi) = -\sum_{m=1}^{\infty} \left( \frac{R^m}{\rho^{m+1}} \right) \cos m(\theta - \phi), & \rho > R \end{cases} \quad (2-10)$$

For the higher-order kernel functions,  $L(s, x)$  and  $M(s, x)$  in Eq. (2-6), are shown below:

$$L(s, x) = \begin{cases} L^i(R, \theta; \rho, \phi) = -\sum_{m=1}^{\infty} \left( \frac{\rho^{m-1}}{R^m} \right) \cos m(\theta - \phi), & R > \rho \\ L^e(R, \theta; \rho, \phi) = \frac{1}{\rho} + \sum_{m=1}^{\infty} \left( \frac{R^m}{\rho^{m+1}} \right) \cos m(\theta - \phi), & \rho > R \end{cases} \quad (2-11)$$

$$M(s, x) = \begin{cases} M^i(R, \theta; \rho, \phi) = \sum_{m=1}^{\infty} \left( \frac{m\rho^{m-1}}{R^{m+1}} \right) \cos m(\theta - \phi), & R \geq \rho \\ M^e(R, \theta; \rho, \phi) = \sum_{m=1}^{\infty} \left( \frac{mR^{m-1}}{\rho^{m+1}} \right) \cos m(\theta - \phi), & \rho > R \end{cases} \quad (2-12)$$

The unknown boundary densities can be represented by using the Fourier series as shown below:

$$G(s_j, \xi) = a_0^j + \sum_{n=1}^{\infty} (a_n^j \cos n\theta_j + b_n^j \sin n\theta_j), \quad s_j \in B_j, \quad j = 1, 2, \dots, N \quad (2-13)$$

$$\frac{\partial G(s_j, \xi)}{\partial n_s} = p_0^j + \sum_{n=1}^{\infty} (p_n^j \cos n\theta_j + q_n^j \sin n\theta_j), \quad s_j \in B_j, \quad j = 1, 2, \dots, N \quad (2-14)$$

where  $N$  is the number of circular boundaries. In real computation, the finite  $M$  terms for expansion of kernel and boundary density are adopted.

### 2.2.3 Adaptive observer system

An adaptive observer system is addressed to fully employ the property of degenerate kernels for circular boundaries as shown in Figures 2-2 (a) and (b). For the integration, the origin of the observer system can be adaptively located on the center of the corresponding boundary contour. The dummy variable in the circular boundary integration is the angle  $\theta$  instead of radial coordinate  $R$ . By using the adaptive system, all the integrations can be easily calculated for multiply connected problems.

### 2.2.4 Vector decomposition technique for the potential gradient in the hypersingular equation

Considering the Green's function problem for the nonconcentric case, we solved the potential gradient by employing the hypersingular integral equation in Eq. (2-4). When we collocate the domain point  $x$  on the  $B_i$  circular boundary, but integrate the  $B_j$  circular boundary, the normal derivative of potential for the domain point  $x$  need special treatment. In Figure 2-3 the true normal direction with respect to the collocation point  $x$  on the  $B_i$  boundary can be superimposed by using the radial direction and angular direction on the  $B_j$  boundary. According to the concept of decomposition technique, the degenerate kernels for the higher-order singular equation of Eq. (2-6) are changed as :

$$L(s, x) = \begin{cases} L^i(R, \theta; \rho, \phi) = \frac{\partial U^i(R, \theta; \rho, \phi)}{\partial \rho} \cos(\phi_i - \phi_j) \\ \quad + \frac{1}{\rho} \frac{\partial U^i(R, \theta; \rho, \phi)}{\partial \phi} \cos\left(\frac{\pi}{2} - \phi_i - \phi_j\right), \quad R > \rho \\ L^e(R, \theta; \rho, \phi) = \frac{\partial U^e(R, \theta; \rho, \phi)}{\partial \rho} \cos(\phi_i - \phi_j) \\ \quad + \frac{1}{\rho} \frac{\partial U^e(R, \theta; \rho, \phi)}{\partial \phi} \cos\left(\frac{\pi}{2} - \phi_i - \phi_j\right), \quad \rho > R \end{cases} \quad (2-15)$$

$$M(s, x) = \begin{cases} M^i(R, \theta; \rho, \phi) = \frac{\partial T^i(R, \theta; \rho, \phi)}{\partial \rho} \cos(\phi_i - \phi_j) \\ \quad + \frac{1}{\rho} \frac{\partial T^i(R, \theta; \rho, \phi)}{\partial \phi} \cos\left(\frac{\pi}{2} - \phi_i - \phi_j\right), \quad R > \rho \\ M^e(R, \theta; \rho, \phi) = \frac{\partial T^e(R, \theta; \rho, \phi)}{\partial \rho} \cos(\zeta - \xi) \\ \quad + \frac{1}{\rho} \frac{\partial T^e(R, \theta; \rho, \phi)}{\partial \phi} \cos\left(\frac{\pi}{2} - \phi_i - \phi_j\right), \quad \rho > R \end{cases} \quad (2-16)$$

where  $\phi_i$  and  $\phi_j$  shows the angle of the domain point  $x$  for the  $i$ th and  $j$ th circles, respectively, in the polar coordinate.

### 2.2.5 Linear algebraic equation

By moving the null-field point  $x_i$  to the  $i$ th circular boundary in the limit sense for Eq. (2-7), we have the linear algebraic equation

$$[\mathbf{U}]\{\mathbf{t}\} = [\mathbf{T}]\{\mathbf{u}\} + \{\mathbf{b}\} \quad (2-17)$$

where  $\{\mathbf{b}\}$  is the vector due to the source of Green's function,  $[\mathbf{U}]$  and  $[\mathbf{T}]$  are the influence matrices with a dimension of  $(N+1)(2M+1)$  by  $(N+1)(2M+1)$ ,  $\{\mathbf{u}\}$  and  $\{\mathbf{t}\}$  denote the column vectors of Fourier coefficients with a dimension of  $(N+1)(2M+1)$  by 1 in which  $[\mathbf{U}]$ ,  $[\mathbf{T}]$ ,  $\{\mathbf{u}\}$ ,  $\{\mathbf{t}\}$  and  $\{\mathbf{b}\}$  can be defined as follows:

$$[\mathbf{U}] = \begin{bmatrix} \mathbf{U}_{00} & \mathbf{U}_{01} & \cdots & \mathbf{U}_{0N} \\ \mathbf{U}_{10} & \mathbf{U}_{11} & \cdots & \mathbf{U}_{1N} \\ \vdots & \vdots & \ddots & \vdots \\ \mathbf{U}_{N0} & \mathbf{U}_{N1} & \cdots & \mathbf{U}_{NN} \end{bmatrix}, \quad [\mathbf{T}] = \begin{bmatrix} \mathbf{T}_{00} & \mathbf{T}_{01} & \cdots & \mathbf{T}_{0N} \\ \mathbf{T}_{10} & \mathbf{T}_{11} & \cdots & \mathbf{T}_{1N} \\ \vdots & \vdots & \ddots & \vdots \\ \mathbf{T}_{N0} & \mathbf{T}_{N1} & \cdots & \mathbf{T}_{NN} \end{bmatrix} \quad (2-18)$$

$$\{\mathbf{u}\} = \begin{bmatrix} \mathbf{u}_0 \\ \mathbf{u}_1 \\ \mathbf{u}_2 \\ \vdots \\ \mathbf{u}_N \end{bmatrix}, \quad \{\mathbf{t}\} = \begin{bmatrix} \mathbf{t}_0 \\ \mathbf{t}_1 \\ \mathbf{t}_2 \\ \vdots \\ \mathbf{t}_N \end{bmatrix}, \quad \{\mathbf{b}\} = \begin{bmatrix} \mathbf{b}_0 \\ \mathbf{b}_1 \\ \mathbf{b}_2 \\ \vdots \\ \mathbf{b}_N \end{bmatrix} \quad (2-19)$$

where the vectors  $\{\mathbf{u}_j\}$  and  $\{\mathbf{t}_j\}$  are in the form of  $\{a_0^j \ a_1^j \ b_1^j \ \cdots \ a_M^j \ b_M^j\}^T$  and  $\{p_0^j \ p_1^j \ q_1^j \ \cdots \ p_M^j \ q_M^j\}^T$  respectively; the first subscript “ $i$ ” ( $i = 0, 1, 2, \dots, N$ ) in  $[\mathbf{U}_{ij}]$  and  $[\mathbf{T}_{ij}]$  denotes the index of the  $i$ th circle where the collocation point is located and the second subscript “ $j$ ” ( $j = 0, 1, 2, \dots, N$ ) denotes the index of the  $j$ th circle where boundary data  $\{\mathbf{u}_j\}$  or  $\{\mathbf{t}_j\}$  are specified,  $N$  is the number of circular apertures in the domain and  $M$  indicates the truncated terms of Fourier series. The coefficient matrix of the linear algebraic system is partitioned into blocks, and each off-diagonal block corresponds to the influence matrices between two different circular cavities. The diagonal blocks are the influence matrices due to itself in each individual hole. After uniformly collocating the point along the  $j$ th circular boundary, the submatrix can be written as

$$[\mathbf{U}_{ij}] = \begin{bmatrix} U_{ij}^{0c}(\phi_1) & U_{ij}^{1c}(\phi_1) & U_{ij}^{1s}(\phi_1) & \cdots & U_{ij}^{Mc}(\phi_1) & U_{ij}^{Ms}(\phi_1) \\ U_{ij}^{0c}(\phi_2) & U_{ij}^{1c}(\phi_2) & U_{ij}^{1s}(\phi_2) & \cdots & U_{ij}^{Mc}(\phi_2) & U_{ij}^{Ms}(\phi_2) \\ U_{ij}^{0c}(\phi_3) & U_{ij}^{1c}(\phi_3) & U_{ij}^{1s}(\phi_3) & \cdots & U_{ij}^{Mc}(\phi_3) & U_{ij}^{Ms}(\phi_3) \\ \vdots & \vdots & \vdots & \ddots & \vdots & \vdots \\ U_{ij}^{0c}(\phi_{2M}) & U_{ij}^{1c}(\phi_{2M}) & U_{ij}^{1s}(\phi_{2M}) & \cdots & U_{ij}^{Mc}(\phi_{2M}) & U_{ij}^{Ms}(\phi_{2M}) \\ U_{ij}^{0c}(\phi_{2M+1}) & U_{ij}^{1c}(\phi_{2M+1}) & U_{ij}^{1s}(\phi_{2M+1}) & \cdots & U_{ij}^{Mc}(\phi_{2M+1}) & U_{ij}^{Ms}(\phi_{2M+1}) \end{bmatrix} \quad (2-20)$$

$$[\mathbf{T}_{ij}] = \begin{bmatrix} T_{ij}^{0c}(\phi_1) & T_{ij}^{1c}(\phi_1) & T_{ij}^{1s}(\phi_1) & \cdots & T_{ij}^{Mc}(\phi_1) & T_{ij}^{Ms}(\phi_1) \\ T_{ij}^{0c}(\phi_2) & T_{ij}^{1c}(\phi_2) & T_{ij}^{1s}(\phi_2) & \cdots & T_{ij}^{Mc}(\phi_2) & T_{ij}^{Ms}(\phi_2) \\ T_{ij}^{0c}(\phi_3) & T_{ij}^{1c}(\phi_3) & T_{ij}^{1s}(\phi_3) & \cdots & T_{ij}^{Mc}(\phi_3) & T_{ij}^{Ms}(\phi_3) \\ \vdots & \vdots & \vdots & \ddots & \vdots & \vdots \\ T_{ij}^{0c}(\phi_{2M}) & T_{ij}^{1c}(\phi_{2M}) & T_{ij}^{1s}(\phi_{2M}) & \cdots & T_{ij}^{Mc}(\phi_{2M}) & T_{ij}^{Ms}(\phi_{2M}) \\ T_{ij}^{0c}(\phi_{2M+1}) & T_{ij}^{1c}(\phi_{2M+1}) & T_{ij}^{1s}(\phi_{2M+1}) & \cdots & T_{ij}^{Mc}(\phi_{2M+1}) & T_{ij}^{Ms}(\phi_{2M+1}) \end{bmatrix} \quad (2-21)$$

$$\{\mathbf{b}_i\} = \begin{bmatrix} \ln|\mathbf{x}(\rho_i, \phi_1) - \xi| \\ \ln|\mathbf{x}(\rho_i, \phi_2) - \xi| \\ \ln|\mathbf{x}(\rho_i, \phi_3) - \xi| \\ \vdots \\ \ln|\mathbf{x}(\rho_i, \phi_{2M+1}) - \xi| \end{bmatrix} \quad (2-22)$$

where  $\phi_i$ ,  $i=1,2,\dots,2M+1$ , are the angles of collocation along the circular boundary. Although both the matrices in Eqs. (2-20) and (2-21) are not sparse, it is found that the higher order harmonics is considered, the lower influence coefficients in numerical experiments is obtained. It is noted that the superscript “0c” in Eqs. (2-20) and (2-21) indicates the first term of Fourier series. The element of  $[\mathbf{U}_{ij}]$  and  $[\mathbf{T}_{ij}]$  are defined respectively as

$$U_{ij}^{nc}(\phi_m) = \int_{B_j} U(s_j, \mathbf{x}_m) \cos(n\theta_j) R_j d\theta_j, \quad (2-23)$$

$$n = 0, 1, 2, \dots, M, \quad m = 1, 2, \dots, 2M+1$$

$$U_{ij}^{ns}(\phi_m) = \int_{B_j} U(s_j, \mathbf{x}_m) \sin(n\theta_j) R_j d\theta_j, \quad (2-24)$$

$$n = 1, 2, \dots, M, \quad m = 1, 2, \dots, 2M+1$$

$$T_{ij}^{nc}(\phi_m) = \int_{B_j} T(s_j, \mathbf{x}_m) \cos(n\theta_j) R_j d\theta_j, \quad (2-25)$$

$$n = 0, 1, 2, \dots, M, \quad m = 1, 2, \dots, 2M+1$$

$$T_{ij}^{ns}(\phi_m) = \int_{B_j} T(s_j, \mathbf{x}_m) \sin(n\theta_j) R_j d\theta_j, \quad (2-26)$$

$$n = 1, 2, \dots, M, \quad m = 1, 2, \dots, 2M+1$$

where  $j$  is no sum,  $s_j = (R_j, \theta_j)$ , and  $\phi_m$  is the polar angle of the collocation

point  $x_m$ . The influence coefficient of  $U_{ij}^{nc}(\phi_m)$  in Eq. (2-23) denotes the response at  $x_m$  due to  $\cos n\theta$  distribution. The direction of contour integration should be taken care, *i.e.*, counterclockwise and clockwise directions are for the interior and exterior problems, respectively. By rearranging the known and unknown sets, the Fourier coefficients can be obtained easily.

## 2.2.6 Matching of interface conditions for problems of apertures and inclusions

Before extending the formulation from aperture to inclusion, subdomain approach by taking free body needs to be used. By decomposing the inclusion problem into two problems, we have two subsystems. One is the problem with apertures and the other is for each single inclusion problem. Figure (2-4) represents the decomposition of the inclusion problem. According to the continuity of displacement and equilibrium of traction along the ideal interface for the subdomain approach, we have the constraints

$$\{u_j^M\} = \{u_j^I\}, \text{ on } B_j \quad (2-27)$$

$$[\mu_M]\{t_j^M\} = -[\mu_I]\{t_j^I\}, \text{ on } B_j \quad (2-28)$$

where  $[\mu_I]$  and  $[\mu_M]$  can be defined as follows:

$$[\mu_I] = \begin{bmatrix} \mu_I & 0 & \cdots & 0 \\ 0 & \mu_I & \cdots & 0 \\ \vdots & \vdots & \ddots & \vdots \\ 0 & 0 & \cdots & \mu_I \end{bmatrix}, \quad [\mu_M] = \begin{bmatrix} \mu_M & 0 & \cdots & 0 \\ 0 & \mu_M & \cdots & 0 \\ \vdots & \vdots & \ddots & \vdots \\ 0 & 0 & \cdots & \mu_M \end{bmatrix}, \quad (2-29)$$

in which  $\mu_I$  and  $\mu_M$  denote the shear modulus of the matrix and the inclusion, respectively. After assembling the null-field integral equations and the interface conditions (displacement continuity and force equilibrium), a global algebraic system can be obtained.

$$\begin{bmatrix} T_j^M & -U_j^M & 0 & 0 \\ 0 & 0 & T_j^I & -U_j^I \\ I & 0 & -I & 0 \\ 0 & \mu_M & 0 & \mu_I \end{bmatrix} \begin{bmatrix} u_j^M \\ t_j^M \\ u_j^I \\ t_j^I \end{bmatrix} = \begin{bmatrix} U_j(x, \xi) \\ 0 \\ 0 \\ 0 \end{bmatrix} \quad (2-30)$$

### 2.2.7 Image technique for solving half-plane problems

The half-plane problem is imbedded to a full-plane problem through the image method. By employing the anti-symmetric property, the boundary condition of half-plane can be satisfied through the image approach. In the real implementation, the full-plane problem is solved, first.

## 2.3 Illustrative examples and discussions

### *Case 1: eccentric ring (semi-analytical solution)*

Figure 2-5(a) depicts the Green's function of the eccentric ring. The source point is located at  $\xi = (0, 0.75)$ . Figures 2-5(b) and 2-5(c) show the potential distribution by using the present method and Melnikov's approach [Melnikov and Melnikov (2001)], respectively. The two radii of inner and outer circles are  $a = 0.4$  and  $b = 1.0$ . The two centers of the inner and outer circles are  $(-0.4, 0)$  and  $(0, 0)$ , respectively. It is noted that outer radius of one is a degenerate scale and needs special treatment as described in detail by Chen and Shen [Chen and Shen (2007)]. Comparison of the present results with MCP and MMP methods [Melnikov and Melnikov (2001)] is shown in the Table 2-2. We can also obtain good data by our method instead of dealing with Green's function  $G(x, \xi)$  by MMP method, beforehand. Good agreement is made.

### *Case 2: a half plane with an aperture (semi-analytical solution)*

Figure 2-6(a) depicts the Green's function for the half plane with a hole. The source point is located at  $\xi = (2, 1)$ . The center and radius of the aperture are  $(0, 3)$  and  $a = 1.0$ . Figures 2-6(b) and 2-6(c) show the potential distribution by using the present method and Melnikov's approach, respectively. Good agreement is made.

### *Case 3: a half-plane problem with a circular boundary subject to the Robin boundary condition.*

A half-plane problem with an aperture is considered. The governing equation and boundary condition are shown in Fig. 2-7(a). The center and radius of the aperture are  $(2, 2)$  and  $a = 1.0$ , respectively. The concentrated source is located at  $(0, 3.5)$ . The Robin boundary condition is  $t = -2u$  imposed on the aperture. Figures 2-7(b) and 2-7(c) show the potential distribution by using the present method and Melnikov's

approach, respectively. Good agreement is obtained.

*Case 4: a half plane problem with a aperture and an inclusion*

A half-plane problem with a circular hole and a half-circular inclusion are considered as composed of two regions  $D_1 = \{0 < r < 1, 0 < \varphi < \pi\}$  and  $D_2 = \{1 < r < \infty, 0 < \varphi < \pi\}$  filled in with different materials ( $\lambda = \lambda_2 / \lambda_1 = 0.1$ ). The governing equation and boundary condition are shown in Fig. 2-8(a). The center and radius of the aperture are  $(r, \varphi; 1.4, \pi/3)$  and  $a_2 = 0.4$ , respectively. The concentrated source is located at  $(r, \varphi; 0.5, \pi/3)$ . Figures 2-8(b) and 2-8(c) show the potential distributions by using the present method and Melnikov's approach, respectively. Good agreement is also made.

## 2.4 Concluding remarks

For the Green's function with circular boundaries, we have proposed a semi-analytical approach to construct the Green's function by using degenerate kernels and Fourier series. Several examples, including the eccentric case and half plane problems with circular apertures and inclusions, were demonstrated to check the validity of the present formulation. Our advantages are five folds: (1) mesh-free generation (2) well-posed model (3) principal value free (4) elimination of boundary-layer effect (5) exponential convergence. A general-purpose program to construct the Green's function for Laplace problems with circular boundaries of arbitrary number, various radius and location was developed. Following the success of Laplace case, we will extend to the Helmholtz equation in the next chapter.

# **Chapter 3 Derivation of anti-plane dynamic Green's function for several circular inclusions with imperfect interfaces**

## **Abstract**

A null-field integral equation is employed to derive the two-dimensional antiplane dynamic Green's functions for a circular inclusion with an imperfect interface. We employ the linear spring model with vanishing thickness to characterize the imperfect interface. Analytical expressions of displacement and stress fields due to time-harmonic antiplane line forces located either in the unbounded matrix or in the circular inclusion are presented. To fully capture the circular geometries, degenerate-kernel expressions of fundamental solutions in the polar coordinate and Fourier series for boundary densities are adopted. Good agreement is made after comparing with the analytical solution derived by Wang and Sudak's results. Parameter study of wave number and interface constant is done. In this chapter, we employ the null-field BIE to derive the analytical Green's function instead of choosing the Trefftz bases by using the Wang and Sudak's approach. Special cases of cavity and ideal bonding as well as static solutions are also examined.

## **3.1 Introduction**

Analytical as well as numerical Green's functions have received many BEM researchers' attention [Ang and Telles (2004)]. Boundary element method (BEM) was employed to solve time-harmonic Green's function [Kitahara (1985); Denda, Wang and Yong (2003); Denda, Araki and Yong (2004)]. Also, dynamic Eshelby problems [Mikata and Nemat-Nasser (1990); Cheng and Batra (1999); Michelitsch, Levin and Gao (2002)], piezoelectricity problems [Chen and Wu (2006); Wang and Zhong (2003)] and scattering problems in elastodynamics [Willis (1980a, b); Talbot and Willis (1983)] were solved. Although a lot of papers on homogenous case were published, only a few of the time-harmonic dynamic Green's functions of a circular cylindrical inclusion can be found [Mura (1988); Mura, Shodja and Hirose (1996)]. Recently, Wang and Sudak [Wang and Sudak (2007)] derived an analytical solution for antiplane time-harmonic Green's functions of a circular inhomogeneity with an

imperfect interface. The interface between the inclusion and the matrix is modeled to the linear springs with vanishing thickness. Interface boundary conditions are tractions equilibrium but the displacements across the interface are discontinuous. In addition, the stress response is proportional to the linear springs interface with vanishing thickness. The key concept of Wang and Sudak's method is that they introduced the Trefftz bases for the solution representation of inclusion and matrix, respectively. However, the completeness of Trefftz bases needs special case. Our main concern is to revisit the problem solved by Wang and Sudak and derive the analytical solution in an alternative way by using the null-field integral equation. Based on the null-field integral formulation, the analytical solution will be derived in a more systematic and straightforward way. Besides, special cases of cavity and ideal bonding as well as static solutions will be examined.

### 3.2 Derivation of anti-plane dynamic Green's function for Helmholtz problems with an imperfect interface

#### 3.2.1 Problem statement and null-field integral formulation

For a two-dimensional problem with an imperfect interface, we consider a unbounded matrix containing a circular inclusion of radius  $a$  with its centre at the origin. A time-harmonic antiplane line force of strength  $pe^{-i\omega t}$  is located at  $(e,0)$  on the  $x$  axis either in the inclusion ( $0 < e < a$ ) or in the matrix ( $a < e$ ) as shown in Figs. 1(a) and 1(b). The  $\mu_M$  and  $\mu_I$  represent the shear moduli of matrix and inclusion, respectively. The anti-plane displacement field subject to the concentrated load in the matrix is shown below

$$(\nabla^2 + k_I^2)G(x, \xi) = -\frac{P}{\mu_I} \delta(x - \xi), \quad x \in D_I \quad \text{if } e < a \quad (3-1)$$

For the infinite matrix with a single inclusion subject to a concentrated load, we have

$$(\nabla^2 + k_M^2)G(x, \xi) = -\frac{P}{\mu_M} \delta(x - \xi), \quad x \in D_M \quad \text{if } e > a \quad (3-2)$$

where  $\nabla^2$  is the Laplacian operator,  $k_I$  and  $k_M$  are the wave numbers for the inclusion and matrix,  $\delta(x - \xi)$  denotes the Dirac-delta function,  $D_I$  and  $D_M$  are domains of the inclusion and matrix, respectively. The time factor  $e^{-i\omega t}$  has been omitted due to the frequency-domain approach after employing the separable property.

For a linear elastic body, the stress components are

$$\sigma_{zr}^I = \mu_I \frac{\partial u_I}{\partial r}, \sigma_{z\theta}^I = \frac{\mu_I}{r} \frac{\partial u_I}{\partial \theta}, \quad x \in D_I \quad (3-3)$$

$$\sigma_{zr}^M = \mu_M \frac{\partial u_M}{\partial r}, \sigma_{z\theta}^M = \frac{\mu_M}{r} \frac{\partial u_M}{\partial \theta}, \quad x \in D_M \quad (3-4)$$

Moreover, we presume that the circular boundary interface is imperfect and homogeneous in the angular direction. The interface boundary conditions are given by [Hashin (1991); Ru and Schiavone (1997); Wang and Meguid (1999)].

$$\sigma_{zr}^I = \sigma_{zr}^M = \beta(u_M - u_I), \text{ on the interface } r = a \quad (3-5)$$

where the non-negative constant  $\beta$  is the parameter of imperfect interface. The circular inclusion is perfectly bonded to the matrix if  $\beta$  approaches infinity. On the other hand, the circular inclusion is fully debonded from the matrix if  $\beta$  approaches zero. In order to employ the Green's third identity as follows

$$\iint_D [u(x)\nabla^2 v(x) - v(x)\nabla^2 u(x)]dD(x) = \int_B [(u(x)\frac{\partial v(x)}{\partial n} - v(x)\frac{\partial u(x)}{\partial n})]dB(x) \quad (3-6)$$

we need two systems,  $u(x)$  and  $v(x)$ . We choose  $u(x)$  as  $G(x, \xi)$  and set  $v(x)$  as the fundamental solution  $U(x, s)$  such that

$$\nabla^2 U(x, s) = 2\pi\delta(x - s) \quad (3-7)$$

Then, we can obtain the fundamental solution as follows

$$U(s, x) = \frac{-i\pi H_0^{(1)}(kr)}{2} \quad (3-8)$$

where  $H_0^{(1)}(kr)$  is the zeroth Hankel function of the first kind and  $r \equiv |s-x|$ . In the present method, we adopt the mathematical tools, degenerate kernels, for the purpose of analytical study. The combination of degenerate kernels and Fourier series plays the major role in handling problems with circular boundaries. Based on the separable property, the kernel function  $U(s, x)$  and  $T(s, x)$  can be expanded into separable form by dividing the source point  $s = (R, \theta)$  and field point  $x = (\rho, \phi)$  in the polar coordinate [Chen, Liu and Hong (2003)]. After exchanging with the variables  $x$  and  $s$ , we have

$$2\pi G(x, \xi) = \int_B T(s, x)G(s, \xi)dB(s) - \int_B U(s, x)\frac{\partial G(s, \xi)}{\partial n_s}dB(s) + U(\xi, x) \quad (3-9)$$

,  $x \in D$

where  $T(s, x)$  is defined by

$$T(s, x) \equiv \frac{\partial U(s, x)}{\partial n_s} \quad (3-10)$$

where  $n_s$  denotes the outward normal vector at the source point  $s$ . To solve the unknown boundary densities  $G(s, \xi)$  and  $\partial G / \partial n_s(s, \xi)$ , the field point  $x$  is located outside the domain to yield the null-field integral equation as shown below:

$$0 = \int_B T(s, x) G(s, \xi) dB(s) - \int_B U(s, x) \frac{\partial G(s, \xi)}{\partial n_s} dB(s) + U(\xi, x), \quad x \in D^c \quad (3-11)$$

where  $D^c$  is the complementary domain. By using the degenerate kernels, the BIE for the “boundary point” can be easily derived through either the null-field integral equation in Eq. (3-11) or the BIE for the domain point of Eq. (3-9) by exactly collocating  $x$  on  $B$  [Chen, Shen and Chen (2006)].

### 3.2.2 Expansions of kernel function and boundary density

Based on the separable property, the kernel function  $U(s, x)$  can be expanded into series form by separating the field point  $x(\rho, \phi)$  and source point  $s(R, \theta)$  in the polar coordinate:

$$U(s, x) = \begin{cases} U^i(s, x) = \frac{-\pi i}{2} \sum_{m=0}^{\infty} \varepsilon_m J_m(k\rho) H_m^{(1)}(kR) \cos(m(\theta - \phi)), & R \geq \rho \\ U^e(s, x) = \frac{-\pi i}{2} \sum_{m=0}^{\infty} \varepsilon_m H_m^{(1)}(k\rho) J_m(kR) \cos(m(\theta - \phi)), & \rho > R \end{cases} \quad (3-12)$$

where the superscripts “ $i$ ” and “ $e$ ” denote the interior and exterior cases for the expressions of kernel, respectively, and  $\varepsilon_m$  is the Neumann factor

$$\varepsilon_m = \begin{cases} 1, & m = 0 \\ 2, & m = 1, 2, \dots, \infty \end{cases} \quad (3-13)$$

It is noted that the larger argument is contained in the complex Hankel function to ensure the series convergence and log singularity. According to the definition of  $T(s, x)$  in Eq. (3-10), we have

$$T(s, x) = \begin{cases} T^i(s, x) = \frac{-\pi k i}{2} \sum_{m=0}^{\infty} \varepsilon_m J_m(k\rho) H_m'^{(1)}(kR) \cos(m(\theta - \phi)), & R > \rho \\ T^e(s, x) = \frac{-\pi k i}{2} \sum_{m=0}^{\infty} \varepsilon_m H_m^{(1)}(k\rho) J_m'(kR) \cos(m(\theta - \phi)), & \rho > R \end{cases} \quad (3-14)$$

The unknown boundary densities can be represented by using the Fourier series as shown below:

$$G(s, \xi) = a_0 + \sum_{n=1}^{\infty} (a_n \cos n\theta + b_n \sin n\theta), \quad s \in B \quad (3-15)$$

$$\frac{\partial G(s, \xi)}{\partial n_s} = p_0 + \sum_{n=1}^{\infty} (p_n \cos n\theta + q_n \sin n\theta), \quad s \in B \quad (3-16)$$

where  $a_0$ ,  $a_n$ ,  $b_n$ ,  $p_0$ ,  $p_n$  and  $q_n$  are the Fourier coefficients. In the real computation, the boundary integrations can be easily calculated by employing the orthogonal property of Fourier series, and only the finite  $M$  terms are used in the summation.

### 3.3 Series representation for the Green's function of an inclusion case

For the problems with inclusion, we can decompose into subsystems of matrix and inclusion after taking the free body on the interface as shown in Fig. 3-1(c). By collocating  $x$  on  $(a^-, \phi)$  and  $(a^+, \phi)$  for matrix and inclusion, respectively, the null-field equations yield

$$\begin{aligned} 0 = & -a_0^e k_M \pi^2 a J_0(k_M a) [Y_0'(k_M a) - iJ_0'(k_M a)] - \sum_{m=1}^{\infty} [a_m^e \cos(m\phi) + b_m^e \sin(m\phi)] \\ & k_M \pi^2 a J_m'(k_M a) [Y_m'(k_M a) - iJ_m'(k_M a)] - p_0^e \pi^2 a J_0(k_M a) [Y_0(k_M a) - iJ_0(k_M a)] \\ & - \sum_{m=1}^{\infty} [p_m^e \cos(m\phi) + q_m^e \sin(m\phi)] \pi^2 a J_m(k_M a) [Y_m(k_M a) - iJ_m(k_M a)] \\ & - \frac{P}{\mu_M} \left\{ \frac{\pi}{2} J_0(k_M a) [Y_0(k_M a) - iJ_0(k_M a)] \right. \\ & \left. + \sum_{m=1}^{\infty} \pi J_m(k_M a) [Y_m(k_M a) - iJ_m(k_M a)] \cos(m\phi) \right\} \\ & , \quad x \rightarrow (a^-, \phi) \end{aligned} \quad (3-17)$$

$$\begin{aligned} 0 = & a_0^i k_I \pi^2 a J_0'(k_I a) [Y_0(k_I a) - iJ_0(k_I a)] + \sum_{m=1}^{\infty} [a_m^i \cos(m\phi) + b_m^i \sin(m\phi)] \\ & k_I \pi^2 a J_m'(k_I a) [Y_m(k_I a) - iJ_m(k_I a)] - p_0^i \pi^2 a J_0(k_I a) [Y_0(k_I a) - iJ_0(k_I a)] \\ & - \sum_{m=1}^{\infty} [p_m^i \cos(m\phi) + q_m^i \sin(m\phi)] \pi^2 a J_m(k_I a) [Y_m(k_I a) - iJ_m(k_I a)] \\ & , \quad x \rightarrow (a^+, \phi) \end{aligned} \quad (3-18)$$

Interface conditions of Eq. (3-5) can be rewritten as

$$t^I = \frac{\beta}{\mu_I} (u^M - u^I), \quad \text{on the interface} \quad (3-19)$$

$$-\mu_M t^M = \mu_I t^I, \quad \text{on the interface} \quad (3-20)$$

By assembling the matrices in Eqs. (3-17), (3-18), (3-19) and (3-20), we have

$$\begin{bmatrix} T_{11}^M & -U_{11}^M & 0 & 0 \\ 0 & 0 & T_{11}^I & -U_{11}^I \\ 0 & \mu_M & 0 & \mu_I \\ \beta & \mu_M & -\beta & 0 \end{bmatrix} \begin{bmatrix} u_1^M \\ t_1^M \\ u_1^I \\ t_1^I \end{bmatrix} = \begin{bmatrix} \frac{p}{\mu_M} U(\xi, x) \\ 0 \\ 0 \\ 0 \end{bmatrix} \quad (3-21)$$

After rearranging Eq. (3-21), we have

$$\begin{bmatrix} T_{11}^M & -U_{11}^M \\ T_{11}^I & \frac{\mu_M}{\beta} T_{11}^I + \frac{\mu_M}{\mu_I} U_{11}^I \end{bmatrix} \begin{bmatrix} u_1^M \\ t_1^M \end{bmatrix} = \begin{bmatrix} \frac{p}{\mu_M} U(\xi, x) \\ 0 \end{bmatrix} \quad (3-22)$$

The unknown coefficients in the algebraic system can be analytically determined as shown below

$$\begin{aligned} a_0^e &= -p[J_0(k_M e) + iY_0(k_M e)][\beta J_0(k_I a) + k_I \mu_I J_0'(k_I a)] \\ &\quad / 2\pi a \{k_I \mu_I J_0'(k_I a)[- \beta [J_0(k_M a) + iY_0(k_M a)] \\ &\quad + k_M \mu_M [J_0'(k_M a) + iY_0'(k_M a)]] + \beta k_M \mu_M J_0(k_I a) \\ &\quad [J_0'(k_M a) + iY_0'(k_M a)]\} \end{aligned} \quad (3-23)$$

$$\begin{aligned} p_0^e &= p\beta k_I \mu_I [J_0(k_M e) + iY_0(k_M e)] J_0'(k_I a) \\ &\quad / 2\pi a \mu_M \{k_I \mu_I J_0'(k_I a)[- \beta [J_0(k_M a) + iY_0(k_M a)] \\ &\quad + k_M \mu_M [J_0'(k_M a) + iY_0'(k_M a)]] + \beta k_M \mu_M J_0(k_I a) \\ &\quad [J_0'(k_M a) + iY_0'(k_M a)]\} \end{aligned} \quad (3-24)$$

$$\begin{aligned} a_m^e &= -p[J_m(k_M e) + iY_m(k_M e)][\beta J_m(k_I a) + k_I \mu_I J_m'(k_I a)] \\ &\quad / \pi a \{k_I \mu_I J_m'(k_I a)[- \beta [J_m(k_M a) + iY_m(k_M a)] \\ &\quad + k_M \mu_M [J_m'(k_M a) + iY_m'(k_M a)]] + \beta k_M \mu_M J_m(k_I a) \\ &\quad [J_m'(k_M a) + iY_m'(k_M a)]\} \end{aligned} \quad (3-25)$$

$$\begin{aligned} p_m^e &= p\beta k_I \mu_I [J_m(k_M e) + iY_m(k_M e)] J_m'(k_I a) \\ &\quad / \pi a \mu_M \{k_I \mu_I J_m'(k_I a)[- \beta [J_m(k_M a) + iY_m(k_M a)] \\ &\quad + k_M \mu_M [J_m'(k_M a) + iY_m'(k_M a)]] + \beta k_M \mu_M J_m(k_I a) \\ &\quad [J_m'(k_M a) + iY_m'(k_M a)]\} \end{aligned} \quad (3-26)$$

where  $a_0^e$ ,  $p_0^e$ ,  $a_m^e$  and  $p_m^e$ ,  $m = 1, 2, 3, \dots$  are the Fourier coefficients of boundary densities for the matrix. According to interface boundary condition of Eqs. (3-19) and (3-20), we obtain the Fourier coefficient of the inclusion as shown below:

$$\begin{bmatrix} a_0^i \\ p_0^i \end{bmatrix} = \begin{bmatrix} \frac{\mu_M}{\beta} p_0^e + a_0^e \\ 0 \end{bmatrix} \quad (3-27)$$

$$\begin{bmatrix} a_m^i \\ p_m^i \end{bmatrix} = \begin{bmatrix} \frac{\mu_M}{\beta} p_m^e + a_m^e \\ -\frac{\mu_M}{\mu_I} p_m^e \end{bmatrix} \quad (3-28)$$

where  $a_0^i, p_0^i, a_m^i$  and  $p_m^i$  are the Fourier coefficients of boundary densities for the inclusion. Then, we can obtain the series-form Green's function for the matrix by applying Eq. (3-9) as shown below:

$$\begin{aligned} G(x, \xi) = & -\frac{\pi a}{2} [a_0^e k_M J_0'(k_M a) + p_0^e J_0(k_M a)] [Y_0(k_M \rho) - iJ_0(k_M \rho)] \\ & - \frac{\pi a}{2} \sum_{m=1}^{\infty} [a_m^e k_M J_m'(k_M a) + p_m^e J_m(k_M a)] [Y_m(k_M \rho) - iJ_m(k_M \rho)] \cos(m\phi) \\ & - \frac{p}{4\mu_M} [Y_0(k_M r) - iJ_0(k_M r)], \quad a \leq \rho < \infty \end{aligned} \quad (3-29)$$

If we expand the fundamental function, we have

$$\begin{aligned} G(x, \xi) = & -\frac{\pi a}{2} [a_0^e k_M J_0'(k_M a) + p_0^e J_0(k_M a)] [Y_0(k_M \rho) - iJ_0(k_M \rho)] \\ & - \frac{\pi a}{2} \sum_{m=1}^{\infty} [a_m^e k_M J_m'(k_M a) + p_m^e J_m(k_M a)] [Y_m(k_M \rho) - iJ_m(k_M \rho)] \cos(m\phi) \\ & - \frac{p}{4\mu_M} \{J_0(k_M e) [Y_0(k_M \rho) - iJ_0(k_M \rho)] \\ & + 2 \sum_{m=1}^{\infty} J_m(k_M e) [Y_m(k_M \rho) - iJ_m(k_M \rho)] \cos(m\phi)\} \\ & , e \leq \rho < \infty \end{aligned} \quad (3-30)$$

$$\begin{aligned} G(x, \xi) = & -\frac{\pi a}{2} [a_0^e k_M J_0'(k_M a) + p_0^e J_0(k_M a)] [Y_0(k_M \rho) - iJ_0(k_M \rho)] \\ & - \frac{\pi a}{2} \sum_{m=1}^{\infty} [a_m^e k_M J_m'(k_M a) + p_m^e J_m(k_M a)] [Y_m(k_M \rho) - iJ_m(k_M \rho)] \cos(m\phi) \\ & - \frac{p}{4\mu_M} \{J_0(k_M \rho) [Y_0(k_M e) - iJ_0(k_M e)] \\ & + 2 \sum_{m=1}^{\infty} J_m(k_M \rho) [Y_m(k_M e) - iJ_m(k_M e)] \cos(m\phi)\} \\ & , a \leq \rho < e \end{aligned} \quad (3-31)$$

### 3.4 Illustrative examples and discussions

#### *Case 1: one inclusion in the matrix with a concentrated force*

Following the same example of Wang and Sudak [Wang and Sudak (2007)], we suppose that  $\mu_I = 4\mu_M$ ,  $c_I = 2c_M$ , and  $e$  is located at  $1.1a$  on the  $x$  axis as shown Fig. 3-1(a). For the static case ( $k=0$ ), we can replace the  $H_0(kr)$  by  $\ln r$  and redo the procedure. The formulation can be found in the Appendix A. On the other hand, the static solution by using the limiting process ( $k \rightarrow 0$ ) is also derived in the Appendix B. The stress  $\sigma_{xz}^*$  along the circular boundary is shown in Fig. 3-2(a). In the real implementation, direct substitution of zero  $k$  value yields the singular behavior in our formulation of Hankel function and can not be carried out in the program. We select  $ka = 0.01$  to simulate the quasi-static result. Good agreement is made in Fig. 3-2(b) after comparing with that of Fig. 3-2(a). Parameter study of  $\beta$  on the stress  $\sigma_{xz}^*$  along the circular boundary is done as shown in Fig. 3-3(a). To simulate the ideally bonded case, we choose  $\beta = 10^{32}$  in the real computation. Good agreement is made after comparing with that of the ideally bonded case ( $\beta = \infty$ ). The derivation of ideally bonded case is also given in the Appendix C. Figs. 3-3(a) and 3-3(b) show that the higher the  $\lambda$  value is, the larger the stress appears. Our results also match well with those of Wang and Sudak's data. Furthermore, test of convergence for the Fourier series using Parseval's sum are shown in Figs. 3-4(a) and 3-4(b). Figs. 3-5(a) and 3-5(b) show the distribution of displacement ( $u_I^* = \mu_M |u_I| / p$ ) along the circular boundary versus the wave number with  $\lambda = 1$  by using the Wang and Sudak's approach and our method, respectively. Good agreement is made. It is expected that higher wave number yield higher oscillation along the angle from  $0 \sim 2\pi$ .

#### *Case 2: infinite matrix with a single inclusion subject to a concentrated force*

We also suppose the same parameters of  $\mu_I = 4\mu_M$  and  $c_I = 2c_M$  as the case 1. Here, the source is located at  $e = 0.9a$  in the inclusion as shown in Fig. 3-1(b). To verify the accuracy of the present solution, we compare with the quasi-static result ( $k_M a = 0.01$ ) for the stress distribution along the interface as shown in Fig. 3-6 using the static solution ( $k_M = 0$ ) as derived in the Appendix A. Also, an alternative method by limiting processes ( $k \rightarrow 0$ ) is also given in the Appendix B. Regarding

the series solution as well as the closed-form solution for the static case, the result is summarized in the Table 3.1. Excellent agreement between the two results is observed from the Fig. 3-6. The stress  $\sigma_{zr}^*$  versus  $k_M a$  for different values of  $\lambda$  is shown in Fig. 3-7. Some amplifications for certain values of  $k_M a$  can be found in the same trend of Fig. 3-3(b). Fig. 3-8 shows the distribution of displacement ( $u_I^* = \mu_M |u_I|/p$ ) along the circular boundary versus the wave number with  $\lambda = 1$ .

### *Case 3: two inclusions in the matrix with a concentrated force*

Following the success of the single-inclusion case to compare well with the Wang and Sudak's result, we extend to two inclusions as shown in Fig. 3-9. We also suppose the same properties of  $\mu_I = 4\mu_M$  and  $c_I = 2c_M$  as the case 1. Here, the concentrated source is located in the matrix of  $e = (2.5, 0)$ . Figure 3-10 shows the variation of  $\sigma_{zr}^* = R|\sigma_{zr}^I|/p = R|\sigma_{zr}^M|/p$  at the point  $(-a_1, 0)$  for various distances  $d = 0.01 \sim 13$ . The local maximum or minimum of  $\sigma_{zr}^*$  occurs in a period of half wavelength. The contour of the displacement for the two-inclusions problem is shown in Fig. 3-11.

## **3.5 Conclusions**

Two-dimensional antiplane dynamic Green's functions for a circular inclusion or two circular inclusions with imperfect interface have been successfully derived by using the present formulation. A limiting case of zero wave number matches well with the static solution. Ideal bonded case can be seen as a special case of our solution. Moreover, good agreement is made after comparing with the analytical solution derived by Wang and Sudak's results. Parameter study of wave number and interface constant is also done.

# Chapter 4 Conclusions and further research

## 4.1 Conclusions

The thesis is concerned about the derivation of Green's function for Laplace and Helmholtz problems with circular aperture and/or inclusions by using the null-field integral equation approach. In the context of this thesis, we have demonstrated that our approach is useful and effective. Based on the proposed formulation for solving the problems involving circular apertures and/or inclusions with perfect or imperfect interface, some concluding remarks are itemized as follows:

1. A systematic approach to solve the Green's function of Laplace or Helmholtz problems with circular apertures and/or inclusions was proposed successfully in this thesis by using the null-field integral equation in conjunction with degenerate kernels and Fourier series. Problems involving infinite, semi-infinite and bounded domains with perfect or imperfect circular boundaries were examined to check the accuracy of the present formulation.
2. The singularity and hypersingularity were avoided by using degenerate kernels for interior and exterior regions separated by the circular boundary. Instead of directly calculating principal values, all the boundary integrals can be performed analytically by using the degenerate kernel and Fourier expansion.
3. Parameter study of wave number ( $k$ ) and interface constant ( $\beta$ ) is done for the two-dimensional antiplane dynamic Green's functions of a circular inclusion with imperfect interface. For the static case ( $k = 0$ ), the Helmholtz problem can be reduced to the Laplace problem. The formulation can be found in the Appendix A. Also, an alternative method by limiting process ( $k \rightarrow 0$ ) is in the Appendix B. When  $\beta$  approaches infinity, the circular inclusion is perfectly bonded to the matrix. When  $\beta$  approaches zero, the circular inclusion is fully debonded from the matrix. The derivation is given in the Appendix C.
4. We derived the analytic Green's function for one inclusion problem by using the

null-field integral equation. Also, the present approach can be utilized to construct semi-analytic Green's functions for several circular aperture or inclusions. Null-field integral equation is seen as a "semi-analytical" approach since error purely ascribes the truncation Fourier series.

5. After introducing the degenerate kernel, the BIE is nothing more than the linear algebra for the unknown coefficients.
  
6. A general-purpose program for deriving the Green's function of Laplace or Helmholtz problems with arbitrary number of circular apertures or inclusions of arbitrary radii and various positions involving Dirichlet or Neumann or mixed boundary condition was developed.

## 4.2 Further research

In this thesis, our formulation has been applied to derive the Green's function with circular boundaries by using the separate form of fundamental solutions and Fourier series expansions. However, several issues are worth to be further investigated as follows:

1. In this thesis, we only consider simpler problems in which the imperfect interface is circumferentially homogeneous. The more general case in which the imperfect interface is circumferentially inhomogeneous can also be solved by using the present method.
2. The extension to Helmholtz problem with a hill can be studied by using the present approach in conjunction with the multiply-domain technique by decomposing the original problem into one interior problem of circular domain and a half-plane problem with a semi-circular canyon.
3. The degenerate kernels are expanded in the polar coordinate and only problems with circular boundaries are solved. For boundary value problems with ellipse or crack, further investigation should be considered.
4. According to our successful experiences for half-plane problems, it is straightforward to quarter-plane problems which can be studied by employing the symmetric or anti-symmetric property of image method.
5. Following the success of applications in two-dimensional problems, it is straightforward to extend this formulation to 3-D problems with spherical inclusions and/or apertures with perfect or imperfect circular boundaries using the corresponding 3-D degenerate kernel functions for fundamental solutions and spherical harmonic expansions for boundary densities.

## References

- [1] **Achenbach, J. D.; Kechter, G. E.; Xu, Y. L.** (1988): Off-boundary approach to the boundary element method. *Computer Methods in Applied Mechanics and Engineering*, vol. 70, pp. 191-201.
- [2] **Adewale, A. O.** (2006): Isotropic clamped-free thin annular plate subjected to a concentrated load. *ASME Journal of Applied Mechanics*, vol. 73, no. 4, pp. 658-663.
- [3] **Ang, W. T.; Telles, J. C. F.** (2004): A numerical Green's function for multiple cracks in anisotropic bodies. *Journal of Engineering Mathematics*, vol. 49, pp. 197-207.
- [4] **Barone, M. R.; Caulk, D. A.** (1981): Special boundary integral equations for approximate solution of Laplace's equation in two-dimensional regions with circular holes. *Quarterly Journal of Mechanics and Applied Mathematics*, vol. 34, pp. 265-286.
- [5] **Barone, M. R.; Caulk, D. A.** (1982): Optimal arrangement of holes in a two-dimensional heat conductor by a special boundary integral method. *International Journal for Numerical Methods in Engineering*, vol. 18, pp. 675-685.
- [6] **Barone, M. R.; Caulk, D. A.** (1985): Special boundary integral equations for approximate solution of potential problems in three-dimensional regions with slender cavities of circular cross-section. *IMA Journal of Applied Mathematics*, vol. 35, pp. 311-325.
- [7] **Barone, M. R.; Caulk, D. A.** (2000): Analysis of liquid metal flow in die casting. *International Journal of Engineering Science*, vol. 38, pp. 1279-1302.
- [8] **Bergman, S.; Schiffer, M.** (1953): Kernel functions and elliptic differential equations in mathematical physics, New York: *Academic Press*.
- [9] **Bird, M. D.** (1992): A Fourier series method for determining the interaction of circular inhomogeneities in harmonic and biharmonic problems, Ph. D. Dissertation, *Department of Mechanical Engineering*, Stanford University, USA.

- [10] **Bird, M. D.; Steele, C. R.** (1991): Separated solution procedure for bending of circular plates with circular holes. *ASME Applied Mechanics Reviews*, vol. 44, pp. 27-35.
- [11] **Bird, M. D.; Steele, C. R.** (1992): A solution procedure for Laplace equation on multiply-connected circular domains. *ASME Journal of Applied Mechanics*, vol. 59, pp. 398-404.
- [12] **Boley, B. A.** (1956): A method for the construction of Green's functions. *Quarterly of Applied Mathematics*, vol. 14, pp. 249-257.
- [13] **Brebbia, C. A.** (1978): Recent advances in Boundary element Methods, Pentech Press, London.
- [14] **Caulk, D. A.** (1983): Analysis of elastic torsion in a bar with circular holes by a special boundary integral method. *ASME Journal of Applied Mechanics*. vol. 50, pp. 101-108.
- [15] **Caulk, D. A.** (1983): Analysis of steady heat conduction in regions with circular holes by a special boundary integral method. *IMA Journal of Applied Mathematics*, vol. 30, pp. 231-246.
- [16] **Caulk, D. A.** (1983): Steady heat conduction from an infinite row of holes in a half-space or a uniform slab. *International Journal of Heat and Mass Transfer*, vol. 26, pp. 1509-1513.
- [17] **Caulk, D. A.** (1984): Special boundary integral equations for potential problems in regions with circular holes. *ASME Journal of Applied Mechanics*, vol. 51, pp. 713-716.
- [18] **Chen, C. T.** (2005): Null-field integral equation approach for Helmholtz (interior and exterior acoustic) problems with circular boundaries, Master Thesis, *Department of Harbor and River Engineering, National Taiwan Ocean University, Keelung, Taiwan.*
- [19] **Chen, C. T.; Chen, I. L.; Chen, J. T.** (2005): Null-field integral equation approach for Helmholtz (interior and exterior acoustic) problems with circular boundaries, 九十四年電子計算機於土木水利工程應用研討會, 台南成大.
- [20] **Chen, H. B.; Lu, P.; Schnack, E.** (2001): Regularized algorithms for the calculation of values on and near boundaries in 2D elastic BEM. *Engineering*

- Analysis with Boundary Elements*, vol. 25, pp. 851-876.
- [21] **Chen, J. T.** (2005): Null-field integral equation approach for boundary value problems with circular boundaries. *International Conference on Computational & Experimental Engineering Sciences*, India.
- [22] **Chen, J. T.; Hong, H. K.** (1994): Dual boundary integral equations at a corner using contour approach around singularity. *Advances in Engineering Software*, vol. 21, pp. 169-178.
- [23] **Chen, J. T.; Hsiao, C. C.; Leu, S. Y.** (2006): Null-field integral equation approach for plate problems with circular boundaries. *ASME Journal of Applied Mechanics*, vol.73, pp. 679-693.
- [24] **Chen, J. T.; Ke, J. N.; Liao, H. Z.** (2007): Construction of Green's function using null-field integral approach for Laplace problems with circular boundaries. *Computers, Materials & Continua*, Accepted.
- [25] **Chen, J. T.; Liu, L. W.; Hong, H. K.** (2003): Spurious and true eigensolutions of Helmholtz BIEs and BEMs for a multiply connected problem. *Proceedings of the Royal Society Series A*, vol. 459, pp. 1891-1924.
- [26] **Chen, J. T.; Shen, W. C.** (2007): Degenerate scale for multiply connected Laplace problems. *Mechanics Research Communications*, vol. 34, pp. 69-77.
- [27] **Chen, J. T.; Shen, W. C.; Wu, A. C.** (2005): Null-field integral equations for stress field around circular holes under anti-plane shear. *Engineering Analysis with Boundary Elements*, vol. 30, pp. 205-217.
- [28] **Chen, J. T.; Shen, W. C.; Chen, P. Y.** (2006): Analysis of circular torsion bar with circular holes using null-field approach. *Computer Modeling in Engineering Science*, vol. 12, pp. 109-119.
- [29] **Chen, J. T.; Wu, A. C.** (2006): Null-field approach for piezoelectricity problems with arbitrary circular inclusions. *Engineering Analysis with Boundary Elements*, vol. 30, pp. 971-993.
- [30] **Chen, J. T.; Wu, A. C.** (2007): Null-field approach for the multi-inclusion problem under anti-plane shears. *ASME Journal of Applied Mechanics*, vol. 74, 469-487.

- [31] **Chen, J. T.; Wu, C. S.** (2006): Alternative derivations for the Poisson integral formula. *International Journal of Mathematical Education in Science and Technology*, vol. 37, pp. 165-185.
- [32] **Chen, J. T.; Wu, C. S.; Lee, Y. T.; Chen, K. H.** (2007): On the equivalence of the Trefftz method and method of fundamental solutions for Laplace and biharmonic equations. *Computers and Mathematics with Applications*, vol. 53, pp. 851-879.
- [33] **Chen, P. Y.; Chen, C. T.; Chen, J. T.** (2005): A semi-analytical approach for dynamic stress concentration factor of Helmholtz problems with circular holes, *The 29<sup>th</sup> National Conference on Theoretical and Applied Mechanics*, NTHU, Hsinchu.
- [34] **Chen, T.** (2001): Thermal conduction of a circular inclusion with variable interface parameter. *International Journal of Solids and Structures*, vol. 38, pp. 3081-3097.
- [35] **Chen, T.; Weng, I. S.** (2001): Torsion of a circular compound bar with imperfect interface. *ASME Journal of Applied Mechanics*, vol. 68, pp. 955-958.
- [36] **Cheng, A. H. D.; Cheng, D. T.** (2005): Heritage and early history of the boundary element method. *Engineering Analysis with Boundary Elements*, vol. 29, pp. 268-302.
- [37] **Cheng, Z. Q.; Batra, R. C.** (1999): Exact Eshelby tensor for a dynamic circular cylindrical inclusion. *ASME Journal of Applied Mechanics*, vol. 66, pp. 563-565.
- [38] **Courant, R.; Hilbert, D.** (1962): *Methods of mathematical physics*, vol. 2, New York: Interscience.
- [39] **Crouch, S. L.; Mogilevskaya, S. G.** (2003): On the use of Somigliana's formula and Fourier series for elasticity problems with circular boundaries. *International Journal for Numerical Methods in Engineering*, vol. 58, pp. 537-578.
- [40] **Cruse, T. A.; Rizzo, F. J.** (1968): A direct formulation and numerical solution of the general transient elastodynamic problem I. *Journal of Mathematical Analysis and Applications*, vol. 22, no. 1, pp. 244-259.

- [41] **Denda, M.; Araki, Y.; Yong, Y. K.** (2004): Time-harmonic BEM for 2-D piezoelectricity applied to eigenvalue problem. *International Journal of Solids and Structures*, vol. 41, pp. 7241-7265.
- [42] **Denda, M.; Wang, C. Y.; Yong, Y. K.** (2003): 2-D time-harmonic BEM for solids of general anisotropy with application to eigenvalue problems. *Journal of Sound and Vibration*, vol. 261, pp. 247-276.
- [43] **Gray, L. J.; Manne, L. L.** (1993): Hypersingular integrals at a corner. *Engineering Analysis with Boundary Elements*, vol. 11, pp. 327-334.
- [44] **Guiggiani, M.** (1995): Hypersingular boundary integral equations have an additional free term. *Computational Mechanics*, vol. 16, pp. 245-248.
- [45] **Hashin, Z.** (1991): The spherical inclusion with imperfect interface. *ASME Journal of Applied Mechanics*, vol. 12, pp. 444-449.
- [46] **Honein, E.; Honein, T.; Herrmann, G.** (1992): On two circular inclusions in harmonic problem. *Quarterly of Applied Mathematics*, vol.50, pp. 479-499.
- [47] **Hong, H. K.; Chen, J. T.** (1988): Derivations of integral equations of elasticity. *Journal of Engineering mechanics*, vol. 114, no. 6, 1028-1044.
- [48] **Hsiao, C. C.** (2005): A semi-analytical approach for Stokes flow and plate problems with circular boundaries, Master Thesis, *Department of Harbor and River Engineering, National Taiwan Ocean University, Taiwan.*
- [49] **Huang, Q.; Cruse, T. A.** (1993): Some notes on singular integral techniques in boundary element analysis. *International Journal for Numerical Methods in Engineering*, vol. 36, pp. 2643-2659.
- [50] **Jaswon, M. A.; Symm, G. T.** (1977): Integral equation methods in potential theory and electrostatics, *Academic Press*, New York.
- [51] **Kellogg, O. D.** (1953): Foundations of potential theory, New York: *Dover*.
- [52] **Kisu, H.; Kawahara, T.** (1988): Boundary element analysis system based on a formulation with relative quantity. *Boundary Elements X*, Brebbia CA, eds., *Springer-Verlag*, vol. 1, pp. 111-121.
- [53] **Kitahara, M.** (1985): Boundary integral equation methods in eigenvalue problems of elastodynamics and thin plates, *Elsevier*, Amsterdam.
- [54] **Kress, R.** (1989): Linear integral equations, *Springer-Verlag*, Berlin.

- [55] **Lebedev, N. N.; Skalskaya, I. P.; Uflyand Y. S.** (1979): Worked problem in applied mathematics, *Dover Publications*, New York.
- [56] **Liu, P. L. F.; Lean, M. H.** (1990): A note on  $\Gamma$ -contours in the integral equation formulation for a multi-connected region. In: Grilli, S., Brebbia, C. A., Cheng, A. H. D. (Eds.). *Computational Engineering with Boundary Elements*, vol. 1, pp. 295-302.
- [57] **Melnikov, Y. A.** (1977): Some application of the Green's function method in mechanics. *International Journal of Solids and Structures*, vol. 13, pp. 1045-1058.
- [58] **Melnikov, Y. A.** (1982): A basis for computation of thermo-mechanical fields in elements of constructions of complex con figuration, *Thesis Dr. Technical Sciences*, Moscow Institute of Civil Engineering (in Russian).
- [59] **Melnikov, Y. A.** (1995): Green's functions in applied mechanics, *Computational Mechanics Publications*, Boston-Southampton.
- [60] **Melnikov, Y. A.; Melnikov, M. Y.** (2001): Modified potential as a tool for computing Green's functions in continuum mechanics. *Computer Modeling in Engineering & Sciences*, vol. 2, pp. 291-305.
- [61] **Melnikov, Y. A.; Melnikov, M. Y.** (2006): Green's functions for mixed boundary value problems in regions of irregular shape. *Electronic Journal of Boundary Elements*, vol. 4, pp. 82-104.
- [62] **Michelitsch, T. M.; Levin, V. M.; Gao, H. J.** (2002): Dynamic potentials and Green's functions of a quasi-plane piezoelectric medium with inclusion. *Proceedings of the Royal Society of London*, vol. A458, pp. 2393-2415.
- [63] **Mikata, Y.; Nemat-Nasser, S.** (1990): Elastic field due to a dynamically transforming spherical inclusion. *ASME Journal of Applied Mechanics*, vol. 57, pp. 845-849.
- [64] **Mogilevskaya, S. G.; Crouch, S. L.** (2001): A Galerkin boundary integral method for multiple circular elastic inclusions. *International Journal for Numerical Methods in Engineering*, vol. 52, pp. 1069-1106.
- [65] **Morse, P. M.; Feshbach, H.** (1953): Methods of theoretical physics, vols. 1 and 2, New York, Toronto, London: *McGraw-Hill*.

- [66] **Mura, T.** (1988): Inclusion problems. *ASME Applied Mechanics Reviews*, vol. 41, pp. 15-20.
- [67] **Mura, T.; Shodja, H. M.; Hirose, Y.** (1996): Inclusion problems. *ASME Applied Mechanics Reviews*, vol. 49, pp. S118-S127.
- [68] **Rashed, Youssef F.** (2004): Green's first identity method for boundary-only solution of self-weight in BEM formulation for thick slabs. *Computers, Materials & Continua*, vol. 1, no. 4, pp. 319-326.
- [69] **Roach, G. F.** (1982): Green's functions, New York: *Cambridge University Press*.
- [70] **Ru, C. Q.; Schiavone, P.** (1997): A circular inclusion with circumferentially inhomogeneous interface in antiplane shear. *Proceedings of the Royal Society of London*, vol. A 453, pp. 2551-2572.
- [71] **Shen, W. C.** (2005): Null-field approach for Laplace problems with circular boundaries using degenerate kernels, Master Thesis, *Department of Harbor and River Engineering*, National Taiwan Ocean University, Taiwan.
- [72] **Shen, W. C.; Chen, P. Y.; Chen, J. T.** (2005): Analysis of circular torsion bar with circular holes using null-field approach, 九十四年電子計算機於土木水利工程應用研討會, 台南成大.
- [73] **Sladek, V.; Sladek, J.** (1991): Elimination of the boundary layer effect in BEM computation of stresses. *Communications in Applied Numerical Methods*, vol. 7, pp. 539-550.
- [74] **Sladek, V.; Sladek, J.; Tanaka, M.** (1993): Regularization of hypersingular and nearly singular integrals in the potential theory and elasticity. *International Journal for Numerical Methods in Engineering*, vol. 36, pp. 1609-1628.
- [75] **Talbot, D. R. S.; Willis, J. R.** (1983): Variational estimates for dispersion and attenuation of waves in random composite—III. Fiber-reinforced materials. *International Journal of Solids and Structures*, vol. 19, pp. 793-811.
- [76] **Telles, J. C. F.** (1987): A self-adaptative coordinate transformation for efficient numerical evaluation of general boundary element integrals. *International Journal for Numerical Methods in Engineering*, vol. 24, pp. 959-973.

- [77] **Telles, J. C. F.; Castor, G. S.; Guimaraes, S.** (1995): Numerical Green's function approach for boundary elements applied to fracture mechanics. *International Journal for Numerical Methods in Engineering*, vol. 38, no. 19, pp. 3259-3274.
- [78] **Wang, X. D.; Meguid, S. A.** (1999): Dynamic interaction between a matrix crack and a circular inhomogeneity with a distinct interphase. *International Journal of Solids and Structures*, vol. 36, pp. 517-531.
- [79] **Wang, X.; Sudak, L. J.** (2007): Antiplane time-harmonic Green's functions for a circular inhomogeneity with an imperfect interface. *Mechanics Research Communications*, vol. 34, pp. 352-358 .
- [80] **Wang, X.; Zhong, Z.** (2003): Two-dimensional time-harmonic dynamic Green's functions in transversely isotropic piezoelectric solids. *Mechanics Research Communications*, vol. 30, pp. 589-593.
- [81] **Willis, J. R.** (1980a): A polarization approach to the scattering of elastic waves — I. scattering by a single inclusion. *Journal of the Mechanics and Physics of Solids*, vol. 28, pp. 287-305.
- [82] **Willis, J. R.** (1980b): A polarization approach to the scattering of elastic waves — II . multiple scattering from inclusions. *Journal of the Mechanics and Physics of Solids*, vol. 28, pp. 307-327.
- [83] **Wu, A. C.** (2006) : Null-field approach for multiple circular inclusion problems in anti-plane piezoelectricity, Master Thesis, *Department of Harbor and River Engineering, National Taiwan Ocean University, Keelung, Taiwan.*
- [84] 陳正宗、李應德，2007，中醫工程分析法—邊界積分方程法(或邊界元素法)與無網格法之研究，國科會-工程技術法展處-學門研究成果成功案例專欄報導，台北。
- [85] 陳正宗、周克勳，2007 數學傳播，圓周積分的三種看法，中央研究院數學研究所發行，台北，接受。

## Appendix 1 Static cases

### Case 1: a concentrated force in the matrix

For the static case ( $k=0$ ) and ideally bonded interface ( $\beta \rightarrow \infty$ ), we can replace the  $H_0(kr)$  by  $\ln r$  and redo the procedure. Then, we follow the formulation for Laplace problems in Chapter 2. For the problem with inclusion, we can decompose into subsystems of matrix and inclusion after taking free body on the interface as shown in Fig. 3-1(c). Then, by collocating  $x$  on  $(a^-, \phi)$  and  $(a^+, \phi)$  for the matrix and inclusion, respectively, the null-field equations yield

$$\begin{aligned}
 0 = & -2\pi a_0^e - \sum_{m=1}^{\infty} \pi(a_m^e \cos m\phi + b_m^e \sin m\phi) \\
 & - 2\pi a \ln a p_0^e + \sum_{m=1}^{\infty} \frac{a\pi}{m} (p_m^e \cos m\phi + p_m^e \sin m\phi) \\
 & - \frac{p}{\mu_M} \left[ \ln e - \sum_{m=1}^{\infty} \frac{1}{m} \left(\frac{a}{e}\right)^m \cos(m\phi) \right] \\
 & , \quad x \rightarrow (a^-, \phi)
 \end{aligned} \tag{A1-1}$$

$$\begin{aligned}
 0 = & - \sum_{m=1}^{\infty} \pi(a_m^i \cos m\phi + b_m^i \sin m\phi) - 2\pi a \ln a p_0^i \\
 & + \sum_{m=1}^{\infty} \frac{a\pi}{m} (p_m^i \cos m\phi + q_m^i \sin m\phi) \\
 & , \quad x \rightarrow (a^+, \phi)
 \end{aligned} \tag{A1-2}$$

Similarly, interface conditions of Eq. (3-5) can be rewritten as

$$t^I = \frac{\beta}{\mu_I} (u^M - u^I), \text{ on the interface} \tag{A1-3}$$

$$-\mu_M t^M = \mu_I t^I, \text{ on the interface} \tag{A1-4}$$

By assembling the matrices in Eqs. (A1-1), (A1-2), (A1-3) and (A1-4), we have

$$\begin{bmatrix} T_{11}^M & -U_{11}^M & 0 & 0 \\ 0 & 0 & T_{11}^I & -U_{11}^I \\ 0 & \mu_M & 0 & \mu_I \\ \beta & \mu_M & -\beta & 0 \end{bmatrix} \begin{bmatrix} u_1^M \\ t_1^M \\ u_1^I \\ t_1^I \end{bmatrix} = \begin{bmatrix} \frac{p}{\mu_M} U(\xi, x) \\ 0 \\ 0 \\ 0 \end{bmatrix} \tag{A1-5}$$

After rearranging Eq. (A1-5), we have

$$\begin{bmatrix} T_{11}^M & -U_{11}^M \\ T_{11}^I & \frac{\mu_M}{\beta} T_{11}^I + \frac{\mu_M}{\mu_I} U_{11}^I \end{bmatrix} \begin{bmatrix} u_1^M \\ t_1^M \end{bmatrix} = \begin{bmatrix} \frac{p}{\mu_M} U(\xi, x) \\ 0 \end{bmatrix} \quad (\text{A1-6})$$

The unknown coefficients in the algebraic system can be determined as shown below:

$$\begin{bmatrix} a_0^e \\ a_m^e \\ b_m^e \\ p_0^e \\ p_m^e \\ q_m^e \end{bmatrix} = \begin{bmatrix} -\frac{p}{2\pi\mu_M} \ln e \\ \frac{p(\beta a + m\mu_I)}{m\pi[m\mu_M\mu_I + \beta a(\mu_M + \mu_I)]} \left(\frac{a}{e}\right)^m \\ 0 \\ 0 \\ -\frac{p\beta\mu_I}{\mu_M\pi[m\mu_M\mu_I + \beta a(\mu_M + \mu_I)]} \left(\frac{a}{e}\right)^m \\ 0 \end{bmatrix} \quad (\text{A1-7})$$

where  $a_0^e, p_0^e, a_m^e$  and  $p_m^e$ ,  $m=1,2,3,\dots$  are the Fourier coefficients of boundary densities for the matrix. As  $\beta$  approaches infinity, we have

$$\begin{bmatrix} a_0^e \\ a_m^e \\ b_m^e \\ p_0^e \\ p_m^e \\ q_m^e \end{bmatrix} = \lim_{\beta \rightarrow \infty} \begin{bmatrix} -\frac{p}{2\pi\mu_M} \ln e \\ \frac{p(\beta a + m\mu_I)}{m\pi[m\mu_M\mu_I + \beta a(\mu_M + \mu_I)]} \left(\frac{a}{e}\right)^m \\ 0 \\ 0 \\ -\frac{p\beta\mu_I}{\mu_M\pi[m\mu_M\mu_I + \beta a(\mu_M + \mu_I)]} \left(\frac{a}{e}\right)^m \\ 0 \end{bmatrix} = \begin{bmatrix} -\frac{p}{2\pi\mu_M} \ln e \\ \frac{p}{m\pi(\mu_M + \mu_I)} \left(\frac{a}{e}\right)^m \\ 0 \\ 0 \\ -\frac{p\mu_I}{a\mu_M\pi(\mu_M + \mu_I)} \left(\frac{a}{e}\right)^m \\ 0 \end{bmatrix} \quad (\text{A1-8})$$

Then, we can obtain the analytical result for static stress ( $\sigma_{zr}^{\star} = a\sigma_{zr}^I / p = a\sigma_{zr}^M / p$ ) of the matrix as shown below:

$$\sigma_{zr}^{\star} = \frac{a}{p} \sigma_{zr}^M = \frac{\mu_I}{\pi(\mu_I + \mu_M)} \sum_{m=1}^{\infty} \left(\frac{a}{e}\right)^m \cos m\theta, \quad e > a \quad (\text{A1-9})$$

The Wang and Sudak's closed-form solution is shown below:

$$\sigma_{zr}^{\star} = \frac{\mu_I}{\pi(\mu_I + \mu_M)} \left( \frac{ea \cos \theta - a^2}{e^2 + a^2 - 2ea \cos \theta} \right), \quad e > a \quad (\text{A1-10})$$

By expanding the Eq. (A1-10) into Fourier series, we have

$$\sigma_{zr}^{\star} = \frac{\mu_I}{\pi(\mu_I + \mu_M)} \sum_{m=1}^{\infty} a_m \cos(m\theta), \quad e > a \quad (\text{A1-11})$$

where the Fourier coefficient of  $a_m$  can be determined by using the Poisson integral formula [Chen and Chou (2007)] as shown below:

$$\begin{aligned} a_m &= \frac{1}{\pi} \int_0^{2\pi} \left( \frac{ea \cos \theta - a^2}{e^2 + a^2 - 2ea \cos \theta} \right) \cos(m\theta) d\theta \\ &= \frac{1}{\pi} \int_0^{2\pi} \left[ \frac{\left(\frac{a}{e}\right) \cos \theta - \left(\frac{a}{e}\right)^2}{1 + \left(\frac{a}{e}\right)^2 - 2\left(\frac{a}{e}\right) \cos \theta} \right] \cos(m\theta) d\theta \\ &= \frac{2}{1 - \left(\frac{a}{e}\right)^2} \frac{\left(\frac{a}{e}\right)^m - \left(\frac{a}{e}\right)^{m+2}}{2}, \quad e > a \\ &= \left(\frac{a}{e}\right)^m \end{aligned} \quad (\text{A1-12})$$

An alternative proof by using the degenerate kernel can also be obtained as shown below:

$$U(s, x) = \ln \sqrt{e^2 + a^2 - 2ea \cos \theta} = \begin{cases} \ln e - \sum_{m=1}^{\infty} \frac{1}{m} \left(\frac{a}{e}\right)^m \cos(m\theta), & e \geq a \\ \ln a - \sum_{m=1}^{\infty} \frac{1}{m} \left(\frac{e}{a}\right)^m \cos(m\theta), & a > e \end{cases} \quad (\text{A1-13})$$

$$L(s, x) = \frac{\partial U(s, x)}{\partial a} = \frac{a - e \cos \theta}{e^2 + a^2 - 2ea \cos \theta} = \begin{cases} - \sum_{m=1}^{\infty} \left(\frac{a^{m-1}}{e^m}\right) \cos(m\theta), & e > a \\ \frac{1}{a} + \sum_{m=1}^{\infty} \left(\frac{e^m}{a^{m+1}}\right) \cos(m\theta), & a > e \end{cases} \quad (\text{A1-14})$$

By multiplying  $(-a)$  into Eq. (A1-14), we can also obtain the result of static case

$$\sigma_{zr}^{\star} = \frac{\mu_I}{\pi(\mu_I + \mu_M)} \sum_{m=1}^{\infty} \left(\frac{a}{e}\right)^m \cos(m\theta), \quad e > a \quad (\text{A1-15})$$

Therefore, we have proved that our series-form solution is mathematically equivalent to the closed-form solution of Wang and Sudak.

### *Case 2: a concentrated force in the inclusion*

Similarly as shown in case 1, we can obtain the unknown coefficients as shown below:

$$\begin{bmatrix} a_0^e \\ a_m^e \\ b_m^e \\ p_0^e \\ p_m^e \\ q_m^e \end{bmatrix} = \begin{bmatrix} -\frac{p\mu_I}{2\pi\mu_M^2} \ln a \\ \frac{p\beta a\mu_I}{m\mu_M[a\pi\beta\mu_M + \pi\mu_I(a\beta + m\mu_M)]} \left(\frac{e}{a}\right)^m \\ 0 \\ \frac{p\mu_I}{2a\pi\mu_M^2} \\ \frac{p\beta\mu_I}{\mu_M[a\pi\beta\mu_M + \pi\mu_I(a\beta + m\mu_M)]} \left(\frac{e}{a}\right)^m \\ 0 \end{bmatrix} \quad (\text{A1-16})$$

where  $a_0^e, p_0^e, a_m^e$  and  $p_m^e$ ,  $m=1,2,3,\dots$  are the Fourier coefficients of boundary densities for the inclusion. As  $\beta$  approaches infinity, we have

$$\begin{bmatrix} a_0^e \\ a_m^e \\ b_m^e \\ p_0^e \\ p_m^e \\ q_m^e \end{bmatrix} = \lim_{\beta \rightarrow \infty} \begin{bmatrix} -\frac{p\mu_I}{2\pi\mu_M^2} \ln a \\ \frac{p\beta a\mu_I}{m\mu_M[a\pi\beta\mu_M + \pi\mu_I(a\beta + m\mu_M)]} \left(\frac{e}{a}\right)^m \\ 0 \\ \frac{p\mu_I}{2a\pi\mu_M^2} \\ \frac{p\beta\mu_I}{\mu_M[a\pi\beta\mu_M + \pi\mu_I(a\beta + m\mu_M)]} \left(\frac{e}{a}\right)^m \\ 0 \end{bmatrix} = \begin{bmatrix} -\frac{p\mu_I}{2\pi\mu_M^2} \ln a \\ \frac{p\mu_I}{m\mu_M\pi(\mu_M + \mu_I)} \left(\frac{e}{a}\right)^m \\ 0 \\ \frac{p\mu_I}{2a\pi\mu_M^2} \\ \frac{p\mu_I}{\mu_M a\pi(\mu_M + \mu_I)} \left(\frac{e}{a}\right)^m \\ 0 \end{bmatrix} \quad (\text{A1-17})$$

Then, we can obtain the analytical result for static stress ( $\sigma_{zr}^{\star} = a\sigma_{zr}^I / p = a\sigma_{zr}^M / p$ ) of the inclusion as shown below:

$$\sigma_{zr}^{\star} = \frac{a}{p} \sigma_{zr}^M = \frac{\mu_I}{2\pi\mu_M} + \frac{\mu_I}{\pi(\mu_I + \mu_M)} \sum_{m=1}^{\infty} \left(\frac{e}{a}\right)^m \cos m\theta, \quad a > e \quad (\text{A1-18})$$

A closed-form solution can be obtained by using degenerate kernel. By multiplying (a) into Eq. (A1-14), we can also obtain the result of closed-form solution for the inclusion

$$\sigma_{zr}^{\star} = \frac{\mu_I}{\pi(\mu_I + \mu_M)} \left( \frac{a^2 - ea \cos \theta}{e^2 + a^2 - 2ea \cos \theta} \right) + \frac{1}{2\pi} \left( \frac{\mu_I^2 - \mu_M \mu_I}{\mu_M^2 + \mu_M \mu_I} \right), \quad a > e \quad (\text{A1-19})$$

Therefore, we have proved that the closed-form solution can be obtained mathematically by using degenerate kernel. Based on the Fourier series expansion, the closed-form solution of Eq. (A1-19) yields

$$\sigma_{zr}^{\star} = a_0 + \frac{\mu_I}{\pi(\mu_I + \mu_M)} \sum_{m=1}^{\infty} a_m \cos(m\theta), \quad a > e \quad (\text{A1-20})$$

where the Fourier coefficient of  $a_0$  and  $a_m$  can be determined by using the Poisson integral formula as shown below:

$$\begin{aligned} a_m &= \frac{1}{\pi} \int_0^{2\pi} \left( \frac{a^2 - ea \cos \theta}{e^2 + a^2 - 2ea \cos \theta} \right) \cos(m\theta) d\theta \\ &= \frac{1}{\pi} \int_0^{2\pi} \left[ \frac{\left(\frac{a}{e}\right)^2 - \left(\frac{a}{e}\right) \cos \theta}{1 + \left(\frac{a}{e}\right)^2 - 2\left(\frac{a}{e}\right) \cos \theta} \right] \cos(m\theta) d\theta \\ &= \frac{2}{\left(\frac{a}{e}\right)^2 - 1} \frac{\left(\frac{a}{e}\right)^{-m+2} - \left(\frac{a}{e}\right)^{-m}}{2} \\ &= \left(\frac{e}{a}\right)^m \\ &, \quad a > e \end{aligned} \quad (\text{A1-21})$$

$$\begin{aligned} a_0 &= \frac{1}{2\pi} \int_0^{2\pi} \left[ \frac{\mu_I}{\pi(\mu_I + \mu_M)} \left( \frac{a^2 - ea \cos \theta}{e^2 + a^2 - 2ea \cos \theta} \right) + \frac{1}{2\pi} \left( \frac{\mu_I^2 - \mu_M \mu_I}{\mu_M^2 + \mu_M \mu_I} \right) \right] d\theta \\ &= \frac{1}{2\pi} \int_0^{2\pi} \frac{\mu_I}{\pi(\mu_I + \mu_M)} \left[ \frac{\left(\frac{a}{e}\right)^2 - \left(\frac{a}{e}\right) \cos \theta}{1 + \left(\frac{a}{e}\right)^2 - 2\left(\frac{a}{e}\right) \cos \theta} \right] d\theta + \frac{1}{2\pi} \left( \frac{\mu_I^2 - \mu_M \mu_I}{\mu_M^2 + \mu_M \mu_I} \right) \\ &= \frac{\mu_I}{\pi(\mu_I + \mu_M)} \frac{\left(\frac{a}{e}\right)^2 - 1}{\left(\frac{a}{e}\right)^2 - 1} + \frac{1}{2\pi} \left( \frac{\mu_I^2 - \mu_M \mu_I}{\mu_M^2 + \mu_M \mu_I} \right) \\ &= \frac{\mu_I}{2\pi\mu_M} \\ &, \quad a > e \end{aligned} \quad (\text{A1-22})$$

It is straightforward to represent the closed-form solution into Fourier series solution. On the contrary, it always needs special treatment, e.g., Watson transformation if we would obtain the closed-form solution by way of Fourier series solution. Here, we do not employ the Watson transformation, but take advantage of expressions of degenerate kernels for fundamental solution. The contours of shear stress  $\sigma_{zx} = \sigma_{zr} \cos \phi - \sigma_{z\theta} \sin \phi$  and  $\sigma_{zy} = \sigma_{zr} \sin \phi + \sigma_{z\theta} \cos \phi$  for a concentrated force in the matrix and inclusion are summarized in the Table 3-2 and 3-3, respectively.

## Appendix 2 Derivation of the static solutions by using the limiting process ( $k \rightarrow 0$ )

	$z \rightarrow 0$	$z \rightarrow 0$
Asymptotic formula	$J_0(z) \sim 1$	$J_m(z) \sim (\frac{1}{2}z)^m / m!$
	$J_0'(z) \sim -(\frac{1}{2}z)^{-1}$	$J_m'(z) \sim (\frac{1}{2}z)^{m-1} / 2(m-1)!$
	$Y_0(z) \sim (2/\pi) \ln z$	$Y_m(z) \sim -\frac{1}{\pi} (m-1)! (\frac{1}{2}z)^{-m}$
	$Y_0'(z) \sim \frac{1}{\pi} (\frac{1}{2}z)^{-1}$	$Y_m'(z) \sim \frac{m!}{2\pi} (\frac{1}{2}z)^{-m-1}$

Case 1

$$\sigma_{zr}^{\star} = \frac{a}{p} \sigma_{zr}^M = -\frac{a}{p} \mu_M [p_0^e + \sum_{m=1}^{\infty} p_m^e \cos(m\theta)] \text{ for the ideally bonded interface and a concentrated force in the matrix}$$

process

$$\begin{aligned} \lim_{\beta \rightarrow \infty} p_0^e &= \lim_{\beta \rightarrow \infty} \frac{p\beta k_I \mu_I [J_0(k_M e) + iY_0(k_M e)] J_0'(k_I a)}{2\pi a \mu_M \{k_I \mu_I J_0'(k_I a) [-\beta [J_0(k_M a) + iY_0(k_M a)] + k_M \mu_M [J_0'(k_M a) + iY_0'(k_M a)]] + \beta k_M \mu_M J_0(k_I a) [J_0'(k_M a) + iY_0'(k_M a)]]\}} \\ &= \frac{-pk_I \mu_I [J_0(k_M e) + iY_0(k_M e)] J_0'(k_I a)}{2\pi a \mu_M \{k_I \mu_I J_0'(k_I a) [J_0(k_M a) + iY_0(k_M a)] - k_M \mu_M J_0(k_I a) [J_0'(k_M a) + iY_0'(k_M a)]\}} \\ \lim_{k \rightarrow 0} p_0^e &= \lim_{k \rightarrow 0} \frac{-pk_I \mu_I [J_0(k_M e) + iY_0(k_M e)] J_0'(k_I a)}{2\pi a \mu_M \{k_I \mu_I J_0'(k_I a) [J_0(k_M a) + iY_0(k_M a)] - k_M \mu_M J_0(k_I a) [J_0'(k_M a) + iY_0'(k_M a)]\}} \end{aligned}$$

Limiting

$$\begin{aligned}
&= \lim_{k \rightarrow 0} \frac{-pk_I \mu_I [1 + i(2 \ln(k_M e) / \pi)] (-k_I a / 2)}{2\pi a \mu_M \{k_I \mu_I (-k_I a / 2) [1 + i(2 \ln(k_M a) / \pi)] - k_M \mu_M [(2i / k_M a \pi)]\}} \\
&= \frac{0}{\pi \mu_M^2 [(2i / a \pi)]} \\
&= 0
\end{aligned}$$

Limiting process

$$\begin{aligned}
\lim_{\beta \rightarrow \infty} p_m^e &= \lim_{\beta \rightarrow \infty} \frac{p\beta k_I \mu_I [J_m(k_M e) + iY_m(k_M e)] J_m'(k_I a)}{\pi a \mu_M \{k_I \mu_I J_m'(k_I a) [-\beta [J_m(k_M a) + iY_m(k_M a)] + k_M \mu_M [J_m'(k_M a) + iY_m'(k_M a)]] + \beta k_M \mu_M J_m(k_I a) [J_m'(k_M a) + iY_m'(k_M a)]\}} \\
p_m^e &= - \frac{pk_I \mu_I [J_m(k_M e) + iY_m(k_M e)] J_m'(k_I a)}{\pi a \mu_M \{k_I \mu_I J_m'(k_I a) [J_m(k_M a) + iY_m(k_M a)] - k_M \mu_M J_m(k_I a) [J_m'(k_M a) + iY_m'(k_M a)]\}} \\
\lim_{k \rightarrow 0} p_m^e &= \lim_{k \rightarrow 0} - \frac{pk_I \mu_I [J_m(k_M e) + iY_m(k_M e)] J_m'(k_I a)}{\pi a \mu_M \{k_I \mu_I J_m'(k_I a) [J_m(k_M a) + iY_m(k_M a)] - k_M \mu_M J_m(k_I a) [J_m'(k_M a) + iY_m'(k_M a)]\}} \\
&= \lim_{k \rightarrow 0} \frac{pk_I \mu_I}{\pi a \mu_M \left\{ \frac{k_M \mu_M J_m(k_I a) [J_m'(k_M a) + iY_m'(k_M a)]}{[J_m(k_M e) + iY_m(k_M e)] J_m'(k_I a)} - \frac{k_I \mu_I J_m'(k_I a) [J_m(k_M a) + iY_m(k_M a)]}{[J_m(k_M e) + iY_m(k_M e)] J_m'(k_I a)} \right\}} \\
&= \lim_{k \rightarrow 0} \frac{pk_I \mu_I}{\pi a \mu_M \left[ \frac{k_M \mu_M J_m(k_I a) Y_m'(k_M a)}{Y_m(k_M e) J_m'(k_I a)} - \frac{k_I \mu_I Y_m(k_M a)}{Y_m(k_M e)} \right]} \\
&= \lim_{k \rightarrow 0} \frac{p\mu_I}{\pi a \mu_M \left[ \frac{(k_M / k_I) \mu_M [(\frac{1}{2} k_I a)^m / m!] [m! / 2\pi (\frac{1}{2} k_M a)^{m+1}] - \mu_I [-(m-1)! / \pi (\frac{1}{2} k_M a)^m]}{[-(m-1)! / \pi (\frac{1}{2} k_M e)^m] [(\frac{1}{2} k_I a)^{m-1} / 2(m-1)!]} - \frac{\mu_I [-(m-1)! / \pi (\frac{1}{2} k_M e)^m]}{[-(m-1)! / \pi (\frac{1}{2} k_M e)^m]} \right]}
\end{aligned}$$

Limiting process

$$= \frac{p\mu_I}{\pi a\mu_M[-\mu_M(\frac{e}{a})^m - \mu_I(\frac{e}{a})^m]}$$

$$= \frac{-p\mu_I(\frac{a}{e})^m}{\pi a\mu_M(\mu_M + \mu_I)}$$

$$\sigma_{zr}^{\star} = \frac{\mu_I}{\pi(\mu_I + \mu_M)} \sum_{m=1}^{\infty} \left(\frac{a}{e}\right)^m \cos(m\theta)$$

Case 2

$$\sigma_{zr}^{\star} = \frac{a}{p} \sigma_{zr}^M = -\frac{a}{p} \mu_M [p_0^e + \sum_{m=1}^{\infty} p_m^e \cos(m\theta)] \text{ for the ideally bonded interface and a concentrated force in the inclusion}$$

process

$$\lim_{\beta \rightarrow \infty} p_0^e = \lim_{\beta \rightarrow \infty} \frac{p\beta k_M \mu_I J_0(k_I e) [J_0'(k_M a) + iY_0'(k_M a)]}{2\pi a \mu_M \{k_I \mu_I J_0'(k_I a) [-\beta [J_0(k_M a) + iY_0(k_M a)] + k_M \mu_M [J_0'(k_M a) + iY_0'(k_M a)]] + \beta k_M \mu_M J_0(k_I a) [J_0'(k_M a) + iY_0'(k_M a)]\}}$$

$$= \frac{pk_M \mu_I J_0(k_I e) [J_0'(k_M a) + iY_0'(k_M a)]}{2\pi a \mu_M \{-k_I \mu_I J_0'(k_I a) [J_0(k_M a) + iY_0(k_M a)] + k_M \mu_M J_0(k_I a) [J_0'(k_M a) + iY_0'(k_M a)]\}}$$

$$\lim_{k \rightarrow 0} p_0^e = \lim_{k \rightarrow 0} \frac{pk_M \mu_I J_0(k_I e) [J_0'(k_M a) + iY_0'(k_M a)]}{2\pi a \mu_M \{-k_I \mu_I J_0'(k_I a) [J_0(k_M a) + iY_0(k_M a)] + k_M \mu_M J_0(k_I a) [J_0'(k_M a) + iY_0'(k_M a)]\}}$$

Limiting

$$\begin{aligned}
&= \lim_{k \rightarrow 0} \frac{p\mu_I}{2\pi a\mu_M \left\{ -\frac{k_I\mu_I J'_0(k_I a)[J_0(k_M a) + iY_0(k_M a)]}{k_M J_0(k_I e)[J'_0(k_M a) + iY'_0(k_M a)]} + \frac{k_M\mu_M J_0(k_I a)[J'_0(k_M a) + iY'_0(k_M a)]}{k_M J_0(k_I e)[J'_0(k_M a) + iY'_0(k_M a)]} \right\}} \\
&= \lim_{k \rightarrow 0} \frac{p\mu_I}{2\pi a\mu_M \left[ -\frac{k_I\mu_I(-k_I a/2)(2/\pi)\ln(k_M a)}{k_M(2/\pi k_M a)} + \frac{\mu_M J_0(k_I a)}{J_0(k_I e)} \right]} \\
&= \frac{p\mu_I}{2\pi a\mu_M^2}
\end{aligned}$$

Limiting process

$$\begin{aligned}
\lim_{\beta \rightarrow \infty} p_m^e &= \lim_{\beta \rightarrow \infty} \frac{p\beta k_M \mu_I J_m(k_I e)[J'_m(k_M a) + iY'_m(k_M a)]}{\pi a\mu_M \{k_I \mu_I J'_m(k_I a)[- \beta[J_m(k_M a) + iY_m(k_M a)] + k_M \mu_M [J'_m(k_M a) + iY'_m(k_M a)]] + \beta k_M \mu_M J_m(k_I a)[J'_m(k_M a) + iY'_m(k_M a)]\}} \\
p_m^e &= \frac{pk_M \mu_I J_m(k_I e)[J'_m(k_M a) + iY'_m(k_M a)]}{\pi a\mu_M \{-k_I \mu_I J'_m(k_I a)[J_m(k_M a) + iY_m(k_M a)] + k_M \mu_M J_m(k_I a)[J'_m(k_M a) + iY'_m(k_M a)]\}} \\
\lim_{k \rightarrow 0} p_m^e &= \lim_{k \rightarrow 0} \frac{pk_M \mu_I J_m(k_I e)[J'_m(k_M a) + iY'_m(k_M a)]}{\pi a\mu_M \{-k_I \mu_I J'_m(k_I a)[J_m(k_M a) + iY_m(k_M a)] + k_M \mu_M J_m(k_I a)[J'_m(k_M a) + iY'_m(k_M a)]\}} \\
&= \lim_{k \rightarrow 0} \frac{p\mu_I}{\pi a\mu_M \left\{ \frac{-k_I \mu_I J'_m(k_I a)[J_m(k_M a) + iY_m(k_M a)]}{k_M J_m(k_I e)[J'_m(k_M a) + iY'_m(k_M a)]} + \frac{k_M \mu_M J_m(k_I a)[J'_m(k_M a) + iY'_m(k_M a)]}{k_M J_m(k_I e)[J'_m(k_M a) + iY'_m(k_M a)]} \right\}} \\
&= \lim_{k \rightarrow 0} \frac{p\mu_I}{\pi a\mu_M \left[ \frac{-k_I \mu_I J'_m(k_I a)Y_m(k_M a)}{k_M J_m(k_I e)Y'_m(k_M a)} + \frac{\mu_M J_m(k_I a)}{J_m(k_I e)} \right]}
\end{aligned}$$

Limiting process

$$\begin{aligned}
 &= \lim_{k \rightarrow 0} \frac{p\mu_I}{\pi a \mu_M \left[ \frac{-(k_I/k_M)\mu_I [(\frac{1}{2}k_I a)^{m-1} / 2(m-1)!] [-(m-1)! / \pi (\frac{1}{2}k_M a)^m]}{[(\frac{1}{2}k_I e)^m / m!] [m! / 2\pi (\frac{1}{2}k_M a)^{m+1}]} + \frac{\mu_M [(\frac{1}{2}k_I a)^m / m!]}{[(\frac{1}{2}k_I e)^m / m!]} \right]} \\
 &= \frac{p\mu_I}{\pi a \mu_M [\mu_I (\frac{a}{e})^m + \mu_M (\frac{a}{e})^m]} \\
 &= \frac{p\mu_I (\frac{e}{a})^m}{\pi a \mu_M (\mu_M + \mu_I)}
 \end{aligned}$$

---


$$\sigma_{zr}^{\star\star} = \frac{\mu_I}{2\pi\mu_M} + \frac{\mu_I}{\pi(\mu_I + \mu_M)} \sum_{m=1}^{\infty} \left(\frac{a}{e}\right)^m \cos(m\theta)$$


---

### Appendix 3 Special cases of $\beta \rightarrow \infty$ and $\beta = 0$

*Case 1: an ideally bonded case ( $\beta \rightarrow \infty$ )*

As the parameter  $\beta$  approaches  $\infty$ , the interface condition yields the force equilibrium and displacement continuous. Then, we follow the formulation for the Helmholtz problem in Chapter 3. For the problem with inclusion, we can decompose into subsystems of matrix and inclusion after taking free body on the interface as shown in Fig. 3-1(c). By collocating  $x$  on  $(a^-, \phi)$  and  $(a^+, \phi)$  for the matrix and inclusion, respectively, the null-field equations yield Eqs. (3-17) and (3-18). Then, the interface conditions of Eq. (3-5) can be rewritten as

$$u^M = u^I, \text{ on the interface} \quad (\text{A3-1})$$

$$-\mu_M t^M = \mu_I t^I, \text{ on the interface} \quad (\text{A3-2})$$

By assembling the matrices in Eqs. (3-17), (3-18), (A3-1) and (A3-2), we have

$$\begin{bmatrix} T_{11}^M & -U_{11}^M & 0 & 0 \\ 0 & 0 & T_{11}^I & -U_{11}^I \\ 0 & \mu_M & 0 & \mu_I \\ I & 0 & -I & 0 \end{bmatrix} \begin{bmatrix} u_1^M \\ t_1^M \\ u_1^I \\ t_1^I \end{bmatrix} = \begin{bmatrix} \frac{P}{\mu_M} U(\xi, x) \\ 0 \\ 0 \\ 0 \end{bmatrix} \quad (\text{A3-3})$$

After rearranging Eq. (A3-3), we have

$$\begin{bmatrix} T_{11}^M & -U_{11}^M \\ T_{11}^I & \frac{\mu_M}{\mu_I} U_{11}^I \end{bmatrix} \begin{bmatrix} u_1^M \\ t_1^M \end{bmatrix} = \begin{bmatrix} \frac{P}{\mu_M} U(\xi, x) \\ 0 \end{bmatrix} \quad (\text{A3-4})$$

The unknown coefficients in the algebraic system can be determined as shown below:

$$\begin{aligned} a_0^e = & -pJ_0(k_I a)[J_0(k_M e) + iY_0(k_M e)] / 2\pi a \{-k_I \mu_I J_0'(k_I a) \\ & [J_0(k_M a) + iY_0(k_M a)] + k_M \mu_M J_0(k_I a)[J_0'(k_M a) + iY_0'(k_M a)]\} \end{aligned} \quad (\text{A3-5})$$

$$\begin{aligned} p_0^e = & -pk_I \mu_I J_0'(k_I a)[J_0(k_M e) + iY_0(k_M e)] / 2\pi a \mu_M \{k_I \mu_I J_0'(k_I a) \\ & [J_0(k_M a) + iY_0(k_M a)] - k_M \mu_M J_0(k_I a)[J_0'(k_M a) + iY_0'(k_M a)]\} \end{aligned} \quad (\text{A3-6})$$

$$\begin{aligned} a_m^e = & -pJ_m(k_I a)[J_m(k_M e) + iY_m(k_M e)] / \pi a \{-k_I \mu_I J_m'(k_I a) \\ & [J_m(k_M a) + iY_m(k_M a)] + k_M \mu_M J_m(k_I a)[J_m'(k_M a) + iY_m'(k_M a)]\} \end{aligned} \quad (\text{A3-7})$$

$$p_m^e = -pk_I \mu_I J_m'(k_I a) [J_m(k_M a) + iY_m(k_M a)] / \pi a \mu_M \{k_I \mu_I J_m'(k_I a) [J_m(k_M a) + iY_m(k_M a)] - k_M \mu_M J_m(k_I a) [J_m'(k_M a) + iY_m'(k_M a)]\} \quad (\text{A3-8})$$

where  $a_0^e, p_0^e, a_m^e$  and  $p_m^e$ ,  $m = 1, 2, 3, \dots$  are the Fourier coefficients of boundary densities for the matrix. According to the interface boundary condition of Eqs. (A3-1) and (A3-2), we obtain the coefficient of the inclusion as shown below:

$$\begin{Bmatrix} a_0^i \\ p_0^i \end{Bmatrix} = \begin{Bmatrix} a_0^e \\ -\mu_M p_0^e / \mu_I \end{Bmatrix} \quad (\text{A3-9})$$

$$\begin{Bmatrix} a_m^i \\ p_m^i \end{Bmatrix} = \begin{Bmatrix} a_m^e \\ -\mu_M p_m^e / \mu_I \end{Bmatrix} \quad (\text{A3-10})$$

where  $a_0^i, p_0^i, a_m^i$  and  $p_m^i$  are the Fourier coefficients of boundary densities for the inclusion. Then, we can obtain the series-form Green's function for the matrix and the inclusion, respectively, by applying Eq. (3-9) to have

$$G(x, \xi) = -\frac{\pi a}{2} [a_0^e k_M J_0'(k_M a) + p_0^e J_0(k_M a)] [Y_0(k_M \rho) - iJ_0(k_M \rho)] - \frac{\pi a}{2} \sum_{m=1}^{\infty} [a_m^e k_M J_m'(k_M a) + p_m^e J_m(k_M a)] [Y_m(k_M \rho) - iJ_m(k_M \rho)] \cos(m\phi) - \frac{p}{4\mu_M} [Y_0(k_M r) - iJ_0(k_M r)], \quad a \leq \rho < \infty \quad (\text{A3-11})$$

$$G(x, \xi) = \frac{\pi a}{2} J_0(k_I \rho) \{a_0^i k_I [Y_0'(k_I a) - iJ_0'(k_I a)] - p_0^i [Y_0(k_I a) - iJ_0(k_I a)]\} - \frac{\pi a}{2} J_m(k_I \rho) \{a_m^i k_I [Y_m'(k_I a) - iJ_m'(k_I a)] - p_m^i [Y_m(k_I a) - iJ_m(k_I a)]\} \cos(m\phi), \quad 0 < \rho < a \quad (\text{A3-12})$$

The absolute amplitude of potential  $|u|$  for the ideally bonded case and for the parameter ( $\beta = 10^{32}$ ) are shown in Figs. (3-12) and (3-13). Good agreement is made.

### Case 2: a cavity case ( $\beta = 0$ )

As the parameter  $\beta$  is zero as shown in Fig. (3-14), the circular inclusion is fully debonded from the matrix. Similarly as shown in the case 1, we can obtain the unknown coefficients as shown below:

$$\begin{bmatrix} a_0^e \\ a_m^e \end{bmatrix} = \begin{bmatrix} -p \frac{Y_0(k_M e) - iJ_0(k_M e)}{2k_M \pi a \mu_M} \frac{Y_0'(k_M a) - iJ_0'(k_M a)}{Y_0(k_M e) - iJ_0(k_M e)} \\ -p \frac{Y_m(k_M e) - iJ_m(k_M e)}{k_M \pi a \mu_M} \frac{Y_m'(k_M a) - iJ_m'(k_M a)}{Y_m(k_M e) - iJ_m(k_M e)} \end{bmatrix} \quad (\text{A3-13})$$

where  $a_0^e$  and  $a_m^e$ ,  $m = 1, 2, 3, \dots$  are the Fourier coefficients of boundary densities for the matrix. Then, we can obtain the series-form Green's function for the matrix by applying Eq. (3-9) to have

$$\begin{aligned} G(x, \xi) = & -\frac{\pi a}{2} a_0^e k_M J_0'(k_M a) [Y_0(k_M \rho) - iJ_0(k_M \rho)] \\ & -\frac{\pi a}{2} \sum_{m=1}^{\infty} a_m^e k_M J_m'(k_M a) [Y_m(k_M \rho) - iJ_m(k_M \rho)] \cos(m\phi) \\ & -\frac{p}{4\mu_M} [Y_0(k_M r) - iJ_0(k_M r)], \quad a \leq \rho < \infty \end{aligned} \quad (\text{A3-14})$$

The absolute amplitude of potential  $|u|$  for the cavity case and for the parameter ( $\beta = 10^{-32}$ ) are shown in Figs. (3-15) and (3-16). Good agreement is also made.

## Number of Papers of FEM, BEM and FDM

Numerical method	Search phrase in topic field	No. of entries	
FEM	‘Finite element’ or ‘finite elements’	66,237	6
FDM	‘Finite difference’ or ‘finite differences’	19,531	2
BEM	‘Boundary element’ or ‘boundary elements’ or ‘boundary integral’	10,126	1
FVM	‘Finite volume method’ or ‘finite volume methods’	1695	
CM	‘Collocation method’ or ‘collocation methods’	1615	

**Table 1-1** Bibliographic database search based on the Web of Science [Cheng A. H. D. (2005)]

BIE		Original problem and auxiliary system	
Present method	$2\pi G(x, \xi) = \int_B T(s, x) G(s, \xi) dB(s) - \int_B U(s, x) \frac{\partial G(s, \xi)}{\partial n_s} dB(s) + U(\xi, x), \quad x \in D \cup B$ <div style="border: 1px dashed red; padding: 5px; margin: 10px auto; width: fit-content;"> <p style="text-align: center; color: red;">Degenerate (separate) form</p> </div> $0 = \int_B T(s, x) G(s, \xi) dB(s) - \int_B U(s, x) \frac{\partial G(s, \xi)}{\partial n_s} dB(s) + U(\xi, s), \quad x \in D^c \cup B$		
Conventional BEM	$2\pi G(x, \xi) = \int_B T(s, x) G(s, \xi) dB(s) - \int_B U(s, x) \frac{\partial G(s, \xi)}{\partial n_s} dB(s) + U(\xi, x), \quad x \in D$ $\pi G(x, \xi) = C.P.V. \int_B T(s, x) G(s, \xi) dB(s) - R.P.V. \int_B U(s, x) \frac{\partial G(s, \xi)}{\partial n_s} dB(s) + U(\xi, x), \quad x \in B$ $0 = \int_B T(s, x) G(s, \xi) dB(s) - \int_B U(s, x) \frac{\partial G(s, \xi)}{\partial n_s} dB(s) + U(\xi, x), \quad x \in D^c$		

where CPV and RPV are the Cauchy principal value and Riemann principal value, respectively. It is noted that the kernel in the present method should be properly expanded in terms interior and exterior expansion of degenerate kernels

**Table 2-1** Comparisons of the BIE between the conventional BIEM and the present method

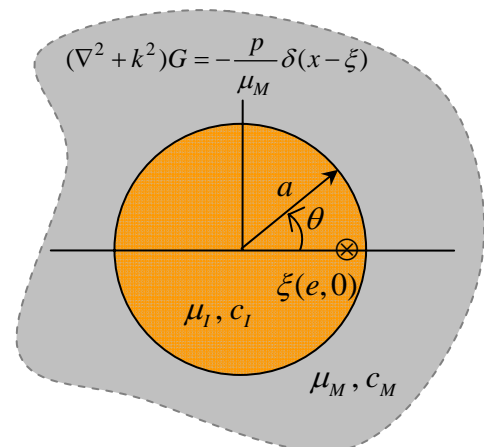
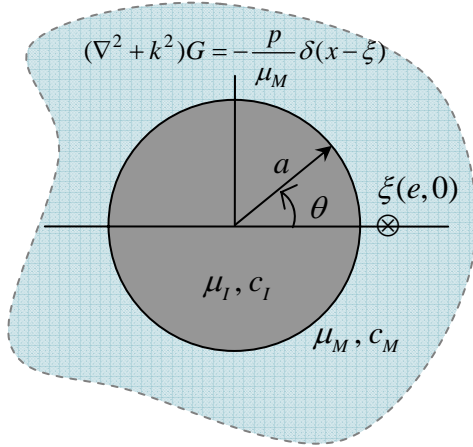
**Table 2-2** Comparison of the numerical results

Field point, $y$	MCP			MMP			Present Method		
	Partitioning number, $k$ [Melnikov and Melnikov (2001)]						Fourier term, $M$		
	$2k \times 2k$			$k \times k$			$2(2M + 1) \times 2(2M + 1)$		
	10	20	50	10	20	50	10	20	50
0	0.000280	0.000128	0.000067	0.000107	0.000049	0.000032	0.000000	0.000000	0.000000
0.2	0.010667	0.010712	0.010781	0.010700	0.010779	0.010798	0.010832	0.010832	0.010832
0.4	0.062359	0.062411	0.062443	0.062407	0.062435	0.062448	0.062458	0.062462	0.062462
0.6	0.177534	0.177574	0.177585	0.177583	0.177590	0.177593	0.177597	0.177596	0.177596
0.8	0.317893	0.317902	0.317911	0.317907	0.317913	0.317914	0.318032	0.317915	0.317915
1.0	0.000014	0.000006	0.000002	0.000000	0.000000	0.000000	0.002014	0.000064	0.000000

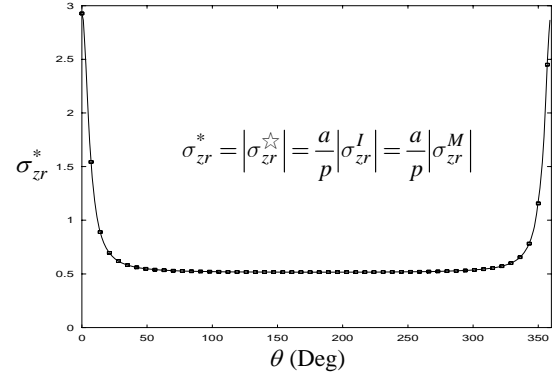
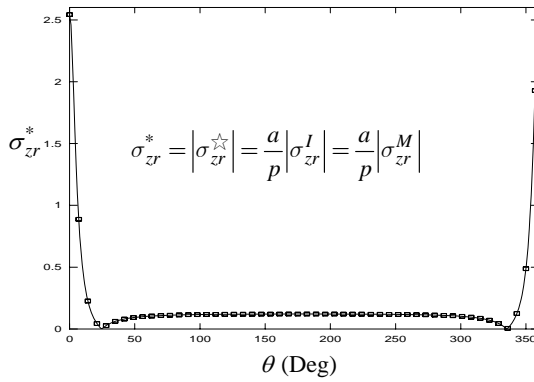
**Table 3-1** Series-form & closed-form solutions for the static case (ideally bonded interface)

Concentrated force in the matrix    Concentrated force in the inclusion

Problem statement



Stress distribution along the interface



Closed-form solution

$$\sigma_{zr}^{\star} = \frac{\mu_I}{\pi(\mu_I + \mu_M)} \left( \frac{ea \cos \theta - a^2}{e^2 + a^2 - 2ea \cos \theta} \right)$$

[Wang and Sudak, (2007)]

$$\sigma_{zr}^{\star} = \frac{\mu_I}{\pi(\mu_I + \mu_M)} \left( \frac{a^2 - ea \cos \theta}{e^2 + a^2 - 2ea \cos \theta} \right) + \frac{1}{2\pi} \left( \frac{\mu_I^2 - \mu_M \mu_I}{\mu_M^2 + \mu_M \mu_I} \right)$$

Series-form solution

$$\sigma_{zr}^{\star} = \frac{\mu_I}{\pi(\mu_I + \mu_M)} \sum_{m=1}^{\infty} \left( \frac{a}{e} \right)^m \cos m\theta$$

$$\sigma_{zr}^{\star} = \frac{\mu_I}{2\pi\mu_M} + \frac{\mu_I}{\pi(\mu_I + \mu_M)} \sum_{m=1}^{\infty} \left( \frac{e}{a} \right)^m \cos m\theta$$

**Table 3-2** Stress contours of  $\sigma_{zx}$  and  $\sigma_{zy}$  for the static and dynamic solutions (a concentrated force in the matrix)

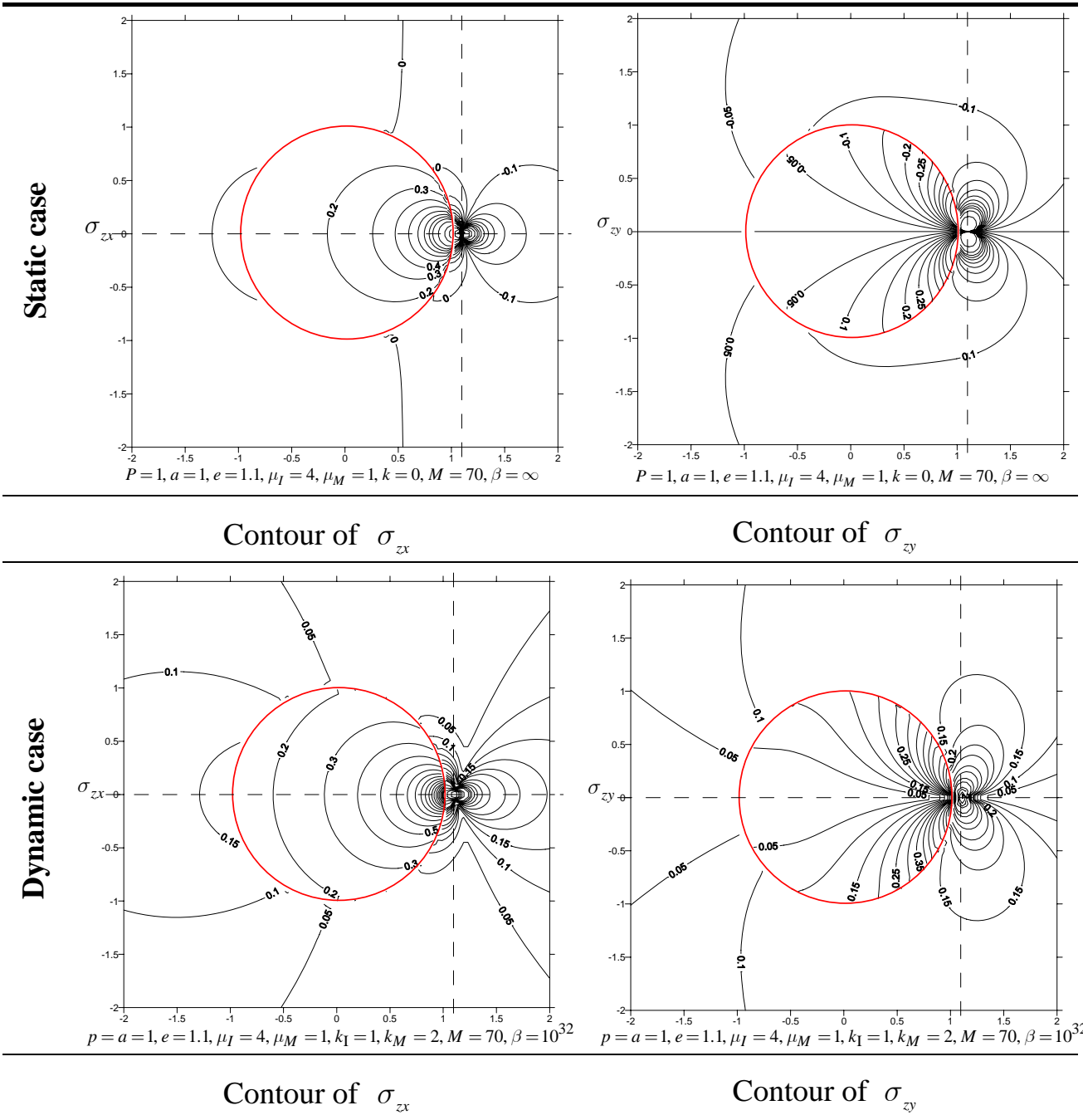
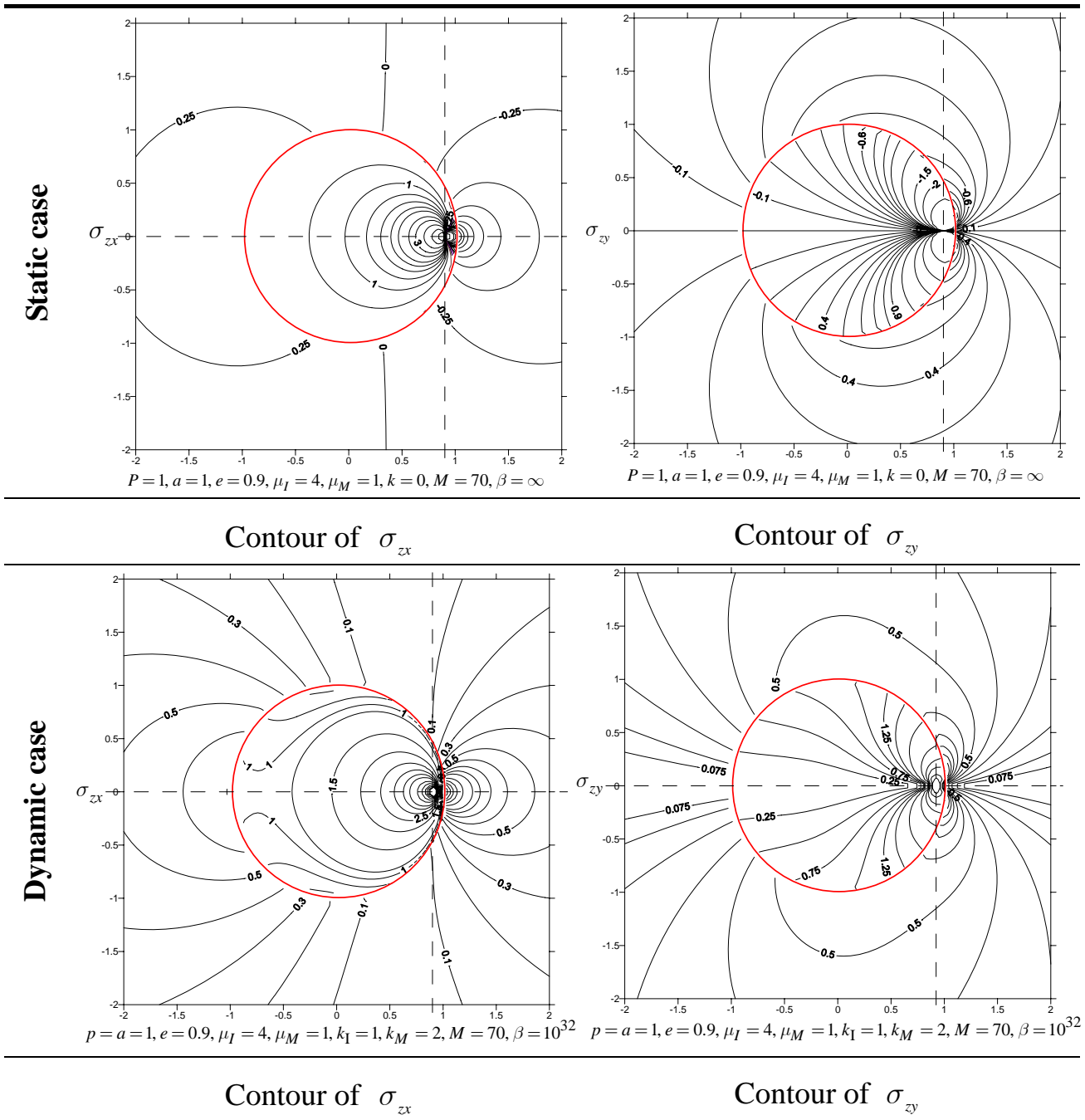
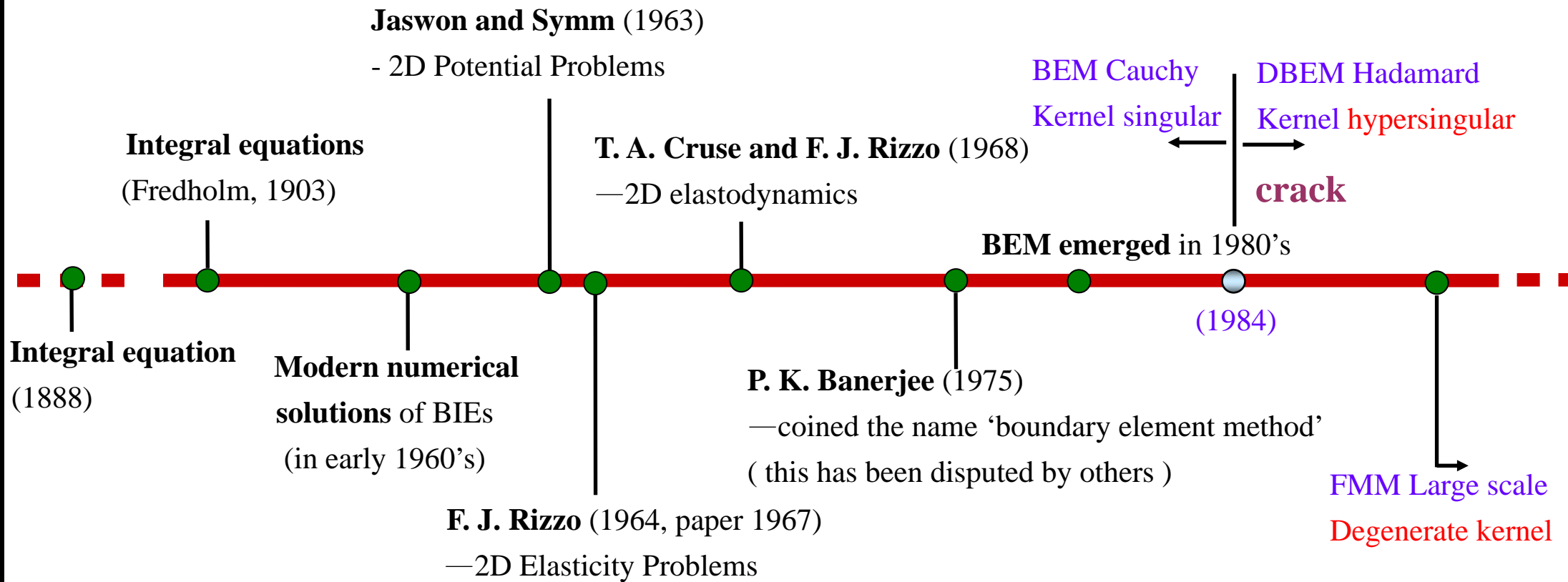


**Table 3-3** Stress contours of  $\sigma_{zx}$  and  $\sigma_{zy}$  for the static and dynamic solutions (a concentrated force in the inclusion)



# A Brief History of the BEM



Original data from Prof. Liu Y J

Figure 1-1 A brief history of the BEM

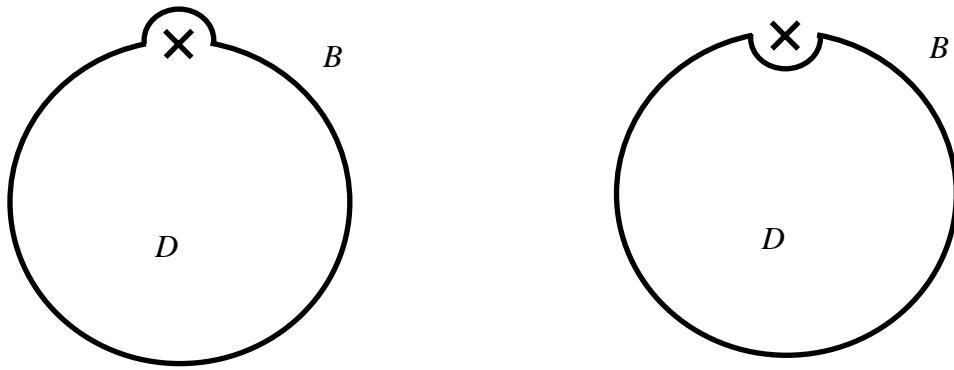


**Figure 1-2 (a)** Bump contour

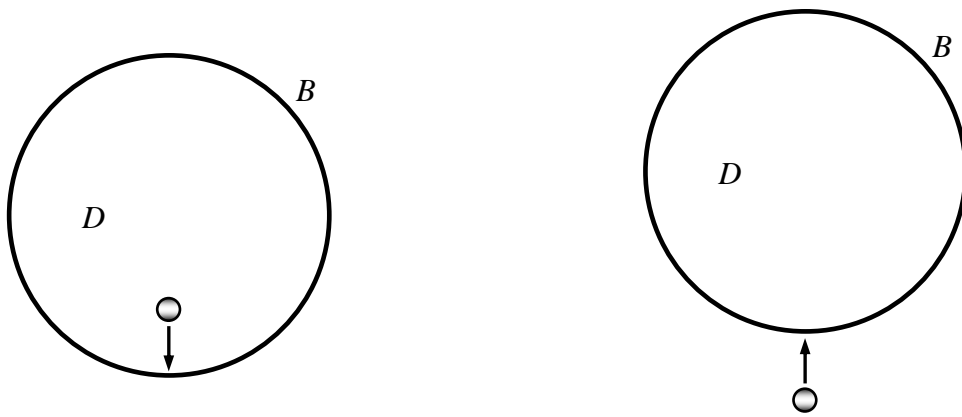


**Figure 1-2 (b)** Limiting process

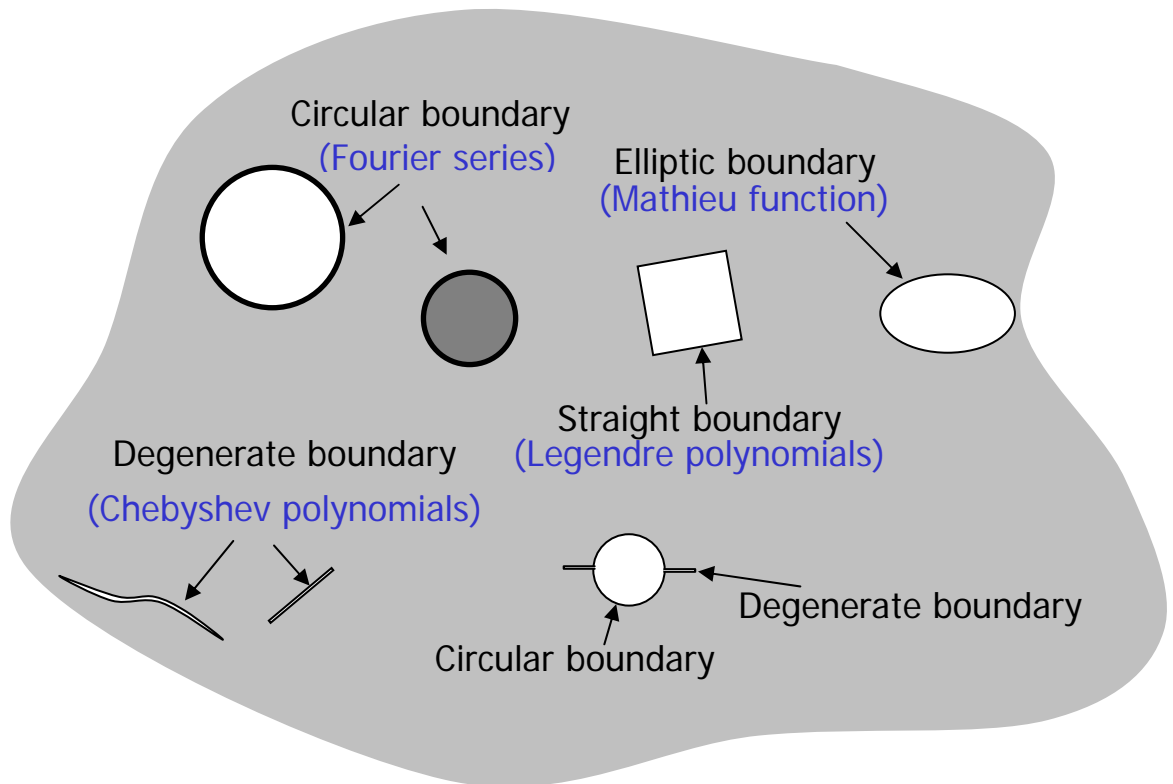


**Figure 1-3** The boundary value problems with arbitrary boundaries

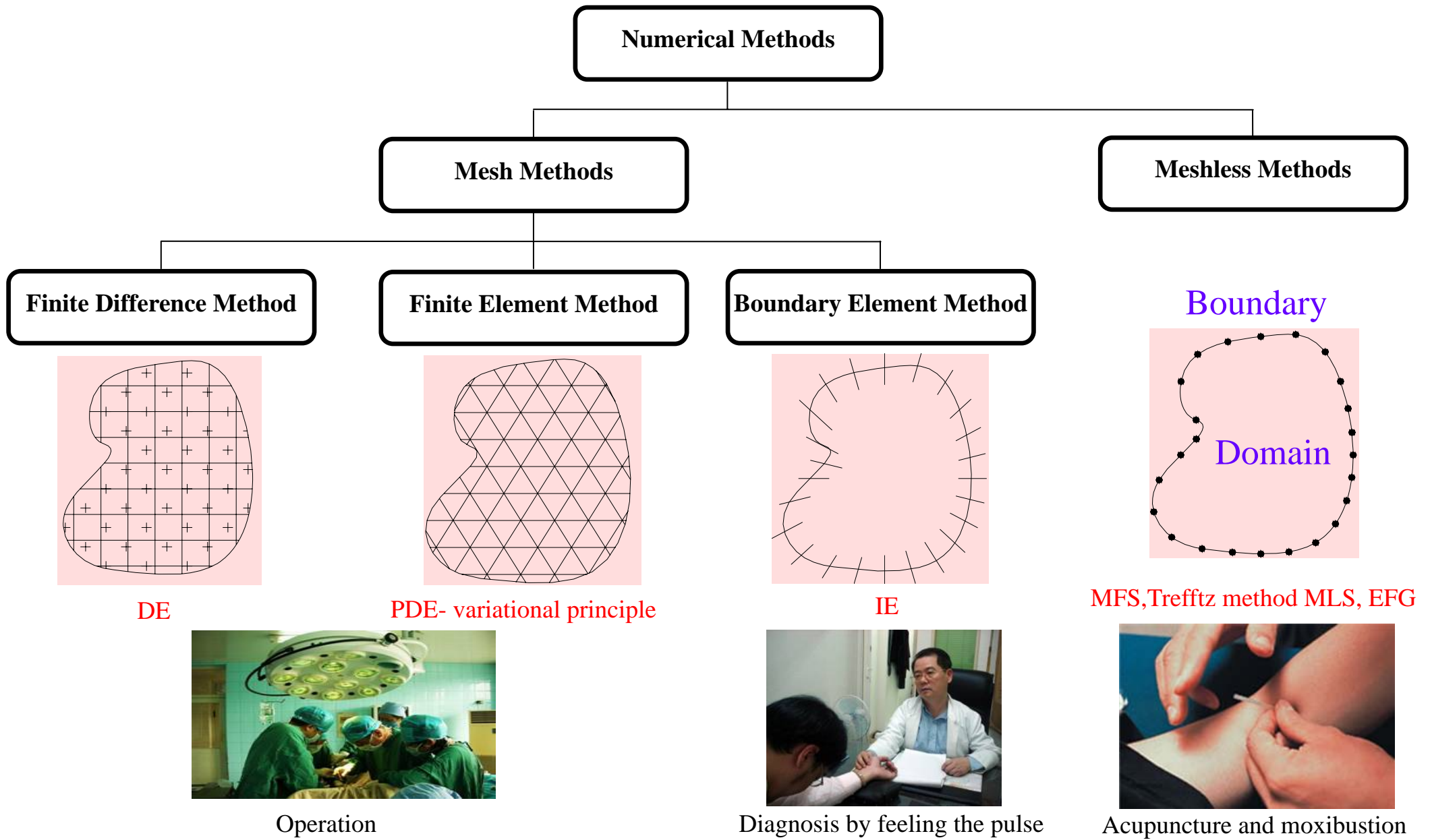


**Figure 1-4** Mesh generation [Chen and Lee (2007)]

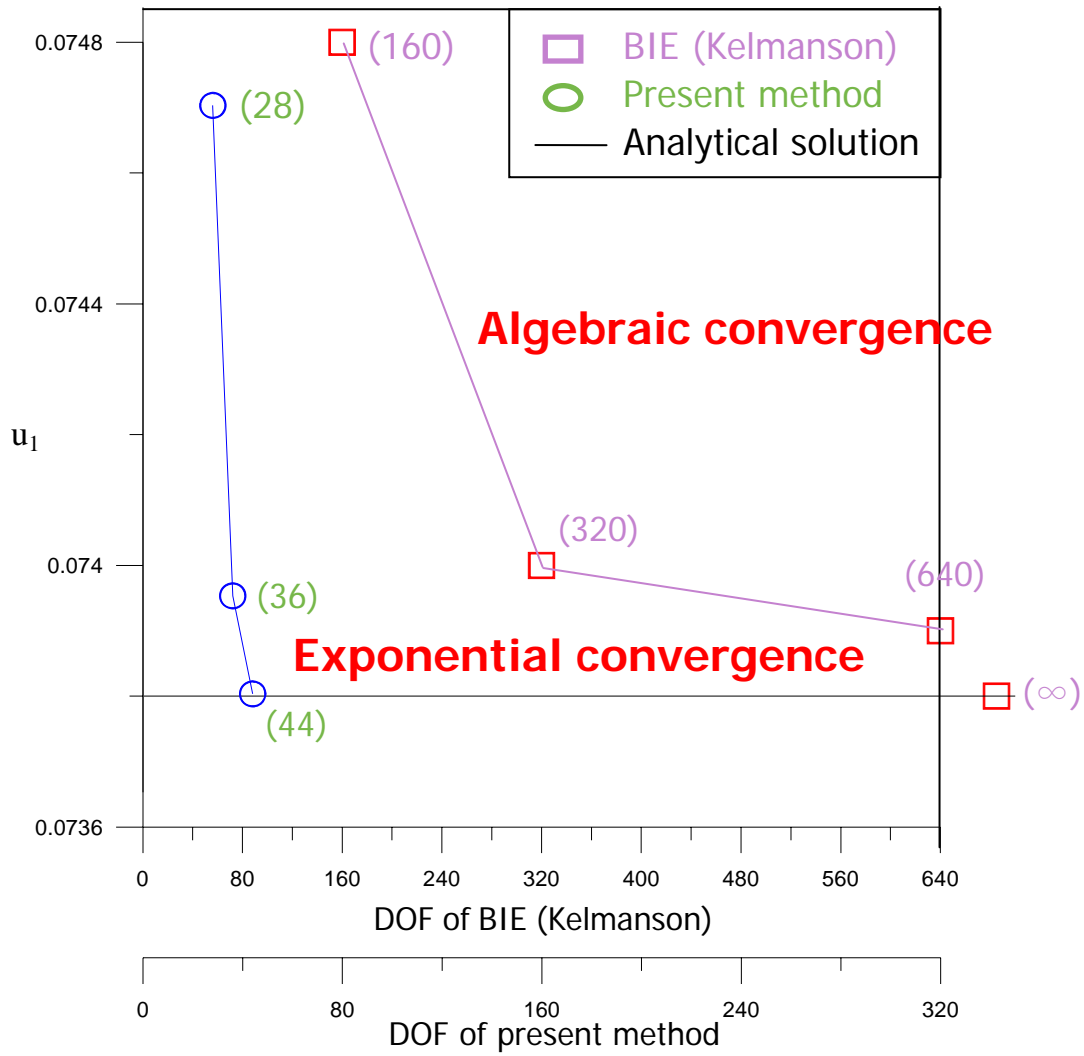


**Figure 1-5** Convergence test [Hsiao (2005)]

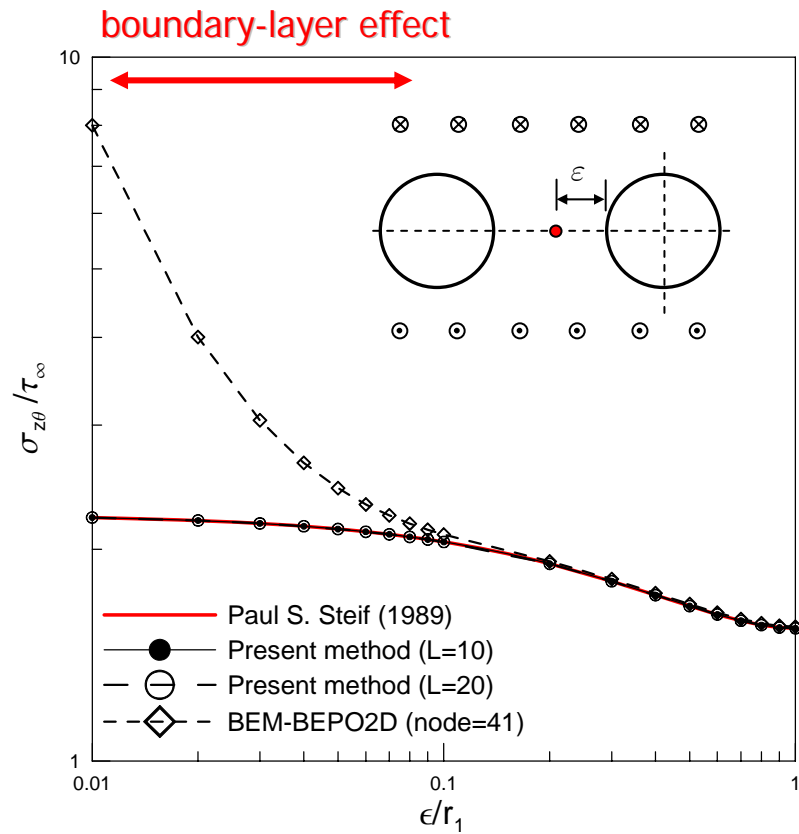
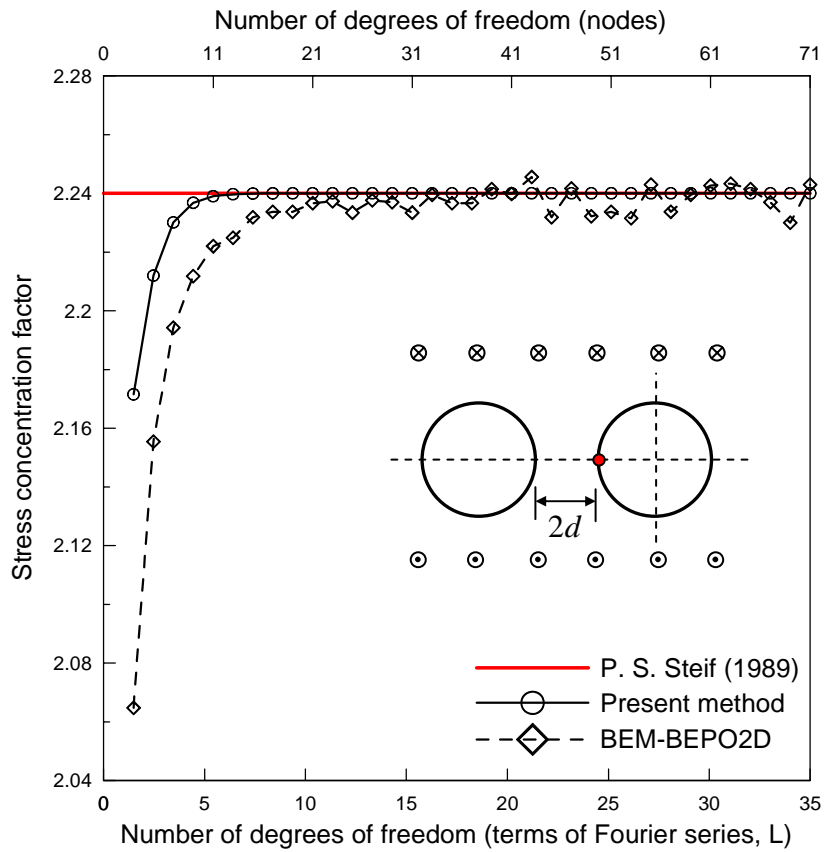


**Figure 1-6** Boundary-layer effect analysis [Wu (2006)]

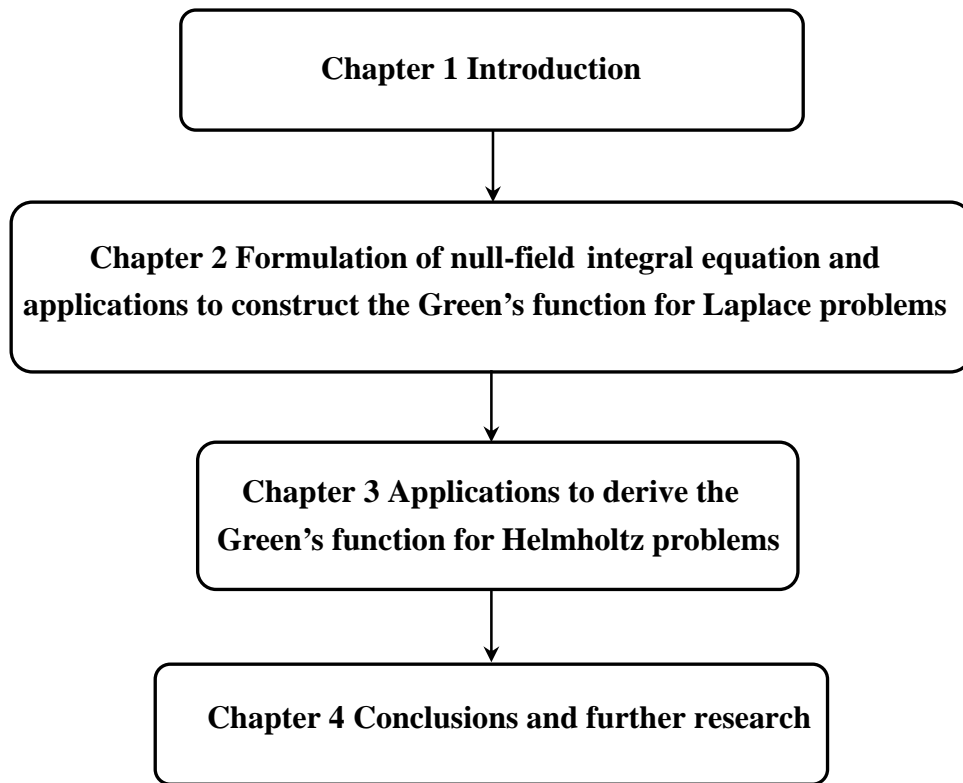


**Figure 1-7** The frame of the thesis

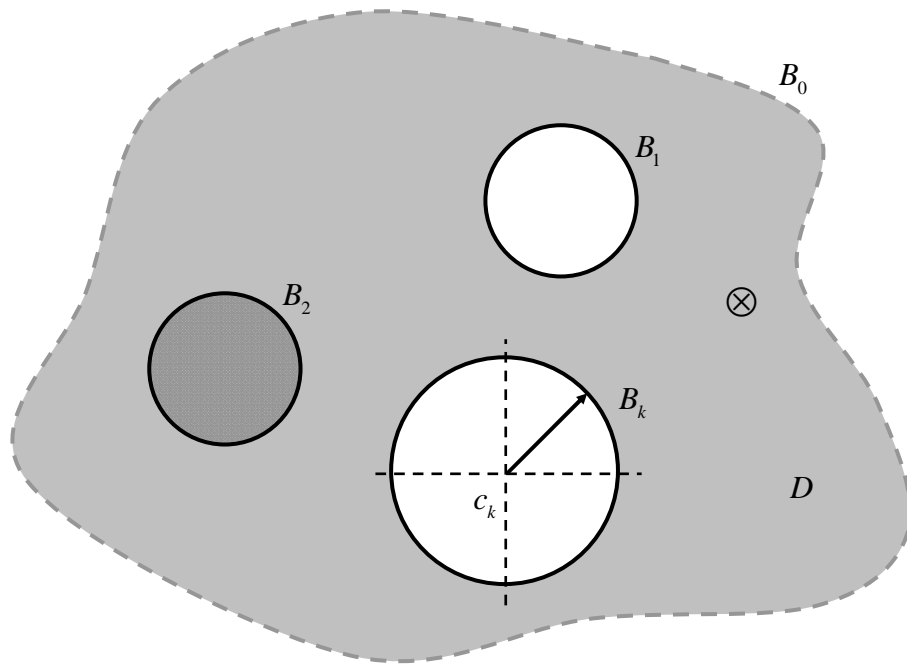


**Figure 2-1** Problem statement

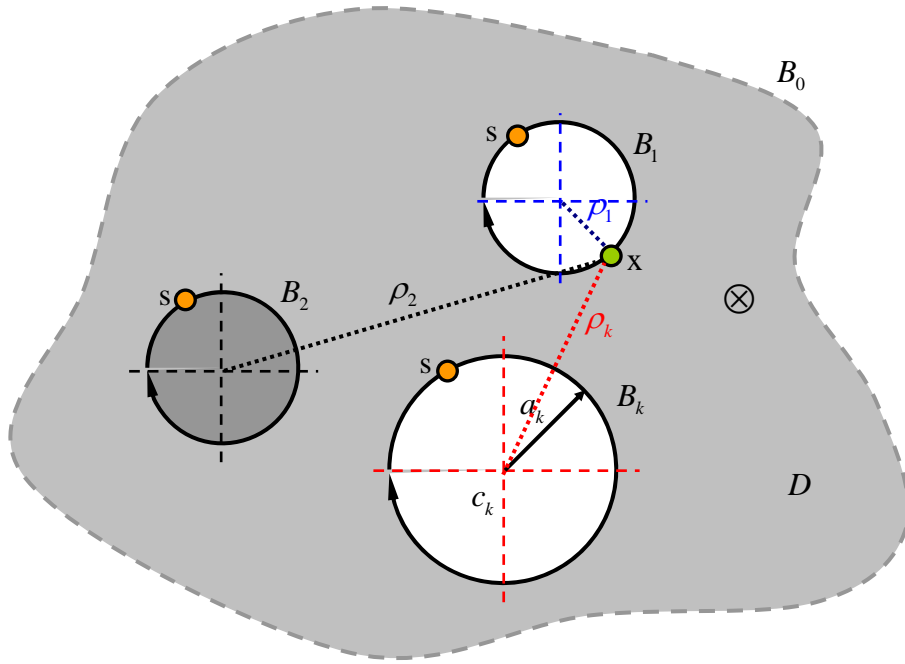


**Figure 2-2 (a)** Sketch of the null-field integral equation in conjunction with the adaptive observer system

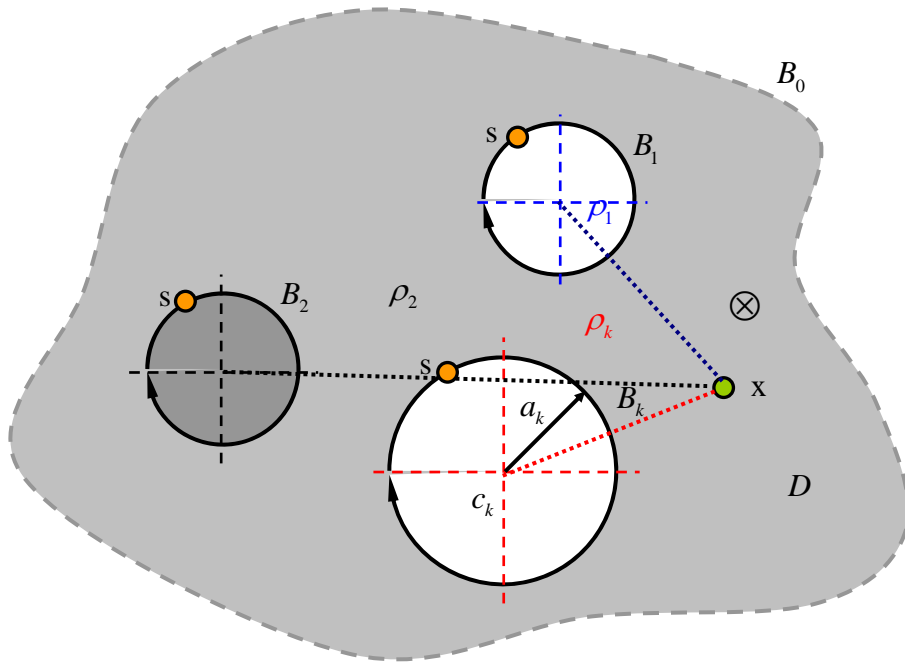


**Figure 2-2 (b)** Sketch of the boundary integral equation for the domain point in conjunction with the adaptive observer system

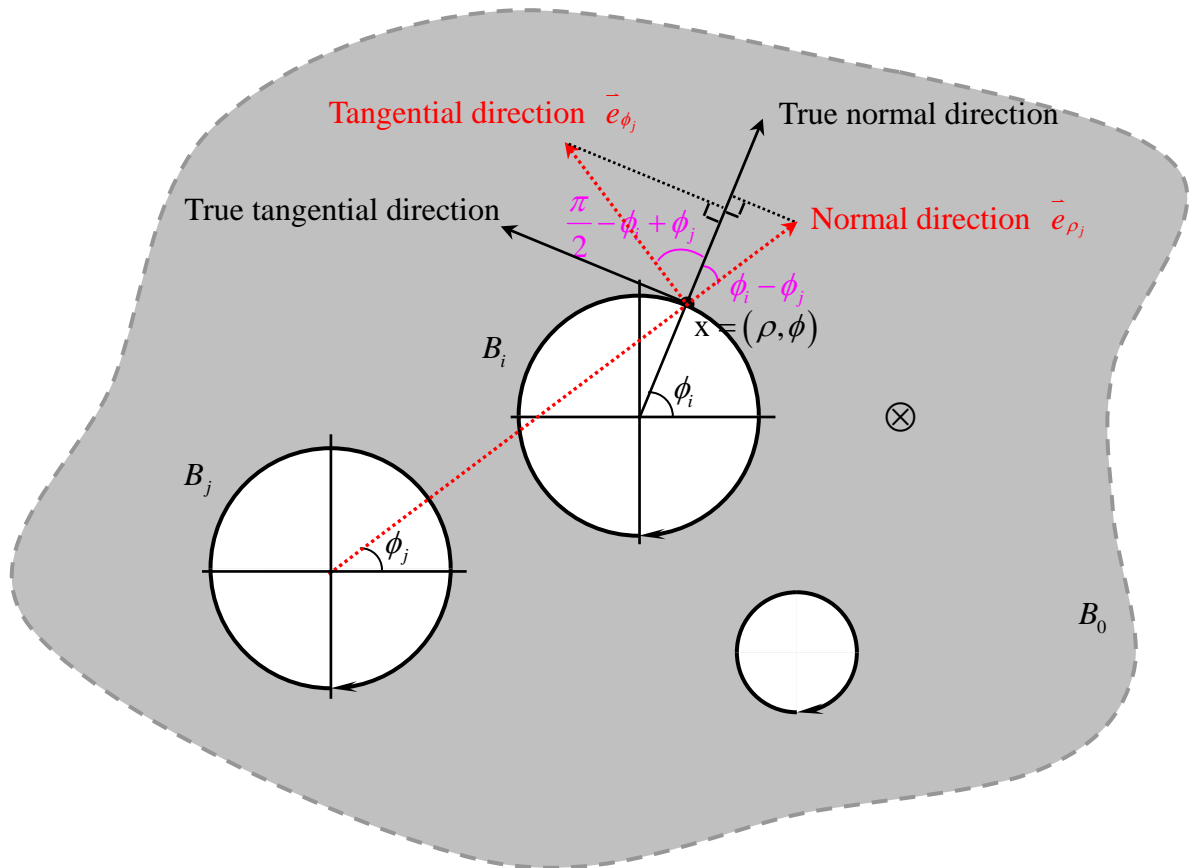


**Figure 2-3** Vector decomposition for the potential gradient in the hypersingular equation (collocation point  $x$  integration on  $B_j$ )

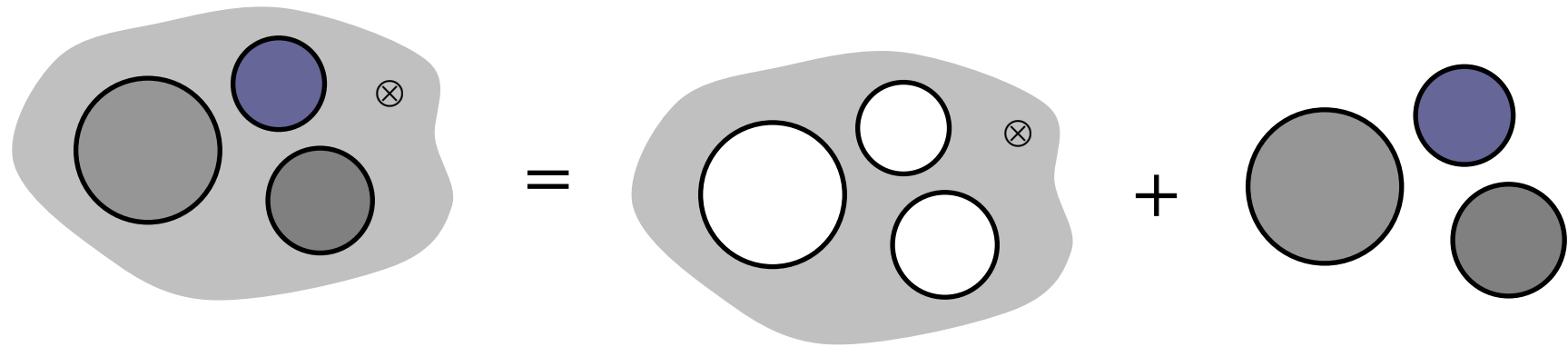


**Figure 2-4** Decomposition of the inclusion problem using the subdomain approach by taking free body

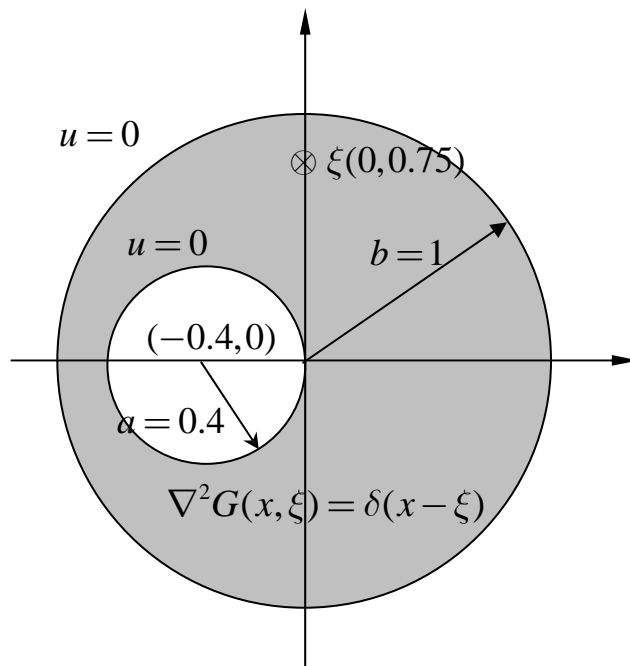


**Figure 2-5(a)** Green's function for the eccentric ring

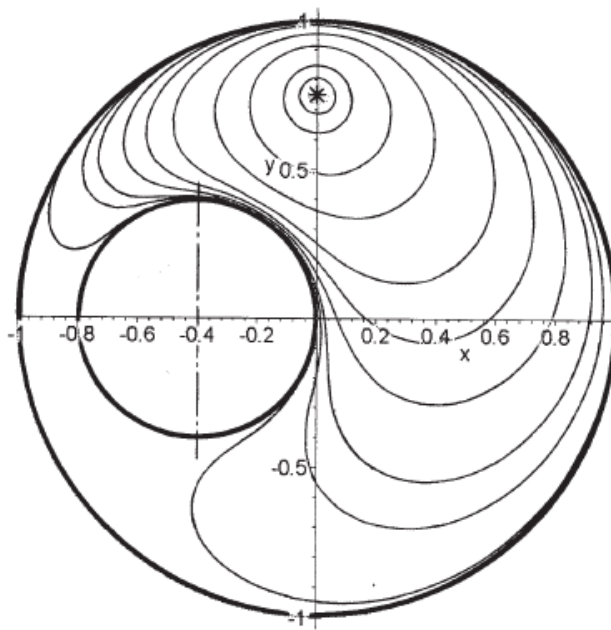


**Figure 2-5(b)** Potential contour using the Melnikov's method [Melnikov and Melnikov (2001)]

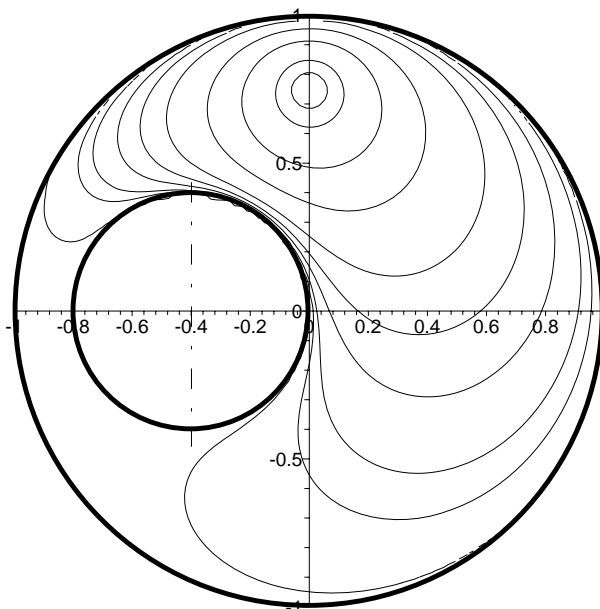


**Figure 2-5(c)** Potential contour using the present method (M=50)

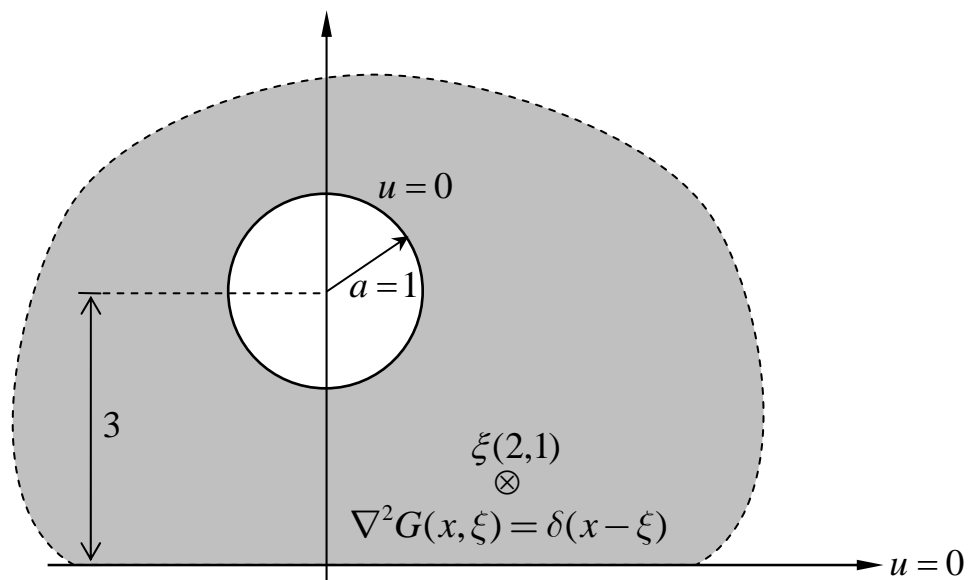


**Figure 2-6(a)** Green's function for the half-plane with an aperture

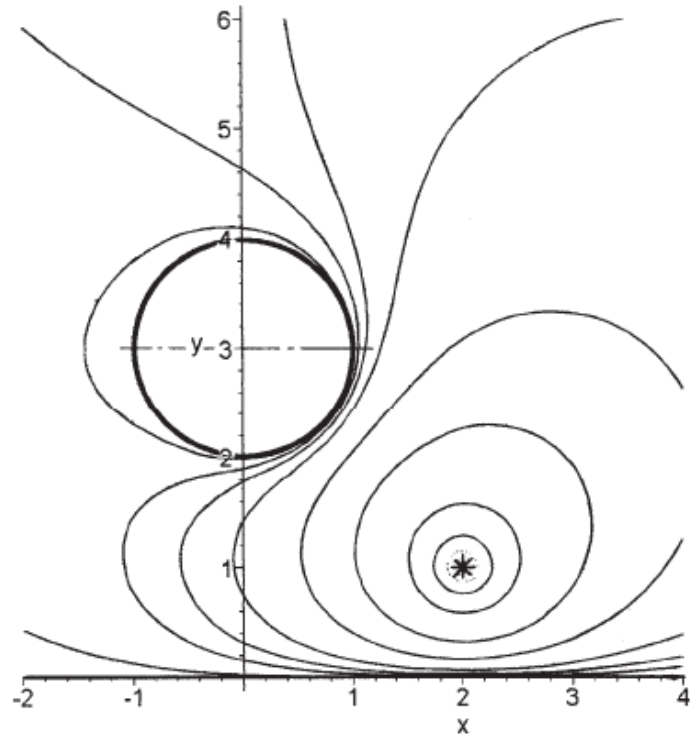


**Figure 2-6(b)** Potential contour using the Melnikov's method [Melnikov and Melnikov (2001)]

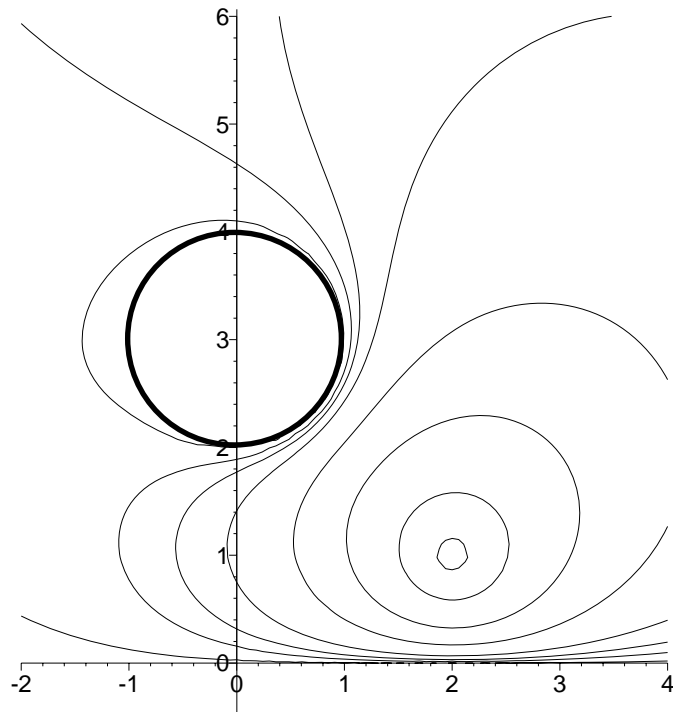


**Figure 2-6(c)** Potential contour using the present method (M=50)

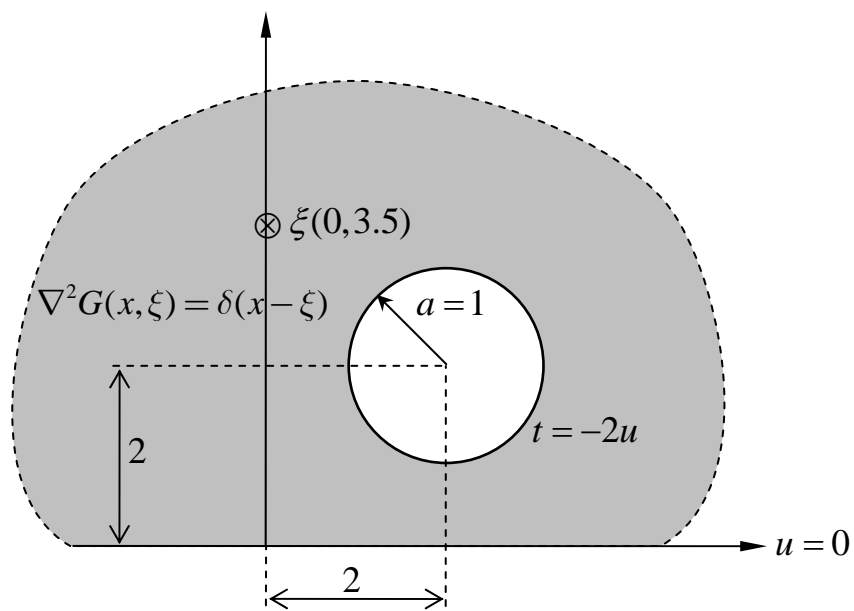


**Figure 2-7(a)** Green's function for the half-plane problem with the Robin boundary condition

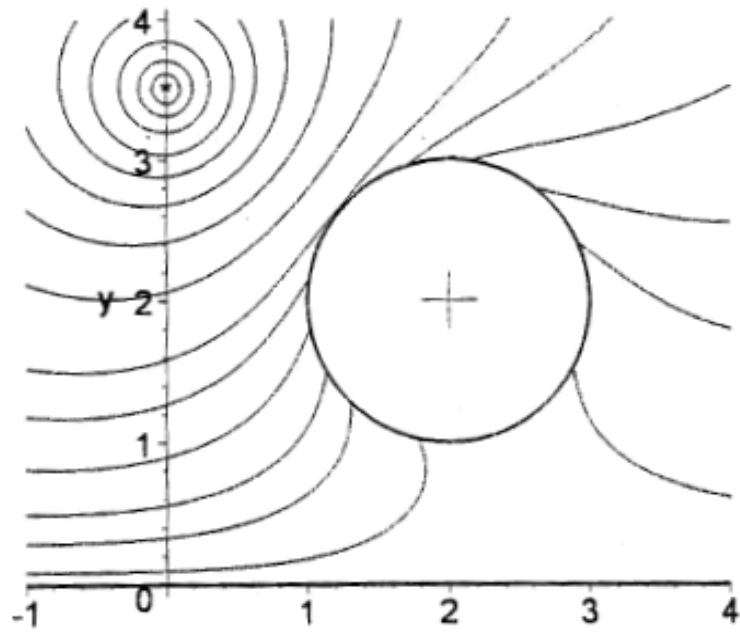


**Figure 2-7(b)** Potential contour by using the Melnikov's approach [Melnikov and Melnikov (2006)]

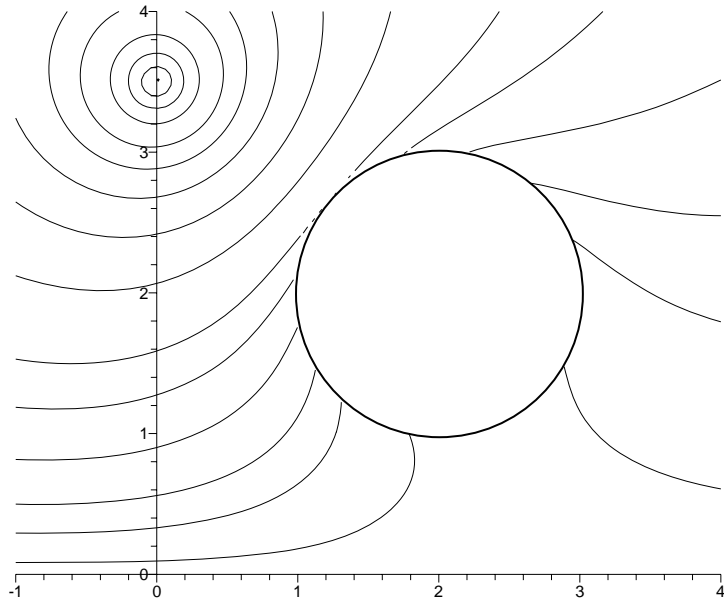


**Figure 2-7(c)** Potential contour by using the null-field integral equation approach (M=50)

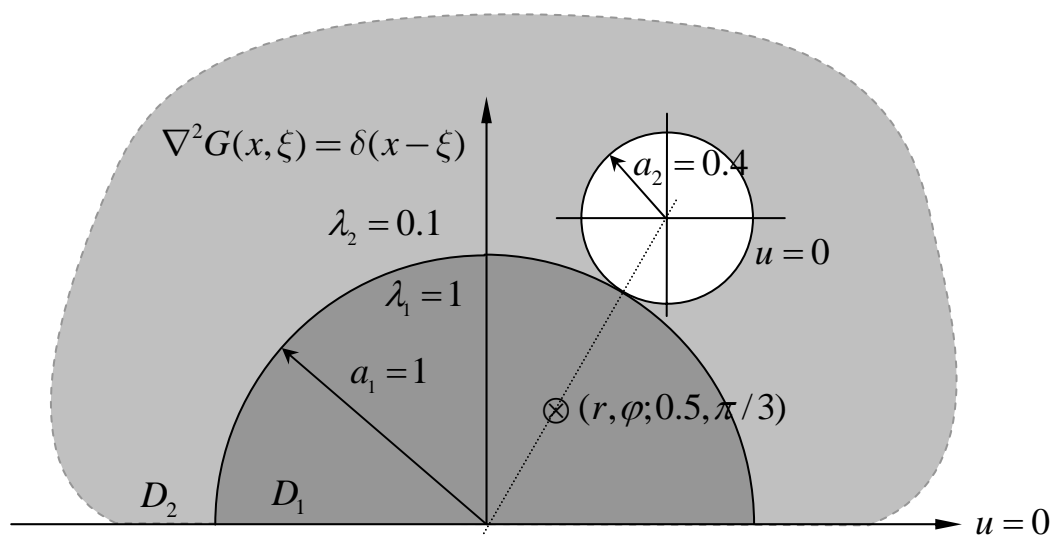


**Figure 2-8(a)** Problem sketch of half-plane problem with a circular hole and a semi-circular inclusion

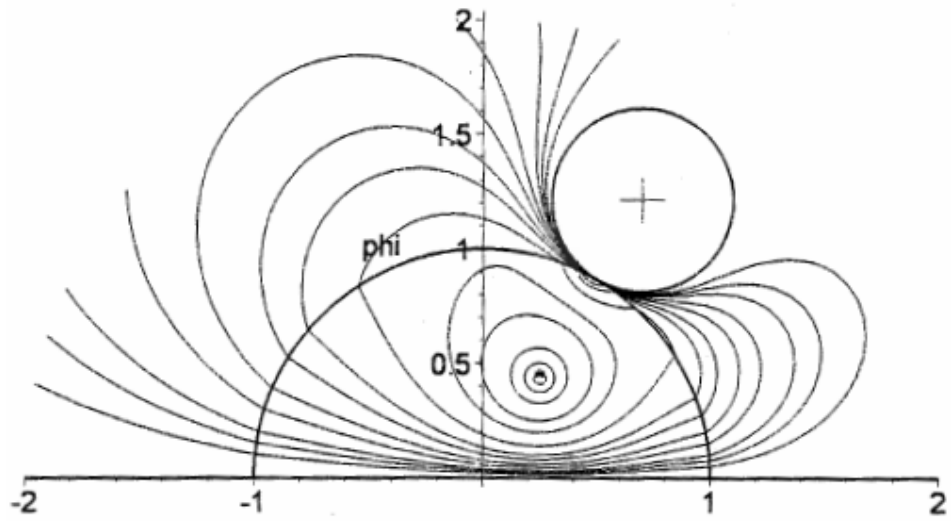


**Figure 2-8(b)** Potential contour by using the Melnikov's method approach  
[Melnikov and Melnikov (2006)]

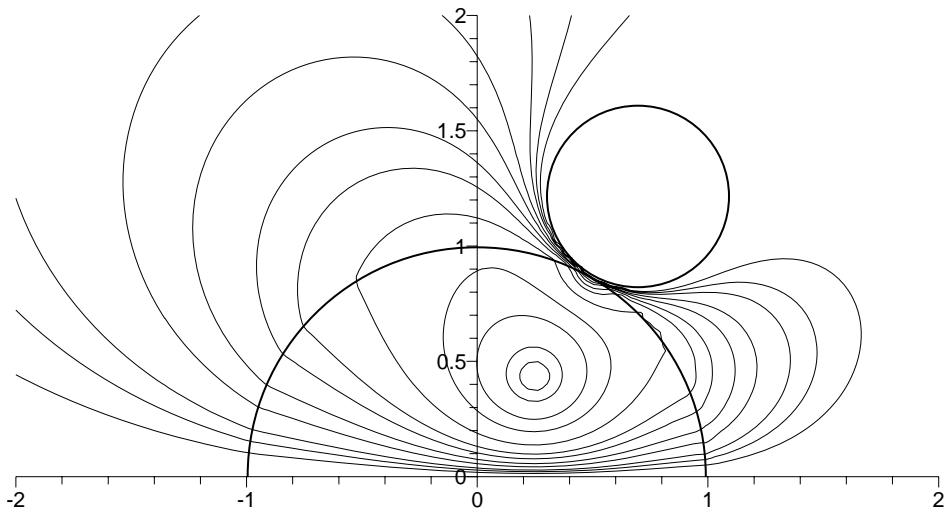


**Figure 2-8(c)** Potential contour by using the null-field integral equation approach  
( $M=50$ )

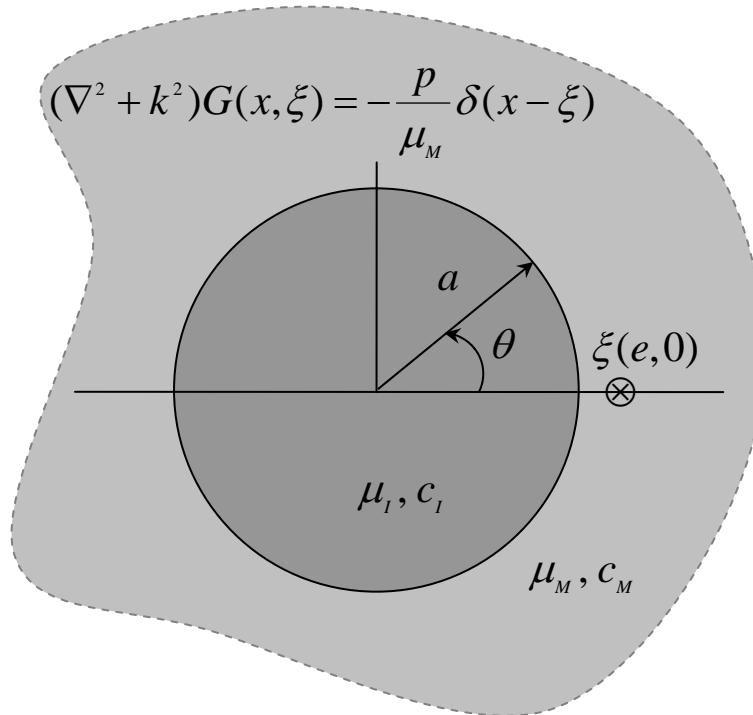


**Figure 3-1(a)** An infinite matrix containing a circular inclusion with a concentrated force at  $\xi$  in the matrix

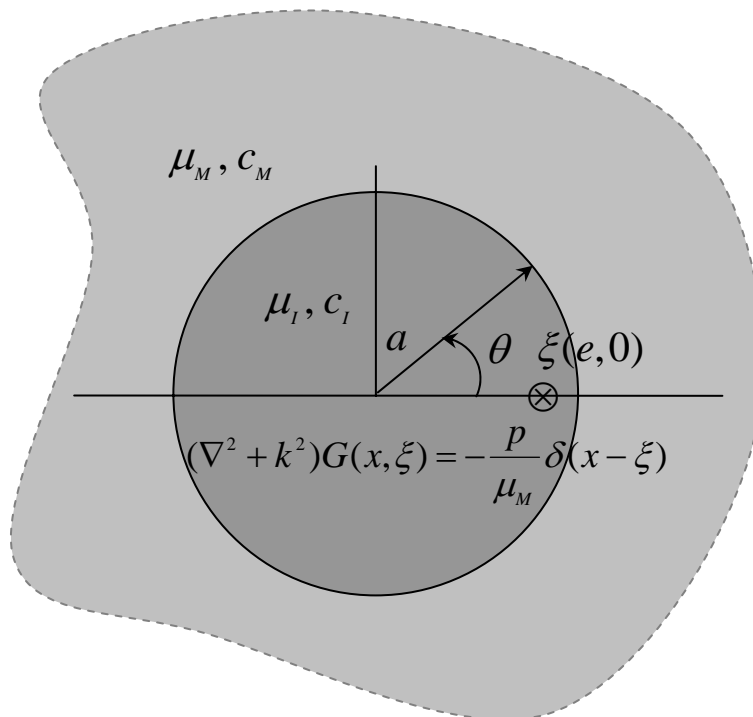


**Figure 3-1(b)** An infinite matrix containing a circular inclusion with a concentrated force at  $\xi$  in the inclusion

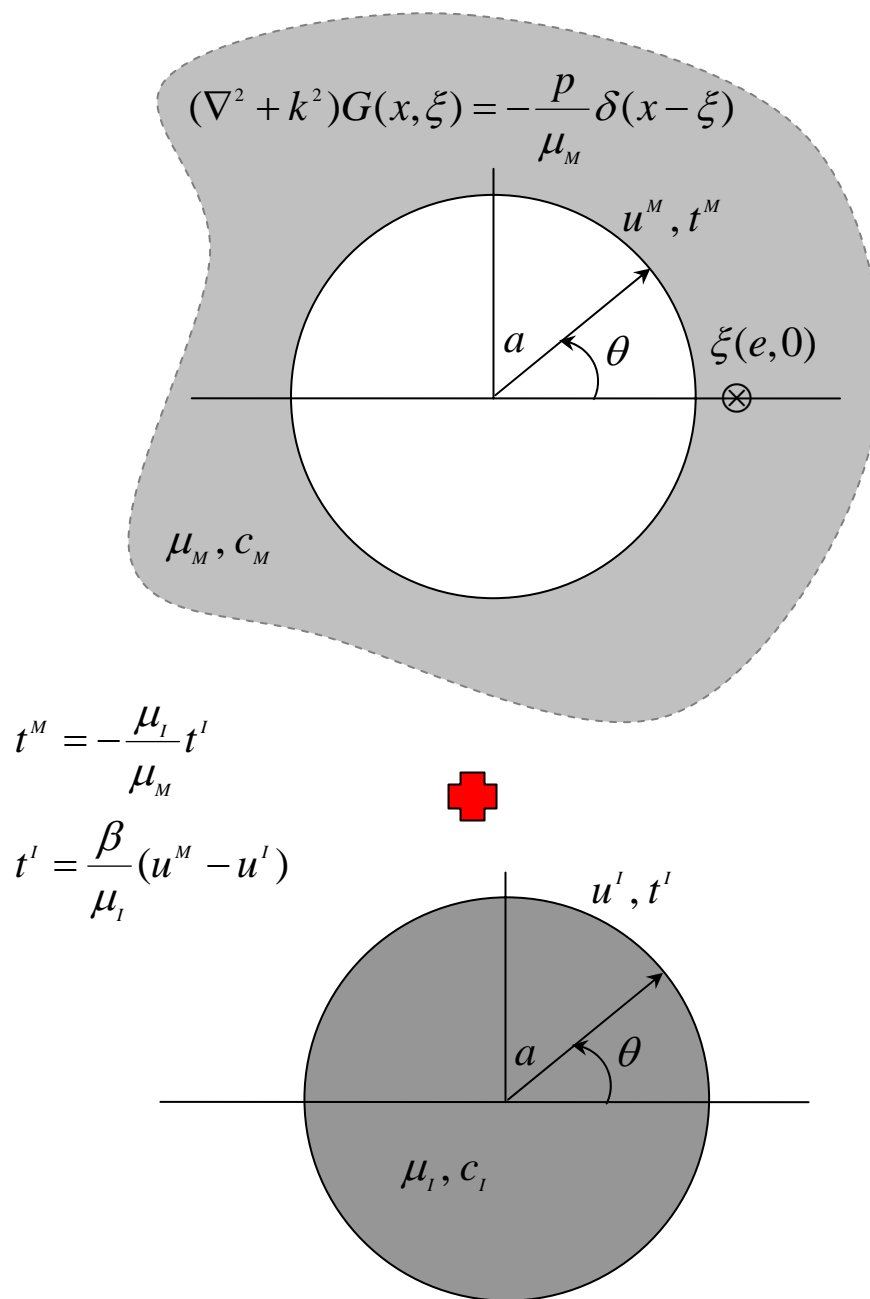


**Figure 3-1(c)** An infinite matrix containing a circular inclusion with a concentrated force at  $\xi$  in the matrix (take free body)

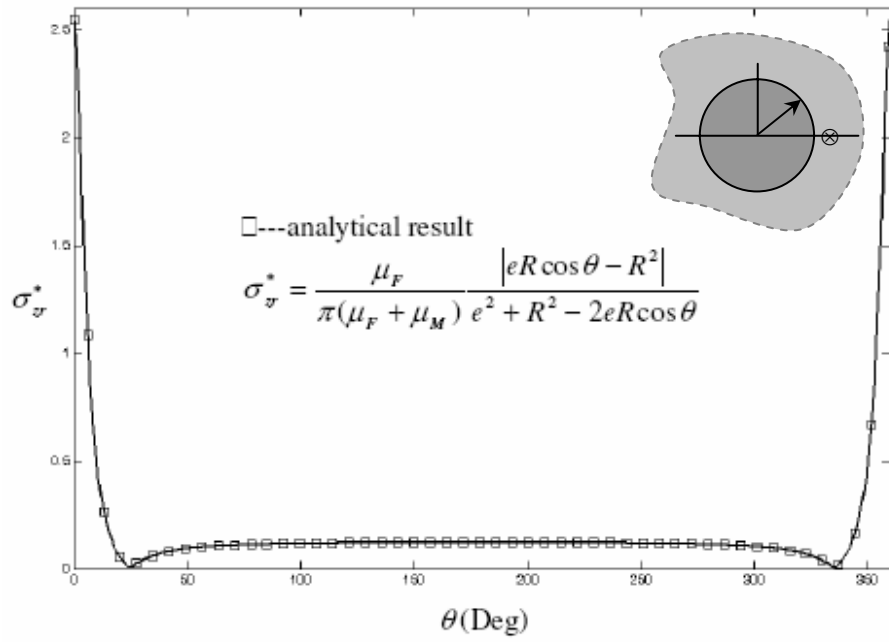


**Figure 3-2(a)** Distribution of  $\sigma_{zr}^*$  for the dynamic ( $k_M a = 0.01$ ) solution along the circular boundary (Wang and Sudak's solution)

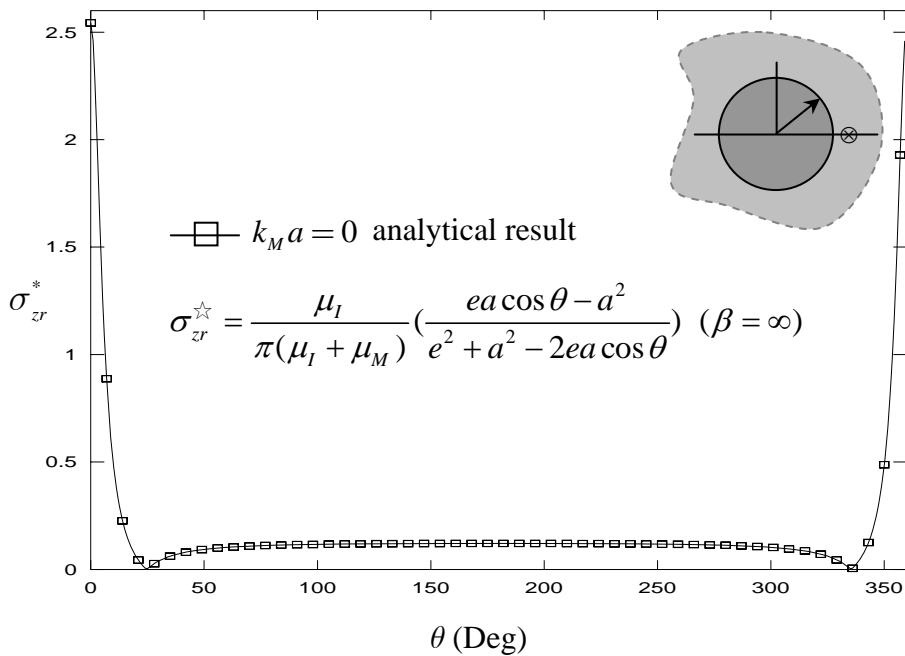


**Figure 3-2(b)** Distribution of  $\sigma_{zr}^*$  for the dynamic ( $k_M a = 0.01$ ) solution along the circular boundary by using the present solution

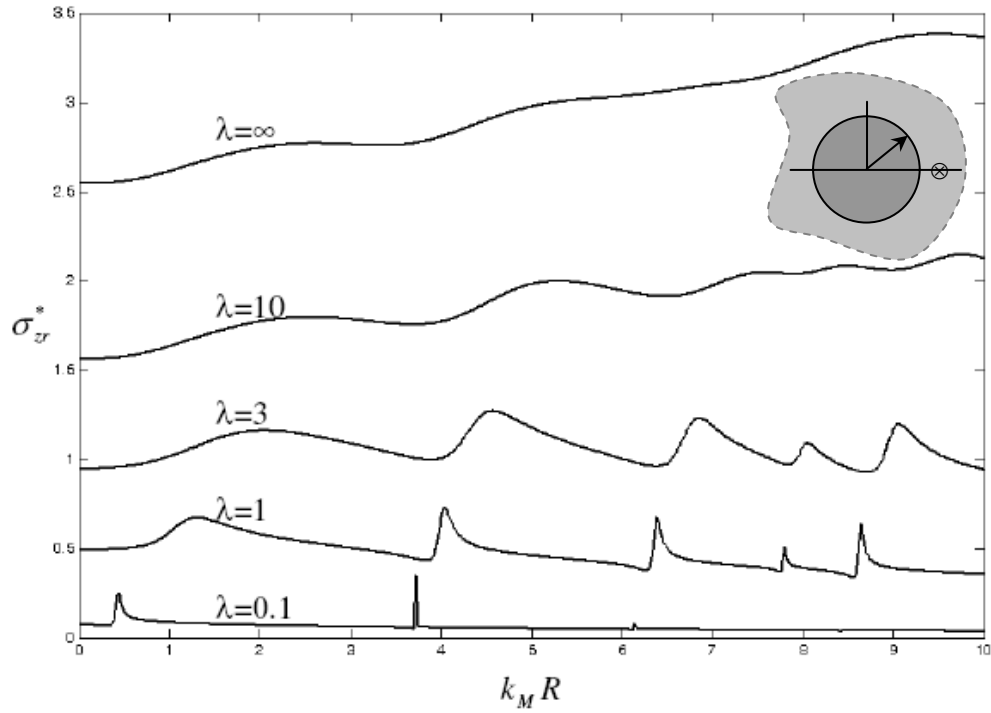


**Figure 3-3(a)** Parameter study of  $\lambda = a\beta/\mu_M$  for the stress response (Wang and Sudak's solution)

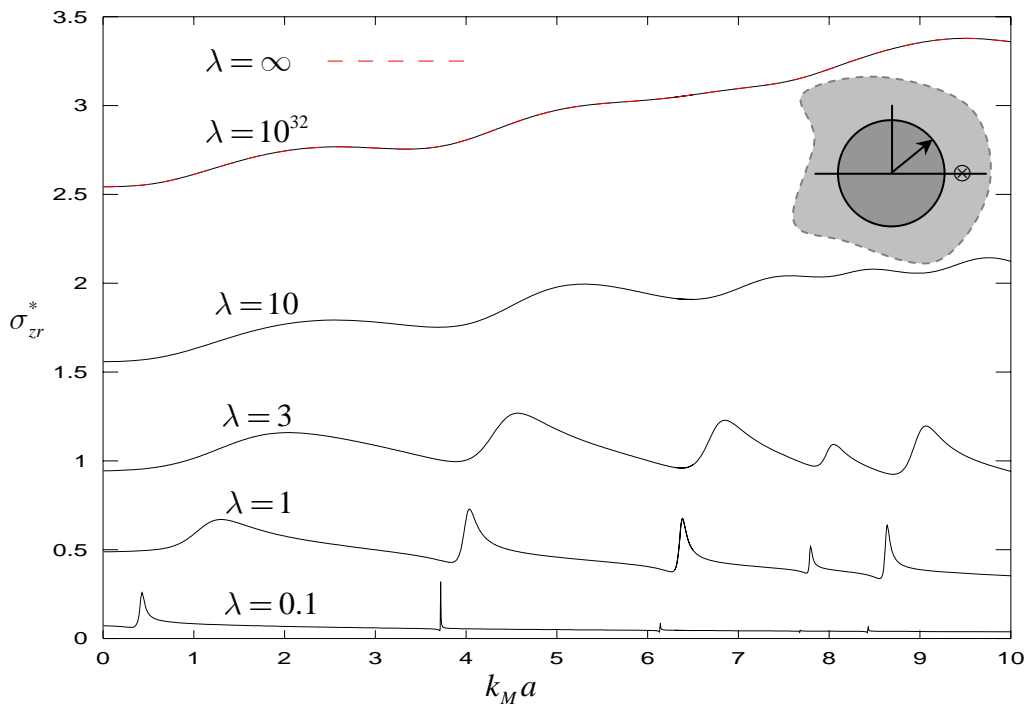


**Figure 3-3(b)** Parameter study of  $\lambda = a\beta/\mu_M$  for the stress response by using the present solution

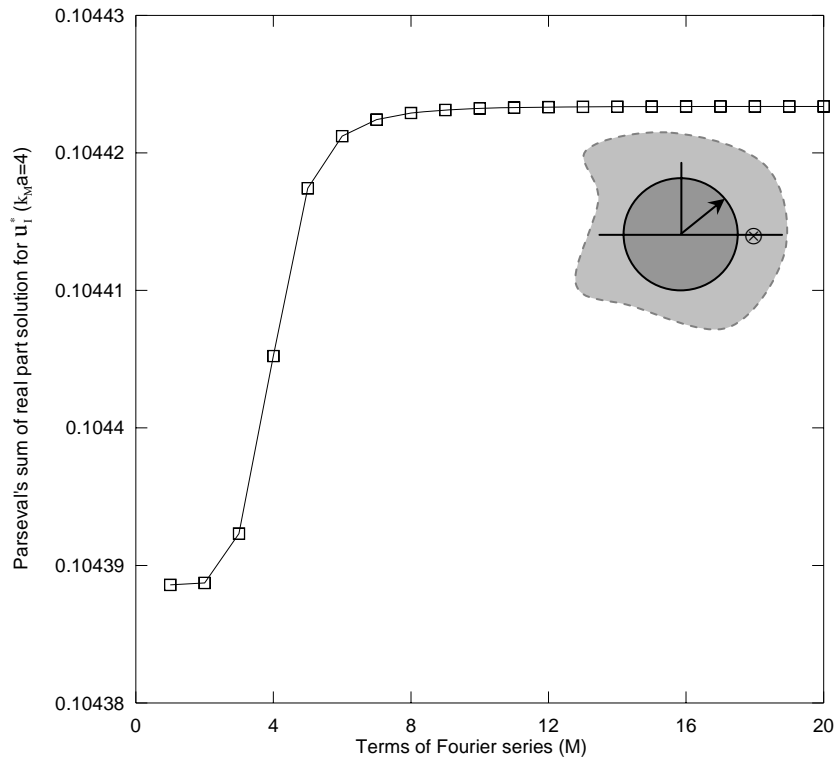


**Figure 3-4(a)** Test of convergence for the Fourier series with a concentrated force in the matrix (real part)

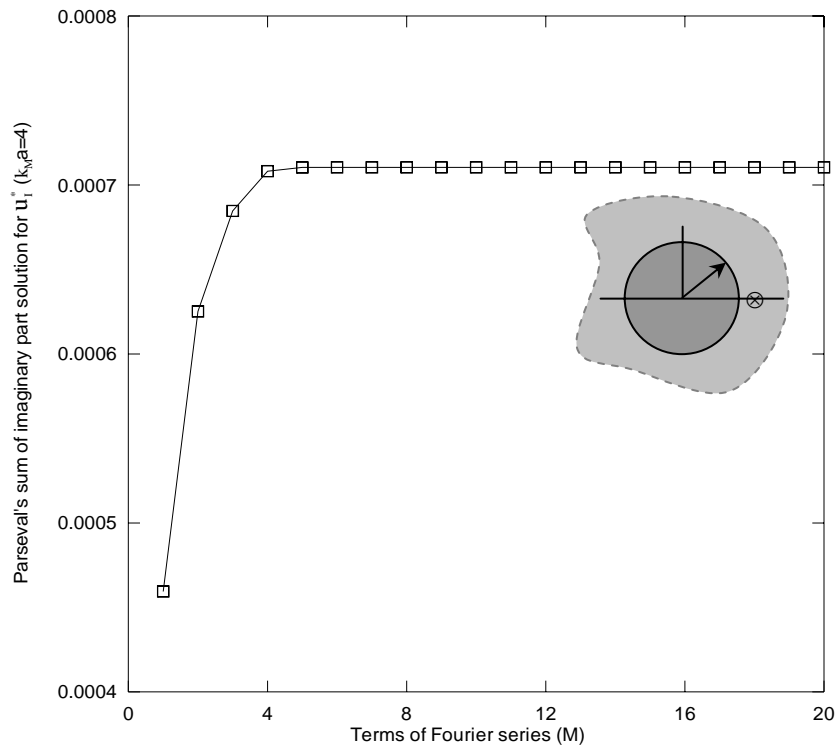


**Figure 3-4(b)** Test of convergence for the Fourier series with a concentrated force in the matrix (imaginary part)

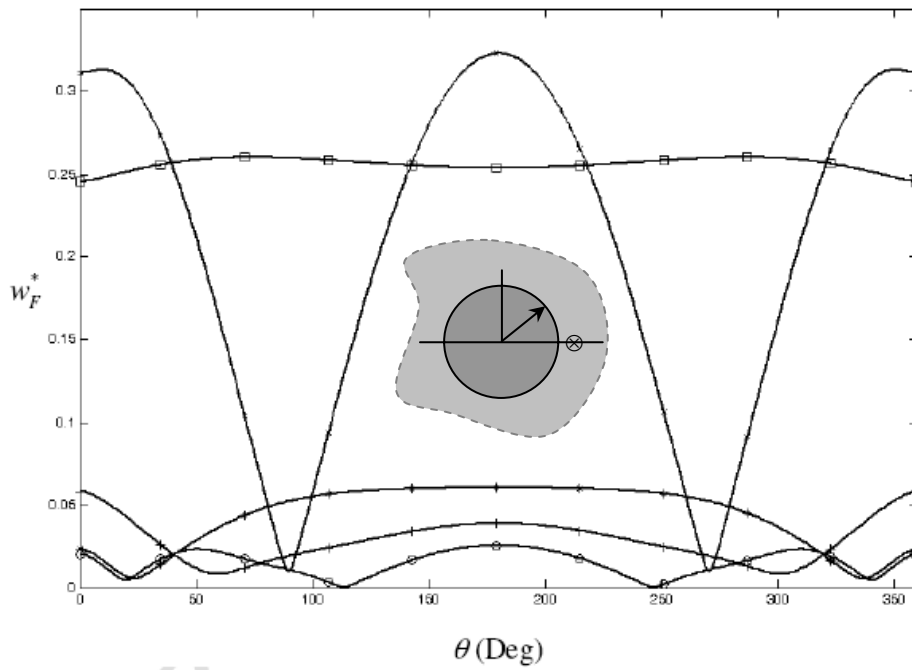


**Figure 3-5(a)** The distribution of displacement  $u_I^*$  along the circular boundary for the case of  $\lambda = 1$  ( $k_M a = 1, 2, 3, 4, 5$ ) (Wang and Sudak's solution)

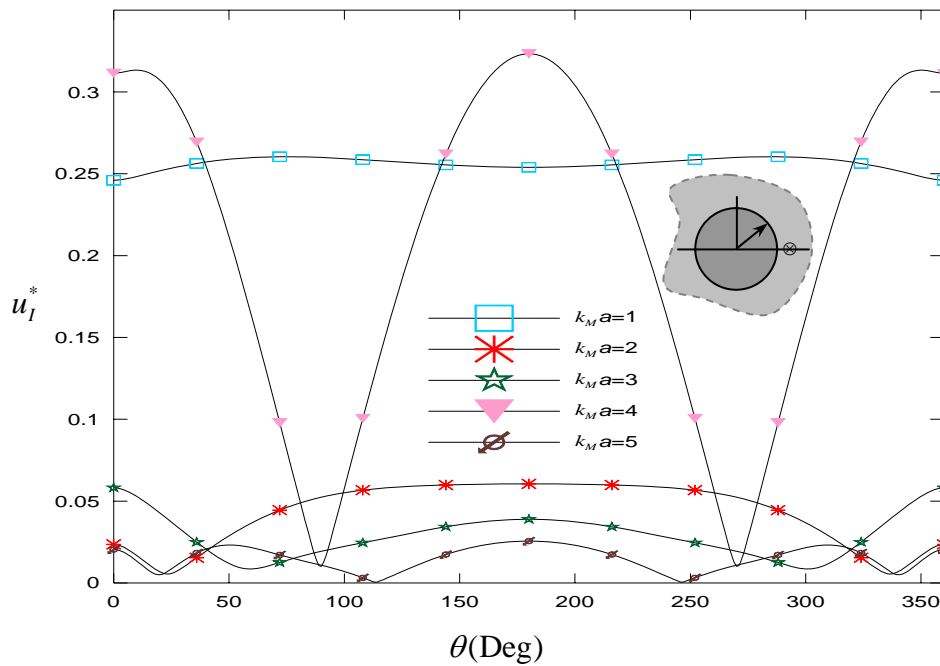


**Figure 3-5(b)** The distribution of displacement  $u_I^*$  along the circular boundary for the case of  $\lambda = 1$  ( $k_M a = 1, 2, 3, 4, 5$ ) by using the present solution

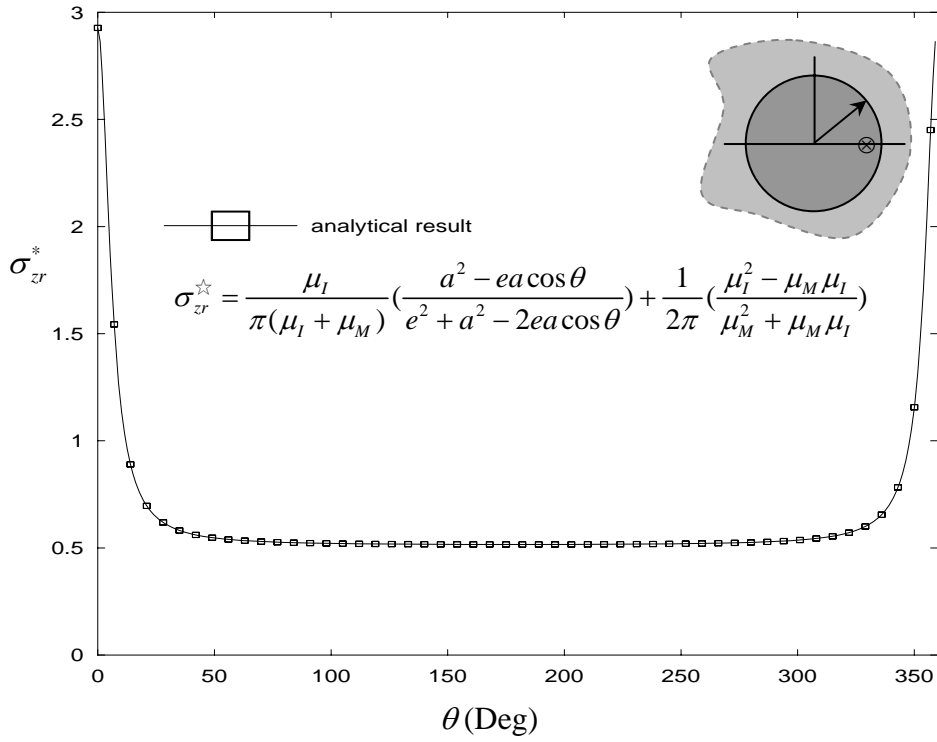


**Figure 3-6** Distribution of  $\sigma_{zr}^*$  for the dynamic ( $k_M a = 0.01$ ) solution along the circular boundary ( $e = 0.9a$ )

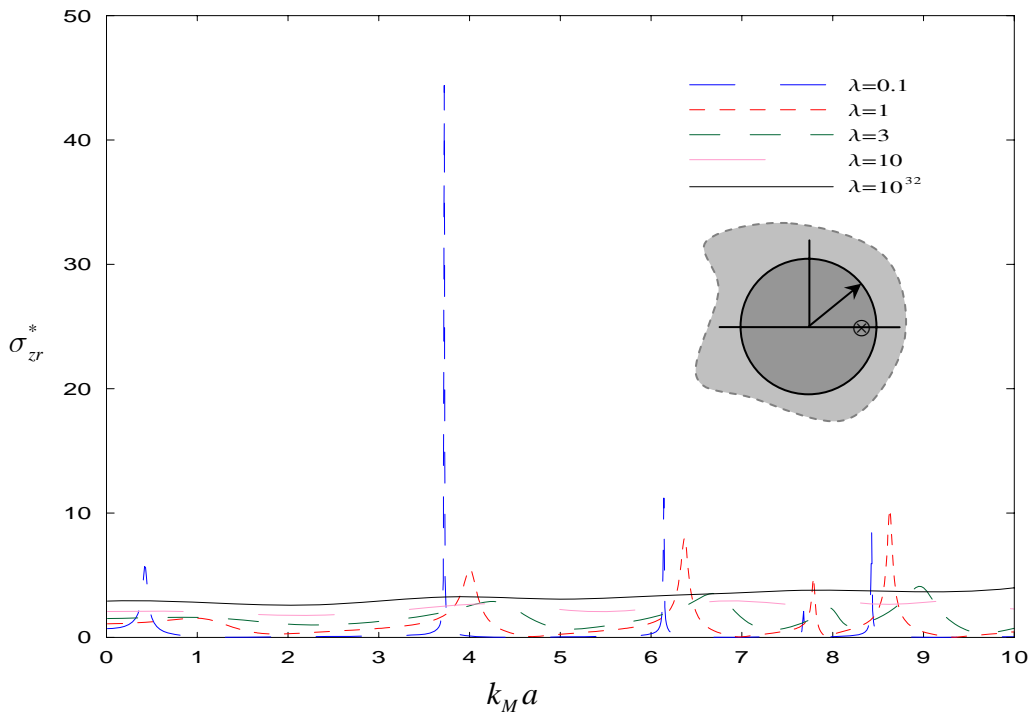


**Figure 3-7** Parameter study of  $\lambda = a\beta / \mu_M$  for the stress response ( $e = 0.9a$ )

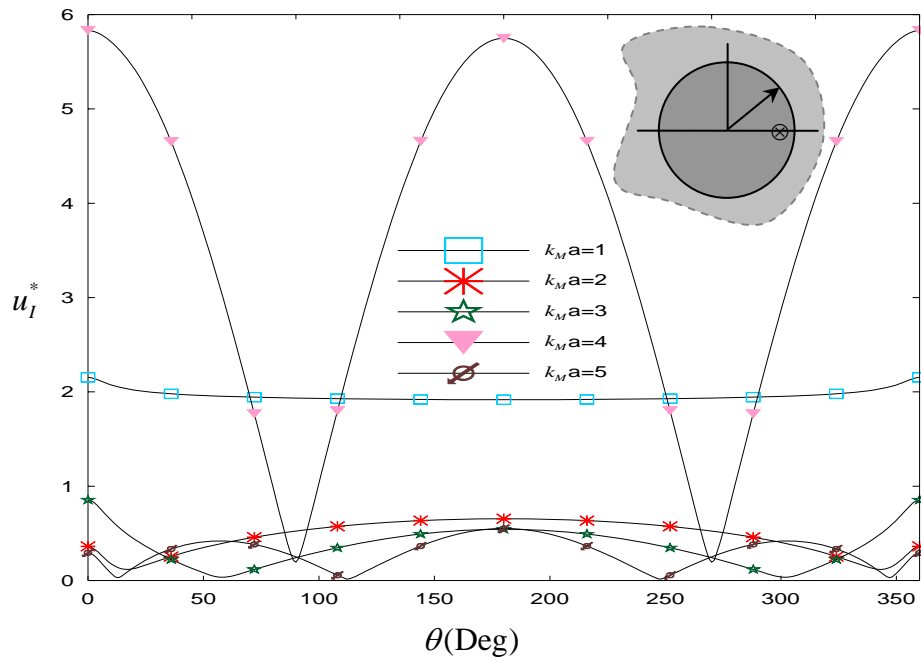


**Figure 3-8** The distribution of displacement  $u_l^*$  along the circular boundary for the case of  $\lambda = 1$  ( $k_M a = 1, 2, 3, 4, 5$ ) ( $e = 0.9a$ )

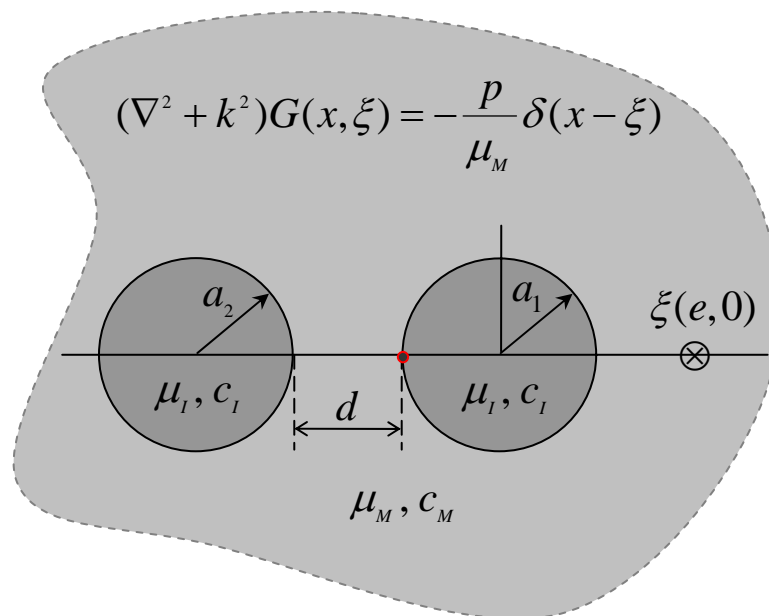


**Figure 3-9** An infinite matrix containing two circular inclusions with a concentrated force at  $\xi$  in the matrix

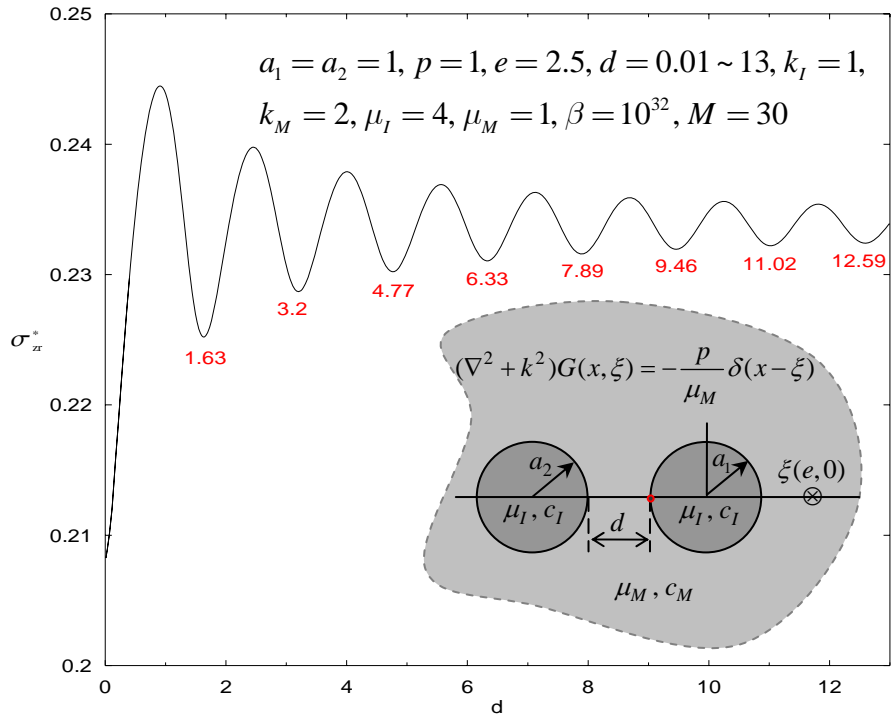


**Figure 3-10** Distribution of  $\sigma_{zz}^*$  of the matrix at the position of  $(a_1, \pi)$  various  $d$

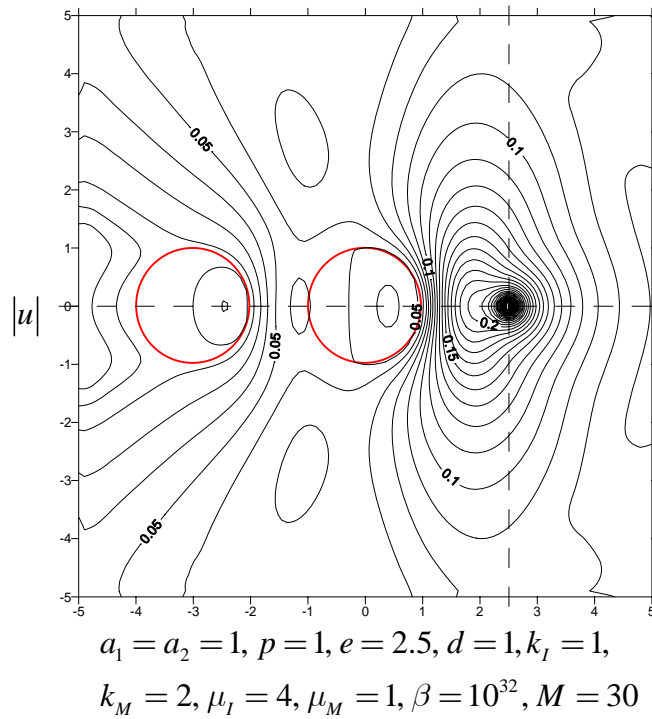
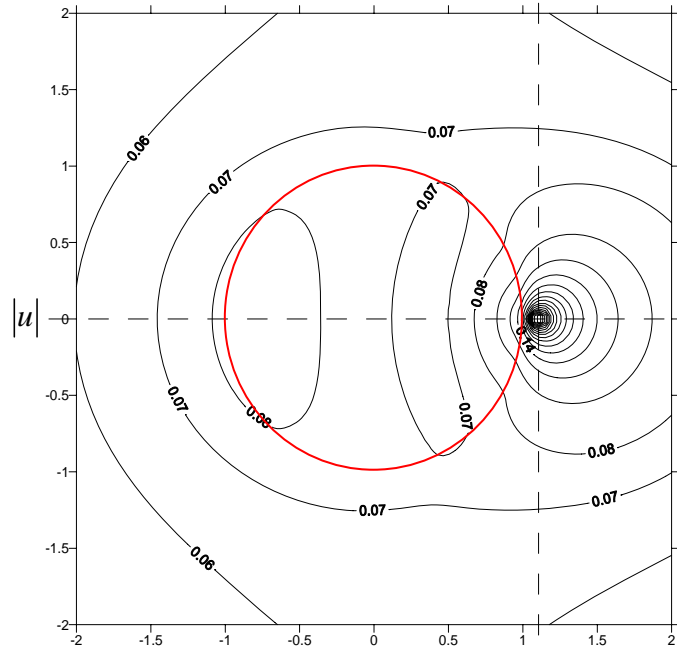
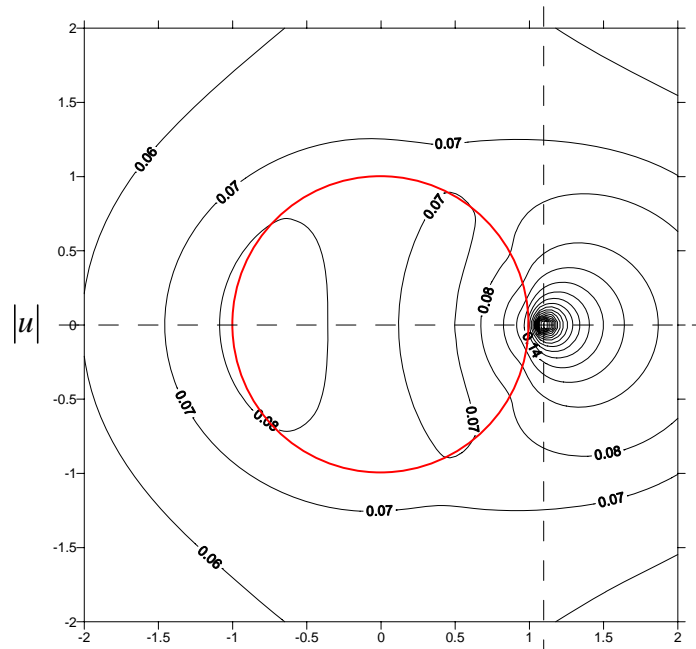


**Figure 3-11** The contour of the displacement for an infinite matrix containing two inclusions with a concentrated force at  $\xi$  in the matrix



$a = 1, P = 1, e = 1.1, k_I = 1, k_M = 2, \mu_I = 4, \mu_M = 1, \beta = \infty, M = 70$

**Figure 3-12** The absolute amplitude of displacement for an ideally bonded case



$a = 1, P = 1, e = 1.1, k_I = 1, k_M = 2, \mu_I = 4, \mu_M = 1, \beta = 10^{32}, M = 70$

**Figure 3-13** The absolute amplitude of displacement for  $\beta = 10^{32}$

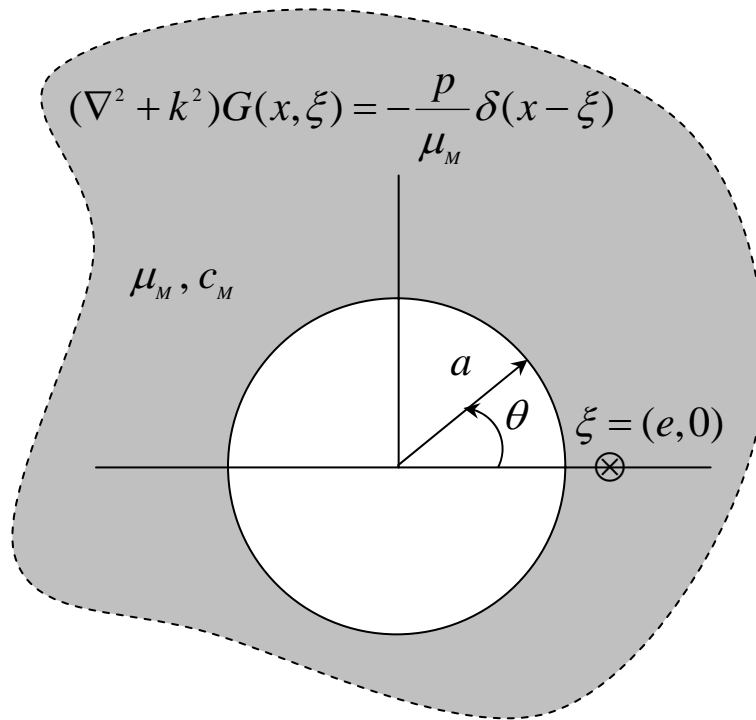
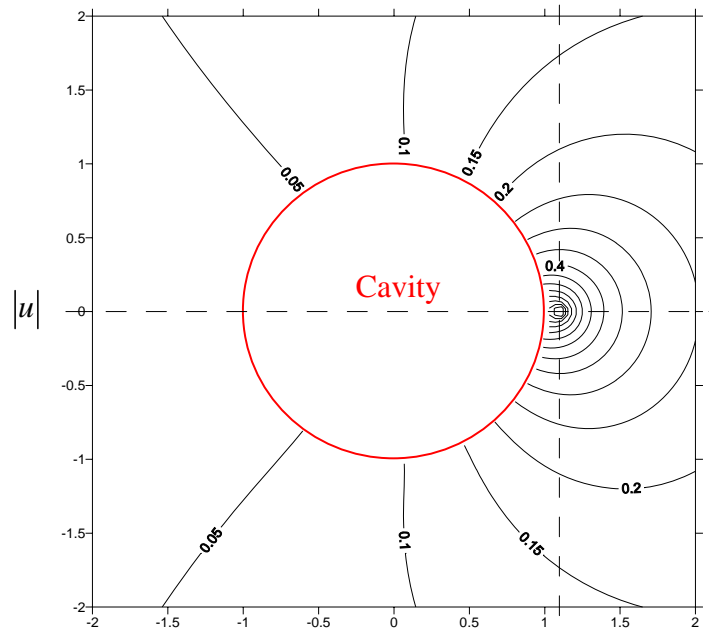
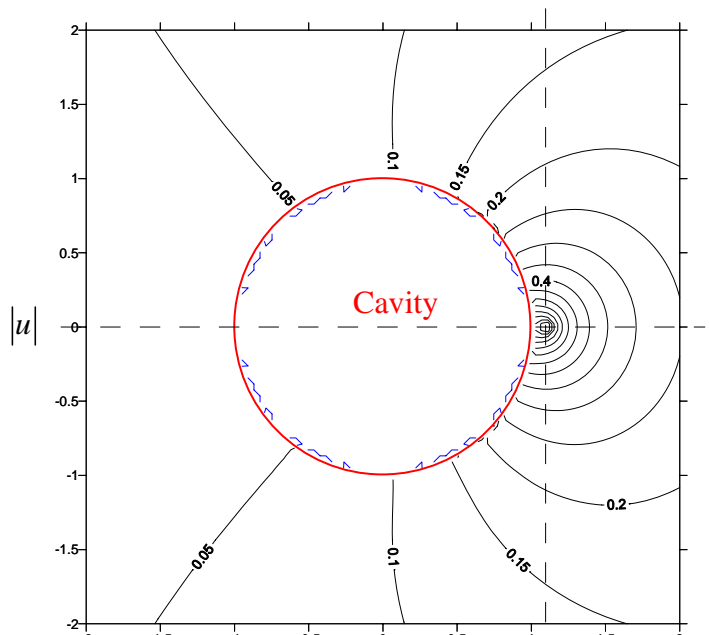


**Figure 3-14** A matrix with a debonded inclusion



$$a = 1, P = 1, e = 1.1, k_I = 1, k_M = 2, \mu_I = 4, \mu_M = 1, \beta = 0, M = 70$$

**Figure 3-15** The absolute amplitude of displacement for the cavity



$$a = 1, P = 1, e = 1.1, k_I = 1, k_M = 2, \mu_I = 4, \mu_M = 1, \beta = 10^{-32}, M = 70$$

**Figure 3-16** The absolute amplitude of displacement for  $\beta = 10^{-32}$

## 作者簡歷

中文姓名：柯佳男

英文姓名：Jia-Nan Ke

出生日期：民國 71 年 12 月 26 日

籍貫：台灣省台中縣

聯絡地址：台中縣沙鹿鎮鹿寮里中山路金星二巷 17 號

聯絡電話：(04) 2665-3767

行動電話：0972158813

電子信箱：[M94520066@mail.ntou.edu.tw](mailto:M94520066@mail.ntou.edu.tw)



學 歷：

國立台灣海洋大學河海工程研究所碩士 (2005.09 ~ 2007.07)

立德管理學院營建科技學系 (2001.09 ~ 2005.06)

台中縣立清水高級中學 (1998.09 ~ 2001.06)

台中縣立鹿寮國民中學 (1995.09 ~ 1998.06)

台中縣立竹林國民小學 (1989.09 ~ 1995.06)

著作目錄：

(A) 期刊論文

- 1 **Chen, J. T.; Ke, J. N.; Liao, H. Z.** (2007): Construction of Green's function using null-field integral approach for Laplace problems with circular boundaries. *Computers, Materials & Continua*, Accepted.
- 2 **Chen, J. T.; Ke, J. N.** (2007): Derivation of anti-plane dynamic Green's function for several circular inclusions with imperfect interfaces. Submitted.

(B) 會議論文

- 1 **Chen, J. T.; Ke, J. N.; Liao, H. Z.** (2007): Null-field equation approach as a tool for computing Green's function for Laplace operator with circular holes and/or inclusions. *International Conference on Computational Methods*, Hiroshima, Japan.